STRESS RELAXATION TESTS ON A LOW ALLOY STEEL

KENOSI NORMAN MOKOLOBATE

A dissertation submitted to the Faculty of Engineering and Built Environment, University of the Witwatersrand, in partial fulfilment of the requirements for the degree of Master of Science in Engineering.

Johannesburg, 2011

ABSTRACT

The deformation behaviour and dislocation substructure of crystalline solids is attributed to the physical processes of dislocation passing obstacles. The energy needed to overcome an obstacle, i.e. an impurity, atom, etc. is provided by activated dislocation caused by either mechanical or thermally activated processes. To verify which deformation mechanism is active in low alloy steel, tensile tests interrupted by stress relaxation periods were studied. These tests were performed over temperatures ranging from 288K to 873K and at constant strain rate.

Strain rates before and after stopping the cross-head and deformation mechanisms were determined. The results of these experiments and how they correlate with the effects of temperature were also discussed. Rather than interpreting the difference to be due to mechanically activated deformation, as has been considered elsewhere, deformation was considered to be thermally activated with a component responsible for hardening and a component unaccompanied by hardening. Creep of low alloy ferrite steel is recovery controlled. Recovery in this material was caused by complex structures of carbides precipitates while dislocation tangles recovery was attributed both to carbide growth and to tangled dislocations re-arrangement and annihilation. Mechanical activation of dislocation glide has not been detected in these experiments.

Flow stresses were calculated from the strain rate differences together with the strains estimated to be due to the hardening component of deformation using a rate equation that describe thermally activated glide controlled deformation. Flow stress–strain curves that were plotted were found to be independent of testing temperature. These curves were compared to hardening curves determined previously from constant force creep tests and were found to be similar.

DECLARATION

I **Kenosi Norman Mokolobate** declare that this research report is my own work except as indicated in the references and acknowledgements. It is submitted in partial fulfillment of the requirements for the degree of Master of Science in Engineering in the University of the Witwatersrand, Johannesburg. It has not been submitted before for any degree or examination in this or any other university.

Signed at ………………………………………………….

On the …………………………….. day of ………………………… 2011

DEDICATION

To my family and friends

You supported me through the long nights and difficult times.

Thank you for believing in me

ACKNOWLEDGEMENTS

There are several people I would like to give my sincere gratitude and appreciation for the quality of this study. First I would like to thank my supervisor Professor D Chandler, without his assistance, encouragement and support this thesis would never have been completed. Your feedback was always appreciated and certainly went a long way in helping me get through this in one piece.

Furthermore I would like to thank my wife Duduzile Mokolobate for her understanding during these trying times and her undying love. Baby you are the best.

Finally, I would like to thank my mother for her love, trust, understanding and support throughout my whole life.

TABLE OF CONTENTS

LIST OF TABLES

LIST OF FIGURES

LIST OF SYMBOLS

T	Temperature
$\dot{\sigma}$	Stress rate
σ	Stress
$\dot{\varepsilon}_p$	Plastic strain rate
ρ_m	Density of mobile dislocations
b	Burgers vector magnitude of the slip system
α	Geometrical constant of the order of 1
$\overline{\upsilon}$	Average dislocation speed
μ	shear modulus of elasticity
(γ_e)	elastic strain
(γ_p)	plastic strain
$\hat{\tau}$	a term representing average obstacle strength
m	the strain hardening exponent
p	describing the shape of tail average of the flow obstacles
q	the shape of the peak of the flow obstacles
t	time in seconds

INTRODUCTION

BACKGROUND

When a metal or alloy is subjected to increasing applied stress, the strains are initially often proportional to the stress. The material regains its shape and or dimensions when the load is removed. For a polycrystalline fcc metal, the initial slope of the shear stress vs. shear strain curve is found to be of the order of 0.05μ (where μ is the shear modulus of elasticity) and independent of temperature [1]. As the stress is increased, a point is reached after which strains are no longer proportional to the stresses; the strains are not recoverable on unloading of the specimen. The slope decreases with increasing stress and the curve then tends towards a saturation value, which is temperature and rate sensitive [2, 3]. This is attributed to increasing dominance of recovery as the dislocation density increases until eventually the effects of hardening and recovery balance [1].

This irreversible deformation is known as plastic deformation and the stress at which this begins is the yield stress. The yield strength, which is a material property, is a measure of the material's resistance to flow at a given temperature and strain rate. Thus, plastic deformation is the deformation of a material beyond the point of yielding. Plastic deformation of a metallic body therefore results in significant modification to the microstructure of the material. The term plasticity describes the deformation of a material undergoing non-reversible changes of shape in response to applied force [4]. As stress increases the strength of most metals decreases thus initiating plastic flow of the material. The continuous plastic flow of a material during plastic deformation can eventually terminate in fracture.

Perfect plasticity is a property of the material to undergo irreversible deformation without any increase in stresses or loads. Plastic materials with hardening require increasingly higher stresses to result in further plastic deformation speeds, i.e. higher stresses have to be applied to increase the rate of deformation. Such materials are viscous-plastic.

Metals capable of sustaining large amounts of plastic deformation before failure are said to behave in a ductile manner. Those that fracture without much plastic deformation behave in a brittle manner. Ductile behaviour occurs on many metals such as low-strength steels, copper and lead. High strength steels typically exemplify brittle behaviour.

In contrast to elastic deformation which depends primarily on stress in the simplest cases, plastic deformation is a function of stress, temperature and the rate of straining [5]; the microstructure of a material is often important as well.

Most materials are polycrystalline, i.e. they consist of many crystalline grains, each of which consists of an ordered array of atoms, i.e. on a lattice. The grains can be more or less aligned to one another and they meet in a boundary, known as, a grain boundary [5]. The grain boundary thickness is of atomic dimensions hence, this is termed deformation of the grains. Dislocations or defects are abrupt changes in the regular ordering of atoms in materials. They occur in high-density materials and are very important in the understanding of mechanical properties of materials as all real crystals contain defects. These may be point, line, surface or volume defects and disturb the regular arrangements of the atoms locally. The behaviour and effects of these imperfections are intimately related.

Polycrystalline metals deform plastically by several alternative, often competing mechanisms depending on the value of the stress, temperature and strain rate. The mechanisms that account for various aspects of plastic deformation are usually treated in two categories:

- Those that permit relative displacement of adjacent portions of the lattice over large distances, and;
- Those that allow displacement only, i.e. lattice spacing or less [5].

The behaviour of polycrystalline metals and alloys at high temperatures has been the subject of an increasing number of studies over years. In particular, investigation on deformation mechanisms motivated by high performance materials used in electrical generation plants for steam turbines, boiler tubes, steam chest, casing covers and boiler tubes, etc. and chemical plants [4]. In such applications, materials operate for periods beyond the design lives anticipated, up 250 000 hours, and in hostile service environments. Since the material performance may impose a limit on the operating stresses and temperatures, a wide range of alloys have therefore been developed. These alloys would be used for service under conditions such that resistance to creep at high temperatures is a major material requirement. Due to metallurgical complexity of most commercial high-temperature materials, it has then meant that studies, which were aimed at identifying the mechanisms by which creep occurred, have usually been undertaken using pure metals and relatively simple alloys.

Some of the uses of plastic deformation processes are for manufacturing of different metals and alloys in the metal industry. These metals perform at varying temperatures depending on the application. Due to mass production, industries now need to validate the deformation theories of materials to identify the controlling factors that influence the deformation of metals. Once these factors have been isolated, efficient ways of production can be utilised to manufacture superior quality in products.

Existing parametric techniques needed to predict reliable plastic deformation properties are mostly complex, time-consuming and expensive. For many engineering applications, it may be useful to be able to estimate plastic deformation properties of a material from inexpensive methods. This should ideally involve using simpler testing procedures such as tensile tests using stress relaxation techniques, which are relatively simple and less time-consuming.

In this study, the behaviour of low alloy ferritic steel under stresses at high temperatures is assessed to better understand deformation mechanisms by which creep occur. These alloys are generally found in hardened state, where tertiary creep controlled by microstructural degradation predominate [5]. This is due to the degradation of the microstructure produced during the initial hardening treatment. These may take the form of precipitate coarsening and or recovery of forest dislocation structures. For such alloys, it should be simpler to describe creep than for pure metals where primary, secondary, as well as tertiary creep may contribute significantly to behaviour [5].

Additionally, processes such as precipitate coarsening tend to accelerate under applied stress. The current study also attempts to determine whether plastic deformation of low alloy steel occurs predominantly by thermal or mechanical activation of dislocation motion.

LITERATURE SURVEY

Plastic Deformation Mechanisms

Crystalline solids plastically deform due to movement of dislocations in response to applied stress. Slip is the movement of these dislocations along definite crystallographic planes. In simple crystals, crystallographic slip is the predominant mode of plastic deformation. The dislocation boundary is described by the slipped and unclipped parts of the crystal.

Slip occurs preferentially on the most closely packed planes and specific directions, but if slip on these planes is constrained, other less closely packed planes become active. The coordination of a particular slip plane and direction is called a system and the most common slip systems are those that require the lowest stress to produce slip, Fig. 1.

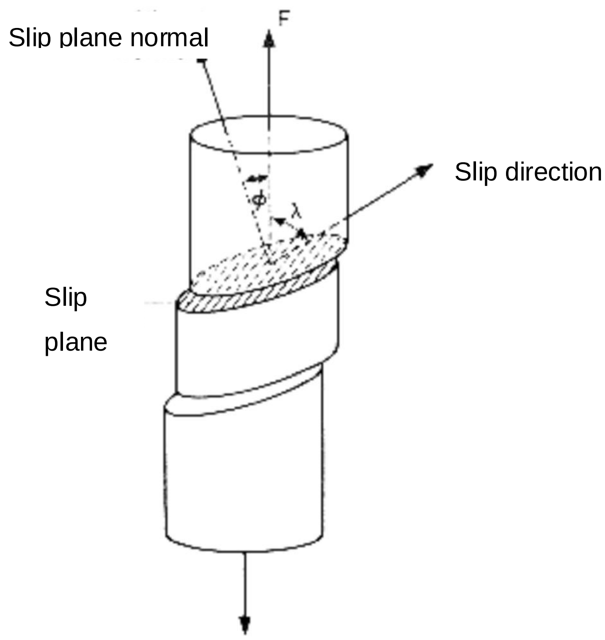

Fig. 1: Illustrations of the geometry of slip in crystalline materials [6].

In slip, plastic deformation is effectively concentrated into the region between atomic planes: in an idealised unit process, one-half of the crystal slips over the other half at an imaginary cut made between two neighbouring atomic planes. A characteristic shear stress is required for slip [5].

In the case where no such alternative modes of deformation are available, the flow stress rises above the cleavage stress and leads to brittle fracture. Apart from slip, the most common mode of plastic flow in metals is twinning.

Twinning is a range of dislocation glide involving the motion of partial dislocation Fig. 2 [5].

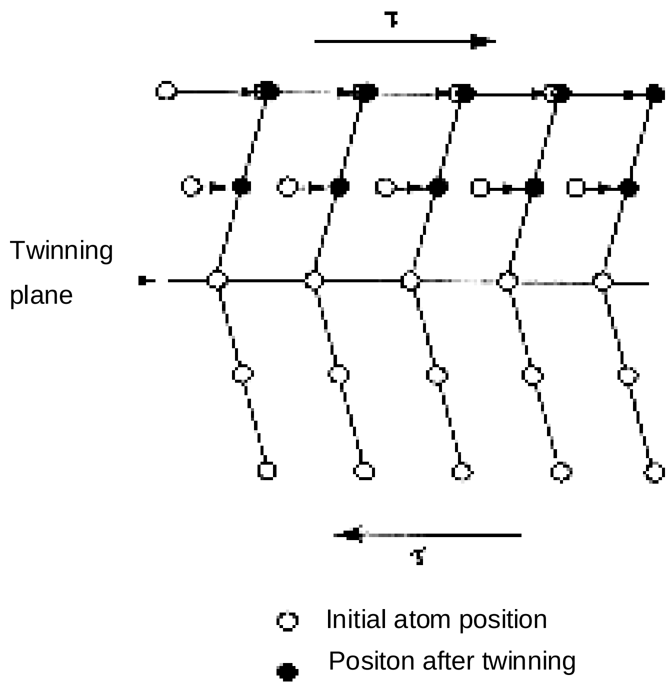

Fig. 2: Twinning in a crystal lattice [7]

It is of importance in the bcc and hcp lattice structures especially at low temperatures [5]. In fcc metals, twinning plays a role at low symmetries and sufficiently low temperatures. For fcc metals the tendency to twin increases with decreasing stalking fault energy. This is the greatest in silver and completely absent in aluminium [5]. Twinning is always preceded by some slip and is a discontinuous process whose occurrence is usually indicated by stress drops on the stress-strain curve and sometimes by an audible “clicking” sound.

Dislocations in crystal structures

Two primary kinds of dislocations are identified: screw dislocation and edge dislocation [5]. An edge dislocation is a defect corresponding to an extra half-plane of atoms introduced mid way between two crystallographic planes, distorting nearby planes of atoms. This kind of dislocation is characterised by a line direction, which is the direction of running along the bottom of the extra half plane, and the Burgers vector, which describes the magnitude and direction of the lattice Fig. 3(a).

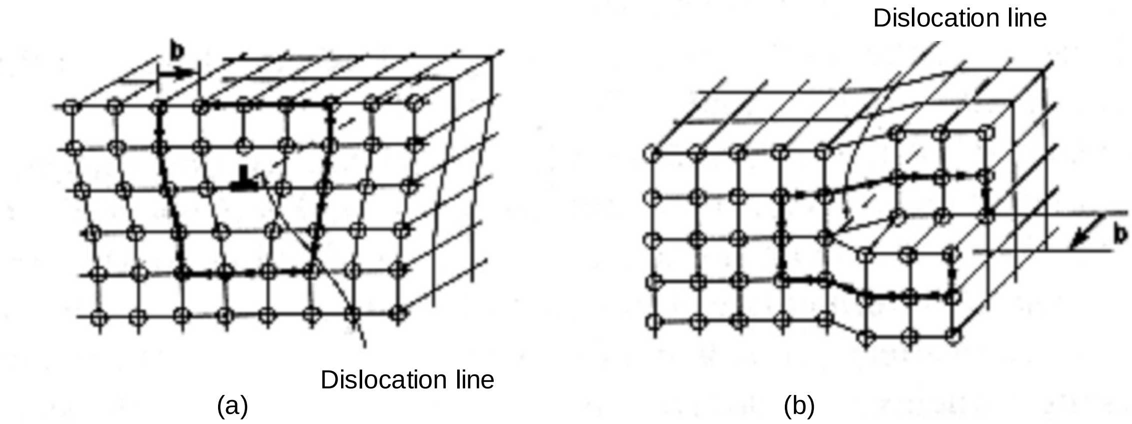

Fig. 3: (a) Edge dislocation; (b) screw dislocation. The Burgers circuit and burgers vector are shown for each case. [7]

For edge dislocation, the Burgers vector is always perpendicular to the dislocation line direction [5]. Edge dislocations attract and collect interstitial atoms dispersed in the lattice [5]. A screw dislocation is constructed by cutting a pathway through a perfect crystal and skewing the crystal one atom spacing Fig. 3(b). In a pure screw dislocation the Burgers vector is then parallel to the dislocation line [5]. Burgers vector is a useful characterisation of atomic distortions around a dislocation line. It has both a magnitude and direction. A method of determining the Burgers vector is illustrated by circuits around the dislocation lines depicted by the bold line traces in Fig. 3.

Mixed dislocation is the intermediate orientation between the two extreme cases, i.e. screw and edge dislocation. In many materials, mixed dislocations are found, i.e. where the line direction and Burgers vector are neither perpendicular nor parallel and consisting of both screw and edge character [5].

At low homologous temperatures, physical processes involved in plastic deformation of metals consist of dislocation motions. This process involves interactions with obstacles such as cross slip, the cutting of attractive dislocation junctions and the passing through obstacles [5]. At these low temperatures and high stresses, rate controlling mechanisms are caused by dislocation glide through an obstacle field provided by a forest dislocation or precipitate.

At very high temperatures, crystallographic slip may be supplemented by diffusion mass transport and grain boundary sliding. This deformation manifests itself at high temperatures and very low stresses. Therefore, slip is considered the controlling mode of plastic deformation in simple crystals [4]. At high temperatures deformation of fcc and bcc pure metals are controlled by recovery processes and not by glide controlled processes [8]. Several factors affect high temperature strength of materials and their deformation at elevated temperatures. Dislocation may move out of their glide planes by thermally activated cross slip since the mobility of atoms and the equilibrium concentration of vacancies increase with temperature. Diffusion controlled processes become more important and the mobility of dislocation is thus increased. Mobile dislocations climb more easily at a higher temperature, as it necessitates the mobility of vacancies in a lattice [5, 8].

Deformation that occurs beyond the point of yield, especially at low temperatures, takes place by shear or slip of one crystal plane over the other and is not strongly time dependent. This action is the result of the movement of microscopic defects such as dislocations through the crystal, occurring by consecutive breaking and forming of new bonds with other atoms across the slip plane [5].

Dislocation could also be due to line defects [9]. These lines caused by dislocation can end at the surface of a crystal and at grain boundaries, but never inside a crystal [9]. Thus, dislocation must either form closed loops or branch into other dislocations. Crystal defects such as precipitates, voids and bubbles can occur under certain circumstances and have important effects on the properties of crystalline solids.

Dislocation in metals can also be due to forest dislocation cutting. It is a collection of fixed and randomly distributed point obstacles. The mechanism of forest dislocation cutting exhibits unusual complexities. These dislocations can interact with glide dislocations to form attractive junctions, where small nodal segments of dislocations can lower significantly the local energy of the two intersecting dislocations making the thermally assisted intersection possible. In work hardened crystals not only are the points of intersection of forest dislocations with slip planes nearly always clustered into cell walls giving a distinctly non-random distribution, but they can also be displaced significantly under the forces exerted by an impinging glide dislocation [10].

When the applied stress is smaller than the mechanical threshold, dislocations are expected to stop at various obstacles. These dislocations may be released by thermal fluctuations and then travel at a drag controlled velocity to the next obstacle. This is known as a jerky glide [10].

Deformation in the various grains depends on each other; certain conditions must be met at the interfaces between them. This is the major role of grain boundaries. The theory of polycrystalline deformation consists of treating these interactions once the properties of the grains are known. The interaction may, however, influence the deformation mechanisms inside the grains themselves and render them different from simple crystals. Thus, when we describe plasticity of crystals we mean that of the grains.

MECHANISMS OF STRENGTHENING METALS

The ability to deform plastically depends on the ability of dislocation to move. Strengthening in metals involves hindering dislocation motion in the material. This could happen in several ways.

Strain Hardening

During deformation of a pure metal at ambient temperatures, hardening usually occurs to some extent. Generation and re-arrangement in the material cause dislocation of substructures. The motion of dislocations may be hindered or resisted by their interaction with other dislocations caused by impurity atoms, grain boundaries, etc. This strain hardening behaviour results in the material becoming stronger or harder as it deforms. In a pure metal, two types of point defects are possible, namely a vacant atomic site or vacancy, and an interstitial atom [5]. Impurity atoms in a crystal are considered extrinsic point defects of a crystal.

If dislocations generated by a source are unable to glide freely along their slip planes, a higher applied stress causes a shape change in the material [5]. At low plastic strain rate amplitudes, elastic accommodation of strain may compensate to some extent for the misfit arising from the non-uniform plastic deformation of adjacent grains. In general, a work hardening law can empirically describe stress-strain curves. For tensile straining tests, this empirical relationship is given by Eq. 1 as:

$$\sigma = \sigma_o + k\varepsilon_p^m \qquad (1)$$

where ε_p is the plastic strain, σ_o is the initial stress and *m* is the strain hardening exponent.

Plastic hardened materials deform plastically only on increasing stress level resulting in changes to their yield condition during the loading process. The performance of such materials depends on the previous states of stress and strain.

In such path-dependent cases, the elastic range of materials is expressed by the thermodynamic forces associated with two internal variables, back stress representing kinetic hardening and drag stress representing isotropic hardening [4].

Material often has viscous or time dependent deformation. Time dependent plasticity is a particular limiting case of viscoplasticity. In the unified theory capable of describing cyclic loading and viscous behaviour, the time dependent effect is unified with the plastic deformation as a viscoplastic term [4].

Solid Solution Strengthening

Alloying elements in solid solutions can make a useful contribution to creep resistance in the metals. Most commercial alloys rely on the presence of a fine dispersion of precipitates for their high temperature strength. The role of particles in a material is to act as obstacles to dislocation movement, i.e. on encountering particles in the glide plane, the moving dislocation attempts to cut through the particles or by-pass them by climb and cross slip [4]. Fine particles dispersion also inhibits re-arrangement and total destruction [4].

Softening - *Recovery*

The basis of the recovery, in creep theories, is the knowledge that material hardens with strain and softens with time while being heated. When these two processes occur simultaneously as in high temperature creep, deformation is bound to take place. These ideas were first formulated by Bailey [11] and Orowan [12], and were subsequently elaborated by Cottrell and Aytekin [13]. According to this theory, a balance between strain hardening and recovery exists in the secondary creep stage, producing a steady state creep rate.

Although the consideration of the concurrent strain hardening and recovery processes certainly has a true physical background, the recovery can be considered as phenomenological in the sense that it frequently does not take into account the detailed mechanism by which glide process or the recovery operates. The formulation of the recovery-creep model is such that in principle it could encompass any thermally activated glide process. The recovery-creep theory model is therefore incompatible with the climb theory.

Although earlier recovery-creep models did not describe details of the deformation process, the most recent formulations by Mclean [14] and Lagneborg [15] consider the mechanisms in some detail. According to the model the increased creep strength in these materials are believed to be caused by a decrease in the recovery rate. This in turn is due to a decrease of the driving force for the recovery process. The mobility of the climbing dislocations is involved in the process. Furthermore, the dislocations are arranged in a three dimensional network. The creep process consists of consecutive events of recovery and strain hardening.

CREEP DEFORMATION

Creep is time dependent strain occurring under a stress that is lower than the yield point. As the temperature increases, the strength of most materials decrease and elongation may continue a long time before rupture occurs. Thus, creep is a time dependent plastic deformation phenomenon. The temperature, above which continuing slow deformations and significant modification to the microstructure of the material occurs may terminate in fracture by creep rupture.

Dislocation creep theories can be classified into two main groups, those in which dislocation glide processes are considered rate controlling and those that depend on dynamic recovery by climb [4]. It has been established in previous studies that immediately after small reductions, during creep of ferritic steels, incubation periods of zero creep rate were recorded before creep recommenced at the reduced stress level [16]. This behaviour indicates that dislocation glide mechanisms cannot be rate controlling [16]. With these processes, a small decrease in stress is followed immediately by new slightly lower creep rate and not by an incubation period of zero creep rates. Instead, the occurrence of incubation periods suggest that the flow stress of the material must decrease by recovery before creep begin again after the stress reduction, i.e. creep of ferrite steel is recovery controlled [16].

Creep deformation under monotonic load or stress is usually performed at high temperatures. This effect is most evident at these temperatures and yields data often represented as a graph of strain against time Fig. 4.

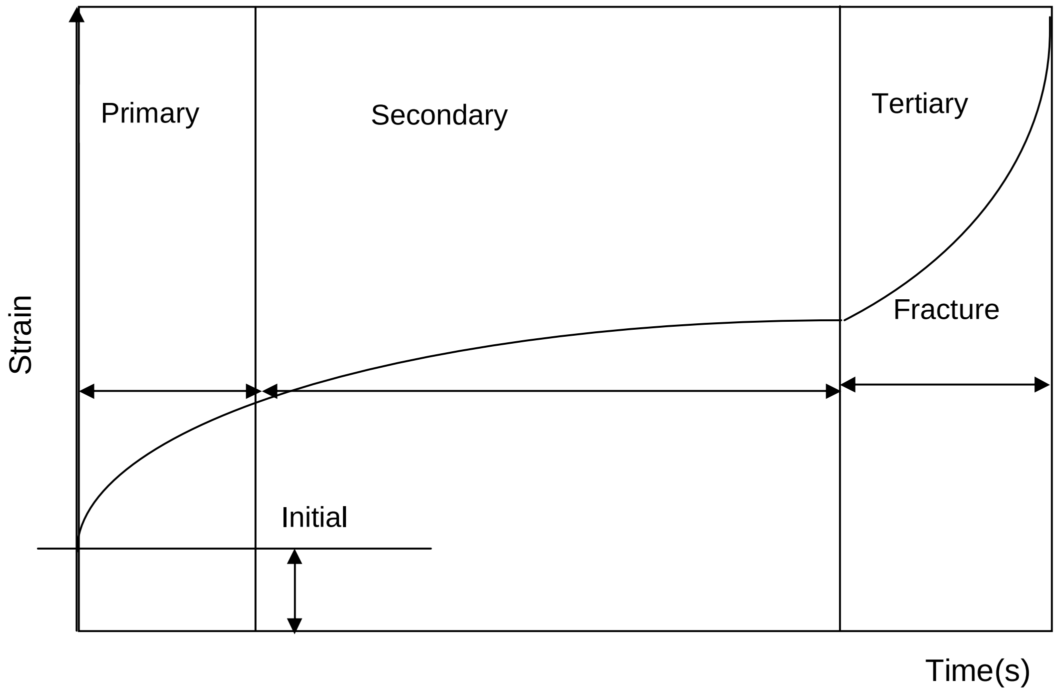

Fig. 4: Strain versus time schematic representation of Creep Curve with basic creep regions under constant load [17]

This monotonic or static creep curve shows three different stages namely primary or transient stage (with decreasing creep strain rate), secondary or steady state stage (of constant and minimum strain rate) and tertiary or unstable stage (with accelerating strain rate).

Primary Creep: Primary creep is a work hardening process during which the strain rate decreases with time.

Secondary Creep: Secondary creep is an equilibrium state between work hardening and softening processes or damage mechanisms producing a constant strain rate.

Tertiary Creep: For tertiary creep, the strain rate increases rapidly, leading to final rupture. The balance between the hardening and softening is lost, with the softening dominating [4, 17].

Creep Deformation Mechanism

Introduction

In general the properties of engineering materials, e.g. mechanical strength, lattice parameter, diffusion coefficient, etc. depend on the thermo-mechanical treatment and become important for creep resistance in low alloy ferritic steels [16]. These alloys derive most of their strength from precipitation hardening [5]. Small changes in thermo mechanical history of materials have large effects on the mechanical behaviour with over-ageing in service an important consideration. In practice, steel is used in one of a few standard states and is limited in its use to temperatures below 600 ^{0}C because of oxidation [17]. Ageing in service becomes important only above 550 ^{0}C. The alloy starts to transform to austenite at above 700 ^{0}C and is never used structurally above 700 ^{0}C, where its strength would be little better than that of pure austenite [18].

Creep occurs by grain boundary sliding. Thus the more grain boundary there is, the easier creep deformations will be [19]. The macroscopic behaviour of almost all real materials reflects the superposition of effects due to many types of obstacles and mechanisms, and occasional effects due to drag and inertia.

Thermally activated deformation processes govern creep deformation [19]. These processes can occur at both low and high temperatures, although most investigations have been at high temperatures. Most of the available data concerning deformation during creep testing are presented as steady state creep rates [20]. Information from such data has led to identification of regions of stress-temperature space in which different and often competing physical mechanisms control the strain rate. Results are often presented as deformation mechanism maps. Creep curves are constructed from rate equations, resulting in increasing stresses with time as the cross sectional area are lost due to void growth. Although steady state creep is possible within the content of the scheme, it does not occur over most of the stress and temperature ranges considered [16].

The physical mechanisms that cause creep deformation differ markedly for different classes of materials. For a given material, different mechanisms are related to microscopic processes such as the motions of atoms, vacancies, dislocations, or molecules, which occur in a time dependent manner and more rapidly at higher temperatures.

In polycrystalline solids, several mechanisms in creep deformation often compete with one another. Among these, the principle mechanisms for fracture are void growth and coalescence. For high strength alloys, microstructure degradation such as precipitates coarsening mechanism is dominant [6]. Three major deformation mechanisms include:

- plasticity controlled by glide of dislocations through an obstacle field,
- power law creep controlled by climb dislocations over obstacles, and
- diffusion creep under the influence of a stress-induced chemical potential difference [6].

The latter two mechanisms occur at high temperatures. Diffusion flow occurs at high temperatures and high stresses while climb occurs at higher temperatures and lower stresses.

For some metals at relatively high stresses and low temperatures, the rate controlling process mechanism is often regarded as dislocation glide through obstacle field that may be provided by forest dislocations or precipitate. At higher temperatures and lower stresses, the rate controlling process becomes dislocation climb rather than glide [20]. At intermediate stress and temperature, conditions between the glide (plasticity) and climb (power law creep) exist. The intermediate behaviour is defined as power law breakdown. Power law breakdown is usually described by empirical equations or could be described by a combination of glide and power law equations. Dislocation glide is by far the most common in plasticity with other forms assisting or facilitating the process.

Fundamentally, the rate controlling mechanism of creep deformation at low temperatures does not, however, differ from that of normal plastic deformation, e.g. as observed during tensile testing [15]. In both cases, all strain is due to thermally activated deformation except for activation that is stress assisted largely during a regular tensile test at ambient temperatures. Recovery causes reductions in strain hardening, whereas the glide process concurrently tends to increase the strain hardening.

In low alloy steels the major mechanism responsible for microstructure degradation is coarsening of the carbide precipitates [16]. The mechanism of solute hardening presents some problems. An extension of the precipitation-hardening model to individual model in individual solute atoms may apply, at best, to very dilute solutions when only interstitial solutes cause any appreciable strengthening. Randomly dispersed substitution solute atoms do not act as discrete obstacles when they are in concentrated solutions, but interact with dislocations cooperatively [2, 3, 21-23]. William and Wilshire [16] observed that as changes in size, spacing and form of the carbide particles occur, the density of dislocations evident within the grains increased very gradually. The individual dislocations observed within the grains were almost invariably found to be held up at carbides suggesting a gradual loss of creep resistance as particle coarsening takes place [16]. For the evaluation of kinetics in alloy steels, where complex structures of carbides precipitates and dislocation tangles because of the quenching process, recovery could be attributed both to carbide growth and to tangled dislocations re-re-arrangement and annihilation.

Most studies on the mechanical behaviour of precipitate-hardened alloys have been concerned with deformation behaviour under steady state conditions usually using creep tests. The work hardening of such materials beyond the yield point where steady state behaviour cannot be assumed has not been studied to such an extent. Furthermore, most work has focused on theoretical issues with little work being done on the practical aspects. An example of extensive practical work involves predicting long-term creep from short-term creep results using extrapolation techniques involving extensive experimental data. There are theories that attempt to predict creep results from tensile tests that usually require information on transient responses for their application [24, 25]. Such measurement involving flow stress changes due to sudden changes in strain rate or temperature tend to be difficult to perform and can lead to ambiguous results since they are subjected to machine stiffness and response characteristics. A possible reason for requiring such a result is that the recovery rates tend to be accelerated for material under stress as compared to unstressed material [18].

Plastic deformation formulation

At sufficiently low temperature effects associated with diffusion can be ignored (i.e. $T < 0.3T_m$), the application of stresses less than the elastic limit result only in elastic strains. When a higher stress is applied to a ductile metal, the resulting instantaneous strain has both elastic and plastic component, with only the elastic component being fully recovered on removal of the stress.

Orowan [26] was the first to present an expression of plastic strain rate in terms of dislocation parameters viz.:

$$\dot{\varepsilon}_p = \alpha b \rho_m \overline{\upsilon} \tag{2}$$

where b is the Burgers vector magnitude of the slip system, α is the geometrical constant of the order of one, ρ_m is the density of mobile dislocations and $\overline{\upsilon}$ is the average dislocation speed. Equation (2) simply says that the deformation rate is proportional to the mobile dislocation speed, i.e. the Burgers vector. The stress, temperature, or microstructure dependence of plastic strain rate must be contained in the non-constant terms, ρ_m and $\overline{\upsilon}$. Therefore, plastic strain rate must be continuous unless the stress, temperature or structure is changed discontinuously.

In-depth understanding of the kind of dependencies is very important when making quantitative predictions of plastic deformation rate. Incidentally, for any deformation at strain rate, $\dot{\varepsilon}_p$ it is a difficult task to evaluate the relative contribution of ρ_m and $\overline{\upsilon}$.

In a constant stress rate testing in which the machine cross-head was stopped to allow for a period of stress relaxation, it has been found that plastic strain rate immediately before stopping the cross-head was greater than that during stress relaxation period [1, 27-31]. The results were generally interpreted in terms of two flow contributions, viz.

- Thermal activation or effective stress component, and
- mechanical activation or athermal [32].

For activated glide, dislocation line segments move under the influence of an effective stress until stopped by a discrete obstacle. Any further glide would occur when either thermal or athermal activation aids the dislocation segment past the obstacle.

THERMAL ACTIVATION

To interpret a variety of temperature and strain rate effects during flow of metals, it is customary to model dislocation movement as a thermally activated process [5, 10, 27, 33-36]. Thermal (effective) stress describes the net stress available to drive dislocations past thermally penetrable obstacles. The energy needed to overcome obstacle barrier is provided not only by the resolved shear stress, but also by thermal energy so that thermally activated deformation theory is named accordingly [5, 10, 26, 37].

In the limit when the thermal stress component is zero, slip is athermal in the sense that obstacle to dislocation motion can be overcome only by increasing the stress or by reducing the obstacles strength through recovery re-arrangement.

“Both thermally and mechanically activated deformation theories are based on physical processes of dislocations passing obstacles and could be described as the combination of kinetic flow theory and structural evolution law"[36]. Enough attention has been given to theory of thermally activated deformation as well as the numerous experiments supporting experimental studies in comparison to the athermal or mechanically activated dislocation glide. This has led to deformation process being generally regarded as dominated by thermally activated processes at temperatures above 0 K [1, 38]. However, this has further resulted in a lack of agreement about the type of mechanisms that bring about the deformation, i.e. in terms of the interrelationships between temperature, stress, microstructure and plastic deformation rate.

Thermally and mechanically activated mechanisms of deformation can be described by flow kinetics and structure evolution kinetics respectively [17]. The flow stress is ascribed to be function of the temperature, deformation rate and a parameter that characterises the mechanical structure of the material. The structure parameter corresponds to a certain configuration of dislocation structure and determines the mechanical state of the materials. It differs from the microstructure, which describes the metallurgical state of materials [39]. The history of the material, for instance heat treatment and pre-deformation, can therefore be represented by the structure parameter [40]. Equations describing these flow mechanisms have similar forms and express the strain rate in terms of the frequency factor, the stress raised to some power and a Arrhenius term.

Work has been done on the subject of unified constitutional theory to describe plastic deformation of metals and alloys with each mechanism of deformation [17] this work describes flow or constitutive equations as governed by two kinds of theories called kinetic flow theory and structural evolution law [4, 10, 35, 36, 41, 42] as was mentioned previously.

Kinetic flow theory

Kinetic flow theory refers to the dislocation glide at fixed structure where point obstacles such as dislocation junctions are regularly distributed on slip plane at a given structure or state of the material. For non-steady state of flow, the state variables, i.e. dislocation density change with time or strain rate. The deformation variables for this process are the stress, structure and temperature [43, 44]. The structure parameter corresponds to a certain configuration of dislocation structure and determines the mechanical state of the material.

Thus, we have $\varepsilon = f(\sigma, T, t)$, so that by integration it gives the strain for the loading history as:

$$\varepsilon = f(\sigma_s, T, t) \tag{3}$$

In general, the total strain is the sum of the elastic (ε_e) and plastic (ε_p) components, that is

$$\varepsilon_e = \frac{\sigma_s}{\mu} + \varepsilon_p \tag{4}$$

Thus, in the case where non-steady state or transient flow occurs, the total strain for loading history, rather than the strain rate, is of paramount importance.

In general, equations for thermally activated glide are often expressed by the steady state shear rate $\dot{\varepsilon}$ as a function of the applied shear stress τ normalised with reference to the temperature compensated shear modulus μ, the activation energy ΔG and the absolute temperature *T* in the form generally described by the Arrhenius equation [4]. The equation for thermally activated glide is written as [5, 39]:

$$\dot{\varepsilon} = \nu \left(\frac{\hat{\tau}}{\mu} \right)^2 \exp\left(\frac{-\Delta G}{kT} \right) \tag{5}$$

where the frequency factor, *V* is usually assigned a value of the order 10^{11} s^{-1}, k is the Boltzmann's constant and μ is the temperature compensated shear modulus. Here, the probability term is a function of the applied stress and ΔG is written as [5]:

$$\Delta G = \Delta F\left\{1-\left(\frac{\hat{\sigma}}{\hat{\tau}}\right)^{p}\right\}^{q} \tag{6}$$

where $\hat{\tau}$ is a material constant, being the shear strength without thermal energy, ΔF is the total free energy (activated energy) required to overcome obstacles without the aid of the external stress ΔF depends on the strength of obstacles to flow. For precipitate hardened alloys, where the precipitates are strong obstacles to flow, the activation energy is assumed to be $\Delta F \cong 2\mu b^3$, and for weak obstacles ΔF can be as low as 0.05 μb^3, $\hat{\tau}$ is a term representing average obstacle strength, with *T* and *k* being respectively the absolute temperature and Boltzmann's constant. The constants *p* and *q* represent the average shapes of the flow obstacles, with *p* describing the shape of the tail and *q* the shape of the peak. Values of unity for each of these would represent an array of cylindrical shaped barriers. If ΔF and $\hat{\tau}$ are functions of the degree of work hardening, i.e. functions of the structure of the material then Eq. (5) would be capable of describing non-steady deformation behaviour under constant-applied stress conditions since these quantities may be expected to increase with increasing strain, causing a falling strain rate.

Solute atoms (alloys or impurities) introduce a friction like resistance to slip, caused by interaction of the moving dislocations with stationary weak obstacles, e.g. single atoms in a very dilute solutions, or local concentration fluctuations in more concentrated solutions. A dispersion of strong and stable particles of a second phase, such as low alloy steels (steel containing dispersions of carbides) cause a gliding dislocation to move only by bowing and bypassing them. This gives a contribution to the flow strength which scales as the reciprocal of the particle spacing and which has a high activation energy (Table 1).

Table 1: Characterisation of obstacle strength [5].

Obstacle Strength	ΔF	$\hat{\tau}$	**Examples**
Strong	$2\mu b^3$	$> \mu b / L$	Dispersion; large or strong precipitate (spacing, L)
Medium	$0.2 - 1.0\mu b^3$	$\approx \mu b / L$	Forest dislocation; radiation damage, small or weak precipitate spacing, L
Weak	$< 0.2\mu b^3$	$<< \mu b / L$	Lattice resistance; solution hardening (solute spacing, L)

Combining Eq. (5) and (6), the rate equation for discrete obstacle controlled plasticity can then be written as:

$$\dot{\varepsilon} = \varepsilon_0 \exp\left[\frac{\Delta F}{kT}\left(1 - \frac{\sigma}{\hat{\sigma}}\right)\right] \tag{7}$$

The data for dislocation glide of precipitate hardened alloys, where the precipitates are strong obstacles to flow, is well described by Eq. (7) with a large value of $\Delta F = 2\mu b^3$. This implies an existence of strong obstacles in the material, presumably carbides, and flow stress which when normalised is insensitive to temperature or strain rate [5].

However, for sufficiently worked alloy the yield stress will regain the temperature dependence that characterises forest hardening. However, where thermally activated cross slip occurs, work hardening becomes relaxed leading to lower flow strength. Precipitates may resist dislocation motion according to their fineness. In finely dispersed form, the moving dislocation can cut precipitates. If the density of the particle is high the flow strength will be high (high $\hat{\tau}$) but strongly temperature dependent (low ΔF). Increasing coarseness of precipitate increasingly causes it to behave like a dispersion of strong particles.

Structural evolution law

Structural evolution law represents the way in which the structure changes during deformation. It describes the influence of strain rate and temperature on the rate of change of structure (state). Kinetic flow law does not account for the evolution of the obstacle structure, i.e. $\hat{\tau}$ is assumed to be at constant strength. For point obstacles such as dislocation intersections, $\hat{\tau}$ should be allowed to change in the course of deformation. Structural evolution law describes the way that obstacle strength changes with time. In a simple metal, at least two effects are needed to describe the kinetics of the structure evolution, namely strain hardening and dynamic recovery [10, 27, 34, 42].

STRESS RELAXATION TESTS

Stress relaxation tests (SRT) have been used to analyse plastic deformation processes. SRT are performed by suddenly applying a finite amount of constraint or initial strain to a specimen and then keeping it constant. The initially imposed strain is purely elastic represented by, $\varepsilon_T = \sigma_T / E$ where σ_T is the initial stress and *E* the Young's modulus. As time progresses the elastic strain is replaced by the inelastic strain. At any time *t*, during stress relaxation, the sum of the elastic strain, ε_e , and the inelastic strain, ε_p , is governed by [45]:

$$\varepsilon_T = \varepsilon_e + \varepsilon_p \qquad (8)$$

where ε_T = instantaneous ε_e = elastic strain and ε_p = plastic strain.

There has been increasing interest in the past to use SRT as a means of discriminating between models of thermally activated and mechanically activated strain [27, 43, 46].

Stress rate change tests during creep experiment have been suggested by Kocks et al. [10] and implemented by Alden [28, 30, 31]. To ensure the minimum change obstacle structure, Alden [28] used lead flow as a weight change mechanism in the

Andrade-Chalmers arm type creep test apparatus to record the strain rate discontinuity.

The procedure for a stress relaxation is illustrated in Fig. 5.

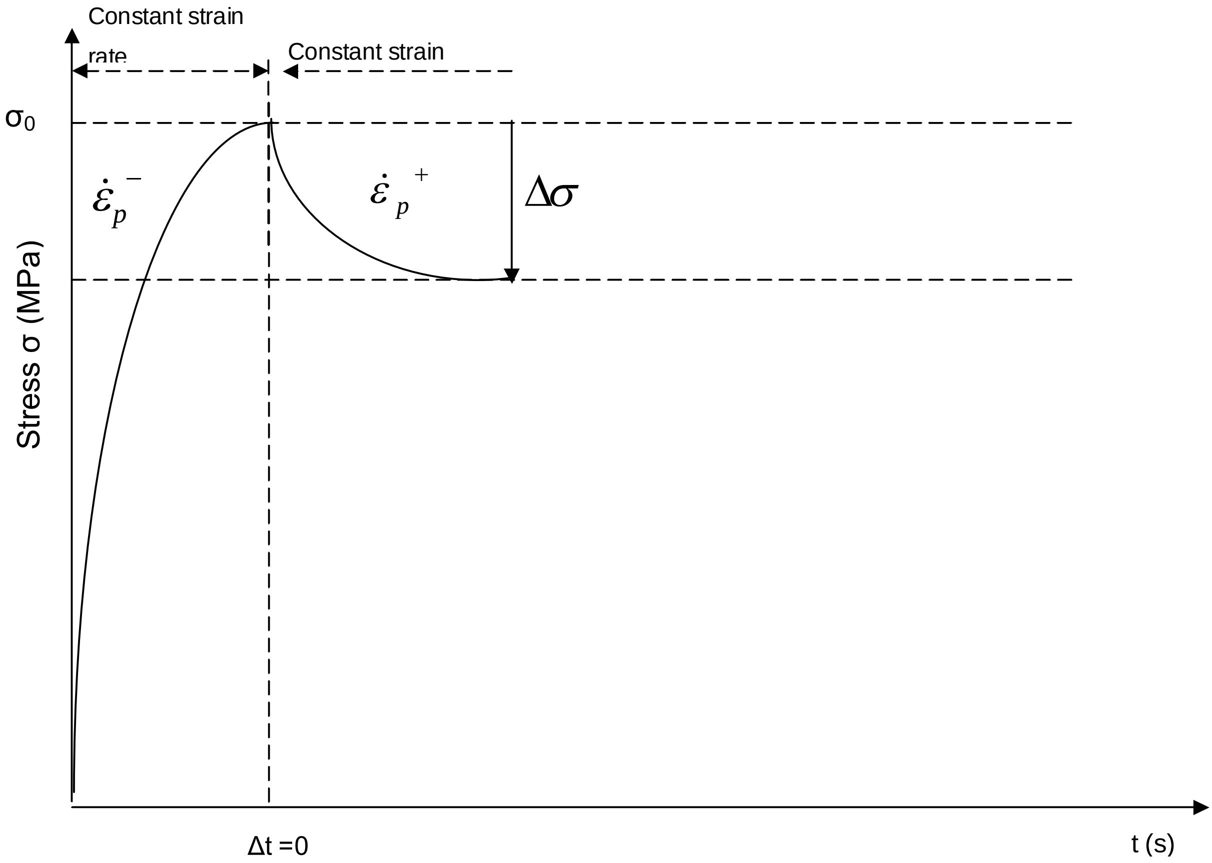

Fig. 5: Schematic diagram of a typical stress rate transient experiment.[47]

While the cross-head is moving $\sigma = \sigma_y$ the yield or flow stress. The test is interrupted and a certain strain kept constant. At time t_o the stress is abruptly changed from $\dot{\sigma}_p^-$ to $\dot{\sigma}_p^+$, Fig. 5. The corresponding inelastic strain rate values, given by, $\dot{\varepsilon}_p^-$ and $\dot{\varepsilon}_p^+$, respectively are extrapolated to check for strain rate continuity, i.e. $\dot{\varepsilon}_p^- = \dot{\varepsilon}_p^+$ [47].

However, because the specimen is experiencing a uniform and homogeneous un-axial deformation in a test machine the relationship between cross-head speed, $\dot{x}$, true plastic strain rate, $\dot{\varepsilon}_p$, and observed true stress, $\dot{\sigma}$, is given to a good approximation by [43]:

$$\frac{\dot{x}}{(1+e_p)L_o} = \dot{\varepsilon}_p + \frac{\dot{\sigma}}{C} \tag{9}$$

In Eq. (9), e_p is the engineering plastic strain, L_o is the initial specimen gauge length. The term C is a combined specimen/ machine modulus defined as

$$\frac{1}{C} = \frac{1}{E} + \frac{1}{M_O(1+e_p)^2} \tag{10}$$

where *E* is Young modulus of the specimen and

$$M_o = K\frac{L_o}{A_o}, \tag{11}$$

A_0 is the initial specimen cross sectional area and *K* is the machine stiffness, which includes elastic effects of the machine, grips and linkage, and specimen elasticity outside the gauge length.

The stress relaxation process starts when the cross-head motion stops, i.e. $\dot{x} = 0$. Therefore, during relaxation

$$\dot{\varepsilon}_p = -\frac{\dot{\sigma}}{C} \tag{12}$$

Eq. (12) allows for determination of the plastic strain rate at time *t*, by measuring the slope of the relaxation curve.

The results from such tests have mostly been presented in terms of a strain rate ratio $\dot{\varepsilon}_p^{\,+}/\dot{\varepsilon}_p^{\,-}$ where $\dot{\varepsilon}_p^{\,+}$ and $\dot{\varepsilon}_p^{\,-}$ are used to indicate respectively the plastic strain rates immediately after, and before stopping the cross-head Fig. 5.

STRAIN RATE CONTINUITY EQUATION

Based on the analyses above strain rate continuity during SRT would then be represented by the ratio as given in Eq. (13):

$$R = \frac{\dot{\varepsilon}_p{}^{+}}{\dot{\varepsilon}_p{}^{-}} = 1 \qquad (13)$$

The results of Eq. (7), indicate that dislocation glide occurs only by thermal activation, i.e. plastic strain rate is continuous. Deformation variables for this process are stress, structure and temperature as was mentioned previously [43, 48]. Specification of these variables will permit, in principle, a calculation of stress at any instant time.

ATHERMAL ACTIVATION

The athermal stress describes the long range kinetic hardening associated with athermal obstacles. Thus for athermal slip the rate of deformation depends not only on stress, temperature and microstructure, but also on the rate of increase of the applied stress [27].

This theory is characterised by a sudden strain rate drop when the stress rate is lowered to zero. The theory has been described theoretically [33, 49, 50] and investigated experimentally [29, 43, 48-56], but was ignored in the development of plastic deformation process. Its proponents have proposed that an exclusively thermal activation model is not a complete representation of plastic flow in metals and that flow past “athermal” obstacles must also be considered [27, 31, 56]. Besides the resolved shear stress and the thermal energy, the applied shear stress should also be included in the analysis for overcoming obstacle barriers.

In one of his seminal papers Alden [28] observed the sudden abrupt decrease in the strain rate during the inelastic extension of α-brass [28]. The decrease he asserted was related to the loss of the athermal component of the strain rate, activated by stress and stress rate. The results were interpreted thus that the strain rate equation contained stress rate as an explicit deformation variable besides those of stress and structure [29].

$$\dot{\varepsilon} = \dot{\varepsilon}(\dot{\sigma}, \sigma, structure) \tag{14}$$

Alden's results suggested that stress rate should be included as a parameter in the expressions describing inelastic deformation, Eq. (14). In athermal theory, the stress rate is not a deformation variable, but merely indicative of structure change in response to strain by strain hardening [31].

The mechanical contribution is a function of stress rate before halting cross-head and is represented by [31]:

$$\dot{\varepsilon}_a = \frac{\dot{\sigma}}{\theta_a} \tag{15}$$

where, $\theta_a, \dot{\varepsilon}_a$ and $\dot{\sigma}$ are respectively athermal work hardening coefficient, strain rate and axial stress rate. In terms of Eq. (15) strain rate is determined by the rate change of stress and structure as opposed to the current values of stress and structure. Strain hardening is the only limiting factor to the strain rate and not thermal process such as impurity, etc. This equation is not dependent explicitly on time or temperature [29]. The derivation and application of Eq. (15) and the nature of stress rate as a deformation variable, where better understood as a result of theoretical study that was undertaken by Alden [50]. The equation applies to a broader class of metals and alloys given simpler conditions of deformation where stress rate is constant.

Therefore, this dependence of plastic strain rate on the stress rate separates Alden's theory most clearly from the thermal activation theory. Alden exploits this distinction in his experiment to argue for mechanical activation. He reports a plastic strain rate discontinuity resulting from a stress rate change at constant stress and temperature; a discontinuity would not exist for thermally activated flow. The mechanically activated glide could also be illustrated by the following functional relationship that describes the kinetics of deformation of a fixed internal structure [55]:

Mechanical activation

$$\varepsilon = f(\sigma) \tag{16a}$$

$$\dot{\varepsilon} = f(\dot{\sigma}) \tag{16b}$$

Strain rate ratio is given by the expression below, Eq. (17):

$$R = \frac{\dot{\varepsilon}_p{}^{+}}{\dot{\varepsilon}_p{}^{-}} < 1 \tag{17}$$

A strain ratio of less than one in the results signifies athermally activated deformation [48, 53].

Few results are presented showing the athermal contribution as a function of either stress rate or temperature [57]. Using stress rate change experiments conducted on a lever arm creep machine, Alden observed strain rate ratios less than unity for copper, 304 stainless steel and α – brass [28, 31]. These observations were also reported by Abe et al [46]. Alden proposed the discontinuity as evidence of mechanically activated deformation theory. In their investigation on OFE Copper, Dunham and Gibeling [47] also found that the results for room temperature stress rate change shows apparent strain rate discontinuity.

Other material where athermal deformation was evidenced include aluminium and iron, solid solution alloys, and precipitation hardened alloy and copper containing 2% cobalt" [27, 31, 43, 48, 53]. These results were also interpreted as evidence for a mechanically activated glide.

However, the existence of such mechanically activated deformation components of flow has been disputed [8, 35, 38, 57, 58]. These mechanically activated observations were subsequently shown to be experimental artefacts caused by insufficient resolution, low stress rate and slow data acquisition, which prevented the detection of dislocation glide [36, 38, 43, 47, 54, 59]. Additionally, some of the previous experiments where athermal deformation is proposed were conducted on various materials using “soft” load controlled machines with higher strain-time resolution [28, 30]. Therefore, the results for 304 stainless steel could not be successfully reproduced using other high resolution methods [41].

Using fluid dynamics concepts, thermally activated kinetic flow theory with structural evolution law numerical methods, Kuo et al [59] could simulate the very abrupt changes in the strain rate that occurs without calling on mechanically activated theory. In the deformation of copper the discontinuity was interpreted in terms of processes involving work hardening giving raise to a component of strain rate which was separated from a component caused by recovery [1].

In another study, Gibeling and Alden [38] reported the results of experiments on Al-Mg, LiF, Interstitial free iron and type 304 stainless steel in which strain rate continuity was detected. They conclude that dislocation motion occurs with the aid of thermal activation for these materials. The mechanical activation of dislocation glide was not detected, even in the range of temperatures for which the yield strength of aluminium exhibited an “athermal” plateau [38]. These evidence disputes further the existence of such a mechanically activated deformation component of flow.

Holbrook et al [43] demonstrated thermal activated deformation by conducting precise relaxation tests at room temperature that deformation of pure Al and Fe is glide controlled. At high temperature, deformation of pure Al and other deformation characteristics of fcc and bcc pure metals are well explained by the recovery controlled process [60]. These studies seem to have caused many investigators to question the validity of athermal deformation processes. Gibeling et al [44] further critically analysed results of strain rate change test performed by Yoshinaga et al [52] and found that their results could be explained by the glide controlled process as well when effects of experimental errors involved in the tests were eliminated. Previous experimental evidence suggests that continuous glide is not observed in fcc metals up to rates of 104 s^{-1} [61].

It is generally desirable to carry out SRT at different temperatures and strain rates to determine material parameters to use in kinetic equations describing deformation. These were then used with the kinetic equation to determine deformation curves. Rather than presenting the results from stress rate tests using Eq. (17) results are shown in the form: $\dot{\varepsilon}_a (= \dot{\varepsilon}_p^- - \dot{\varepsilon}_p^+)$.

EXPERIMENTAL PROCEDURE AND DATA PROCESSING

Materials

The material used was low alloy steel, 709M90, with chemical analysis shown in Table 2.

Table 2: Chemical analysis of 709M40 steel, wt-%

C	Si	Mn	Cr	Mo	Fe
0.39	0.23	0.77	0.96	0.28	Bal

The material was machined into threaded end specimens having a gauge length of 50 mm and a diameter of 5 mm, Fig. 6.

Fig. 6: Machined low alloy steel, 709M90 specimen

The specimens were received in the quenched and tempered condition and were tested as received.

Method

Stress Relaxation Tests

Determination of Deformation Mechanisms

SRT was carried out on a screw-driven machine (JJ Lloyd L2000R, research grade), of maximum capacity of 30kN which was operated in displacement mode Fig. 7.

Fig. 7: Lloyd machine with auxiliary components including a desktop computer and a control panel

All specimens were tested in fixtures suspended from the top of the cross-head. These fixtures allow experiments to be done at room temperature or surrounded by a furnace for elevated temperature tests. In this study, a set of tests was carried out at a displacement rate corresponding to an initial strain rate of $2\times10^{-3}s^{-1}$ at five temperatures in the range 11°C to 590°C. Allowances for machine stiffness and temperature dependent modulus effects were made (appendix A). The procedure used is illustrated in Fig. 8.

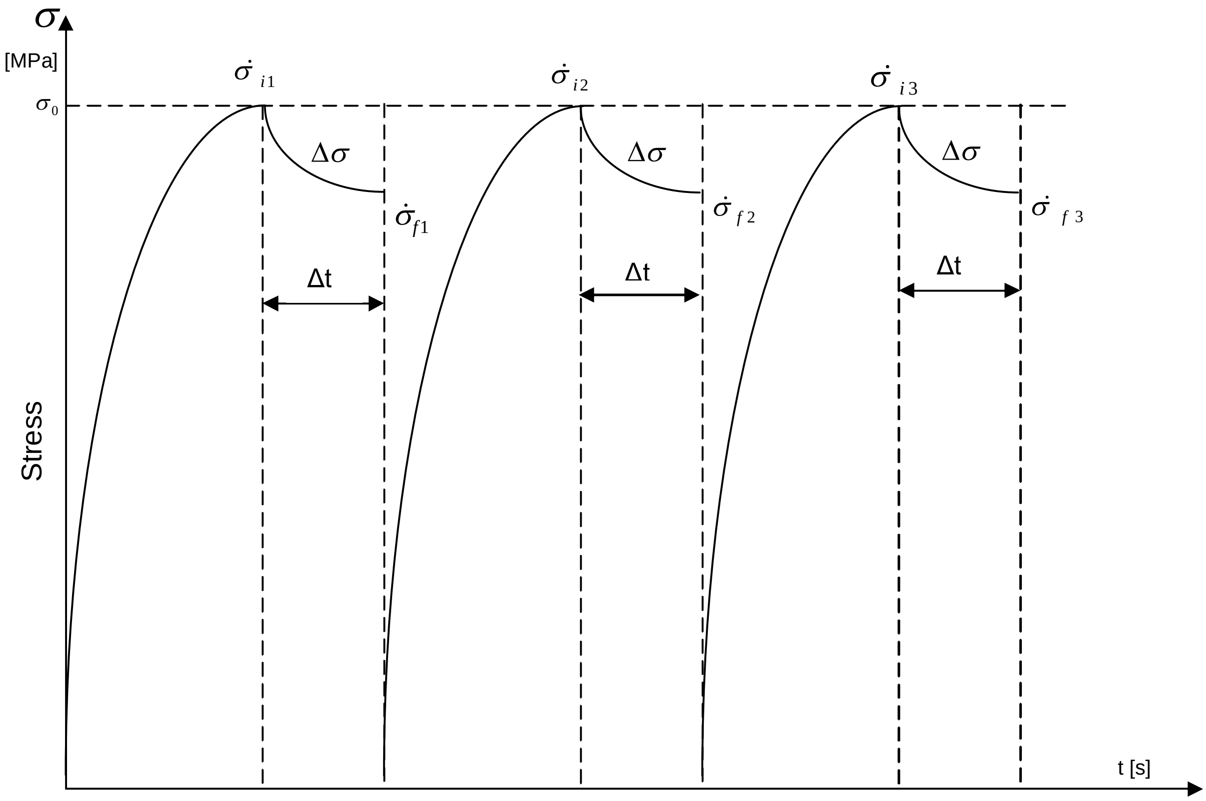

Fig. 8: The procedure of successive stress relaxations (schematics), adapted from [58].

The cross-head was halted at intervals during each test and the relaxation behaviour recorded for 5s at the data capture rate of 12.5 Hz before continuing with loading. Each test was interrupted at intervals with the relaxation times being scaled as displacement rate such that approximately the same number of data points was collected for each relaxation period. The first relaxation starts at stress σ_0, over time interval *Δt*, with a corresponding stress decrease $\Delta\sigma_1$, Fig. 8 The specimen is then unloaded to zero and reloaded to σ_0, fast enough to obtain quasi-elastic conditions. It is then allowed to relax by an amount $\Delta\sigma_2$ during Δt, and then reloaded to σ_0, etc. As a rule, a series consists of 4-5 relaxations tests of 5s each.

Since the relaxation data was collected for 5 seconds, the temperature control was not a critical problem. During each test of 4-5 relaxations temperature was kept constant to approximately 0.5K. All room temperature tests were done in air. To record data with sufficient resolution to permit accurate determinations of plastic strain rates, a computer based data acquisition system was used. Data from the experiments was obtained automatically with the aid of the integrated desktop computer using the appropriate programs.

During relaxation, measurements of stress as a function of time can be used to determine curves of stress decrements, $(\Delta\sigma)$ against stress rate $\dot{\sigma}$ as $\log(-\dot{\sigma})$ [1, 45, 62]. Such curves tend to be linear and the slope can be used to calculate the strain rate sensitivity to stress via machine and specimen stiffness parameters [1]. Linearity is achieved soon after the commencement of relaxation and by extrapolating curves to zero stress rate, $(\Delta\sigma)$, strain rate value at the commencement of relaxation may be estimated [62].

Using a range of deformation temperatures strain rate sensitivity and activation volume of low alloy steel was explored. Using SRT, an apparent activation volume *ΔV* was obtained from the following equation:

$$V = \frac{\sqrt{3}kT\ln(\dot{\varepsilon}_2/\dot{\varepsilon}_1)}{\Delta\sigma} \tag{20}$$

where σ is the flow stress and $\dot{\varepsilon}$ is the strain rate. These two parameters are known as signatures of the deformation (dislocation) mechanism.

Tensile tests

Stress vs. strain curves obtained from tensile tests carried out using a computer integrated Lloyd machine as shown in Fig. 7. The purpose of these tests was to determine the material–machine stiffness at different temperatures that were compared with the temperature compensated Young's modulus, μ.

Thermocouples

Temperature was measured by a thermocouple, which was inserted through the asbestos seal of the furnace. This enabled the accurate finding of the temperature in the furnace.

RESULTS AND DISCUSSION

A typical stress-strain curve conducted by standard tensile test is shown in Fig. 9.

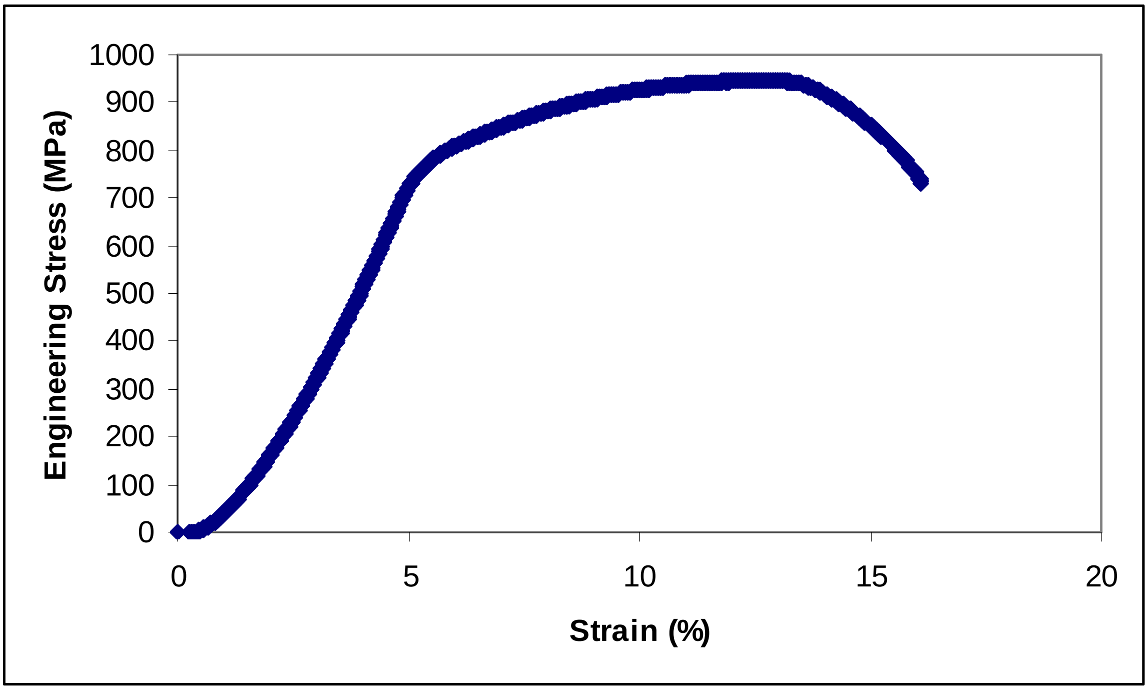

Fig. 9: Tensile stress-strain curve of the low Alloy Steel at 500^{0}C

Standard tensile tests show Young's modulus μ, yield strength and ultimate tensile strength of 143 GPa 763 MPa, 930 MPa respectively for the low alloy steel. The measured Young's modulus value is much less than the theoretical value due to machine stiffness and the effect of temperature on the strength of the material.

Typical stress – time curves obtained for stress relaxations tests in low alloy steel are illustrated in Fig. 10.

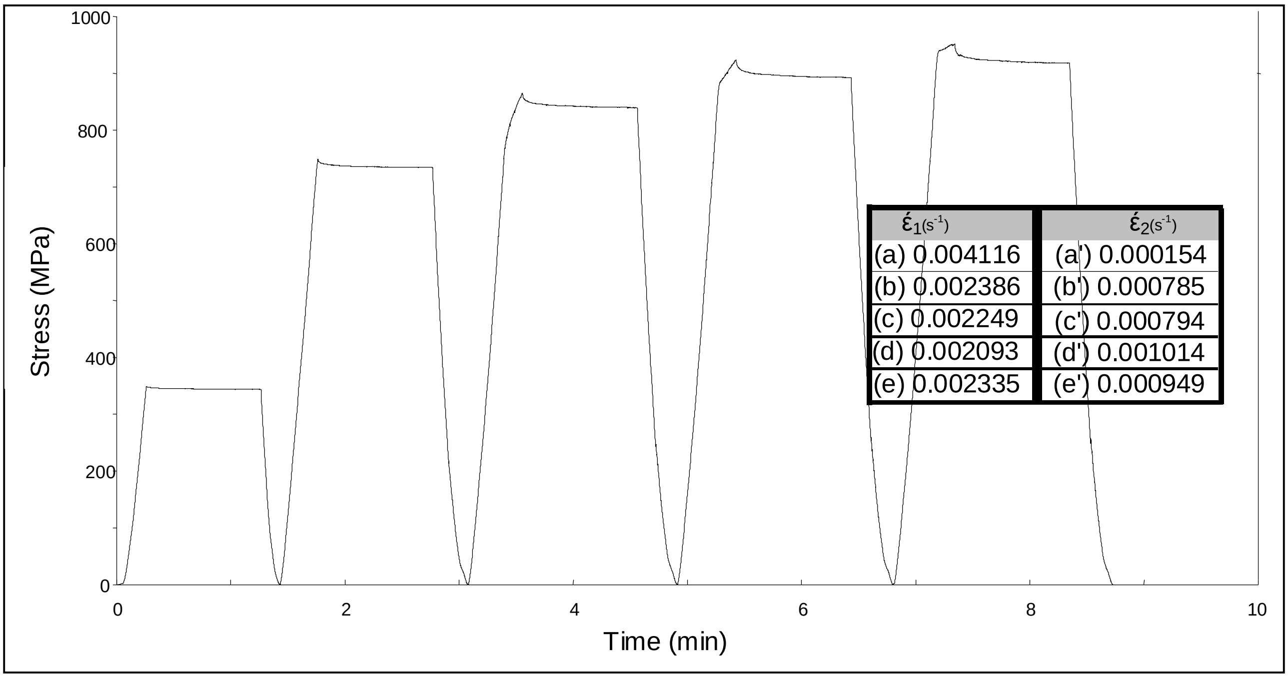

Fig. 10: Succession of five relaxations in low alloy steel. T = 15^0 C 347,742,858,921, 944 MPa respectively.

The relaxation behaviour of low alloy steel suggests activity of diffusion mechanisms, which have an effect of slowing down mobile dislocation under certain conditions, Fig. 10.

Relaxation rates were obtained from data at a temperature of 15°C and displacement rate corresponding to an initial strain rate of 2 x $10^{-3}s^{-1}$, in Fig. 10. Multiple points at the same stress were obtained due to limited stress resolution of around 0.125 MPa especially at longer times, Fig 11.

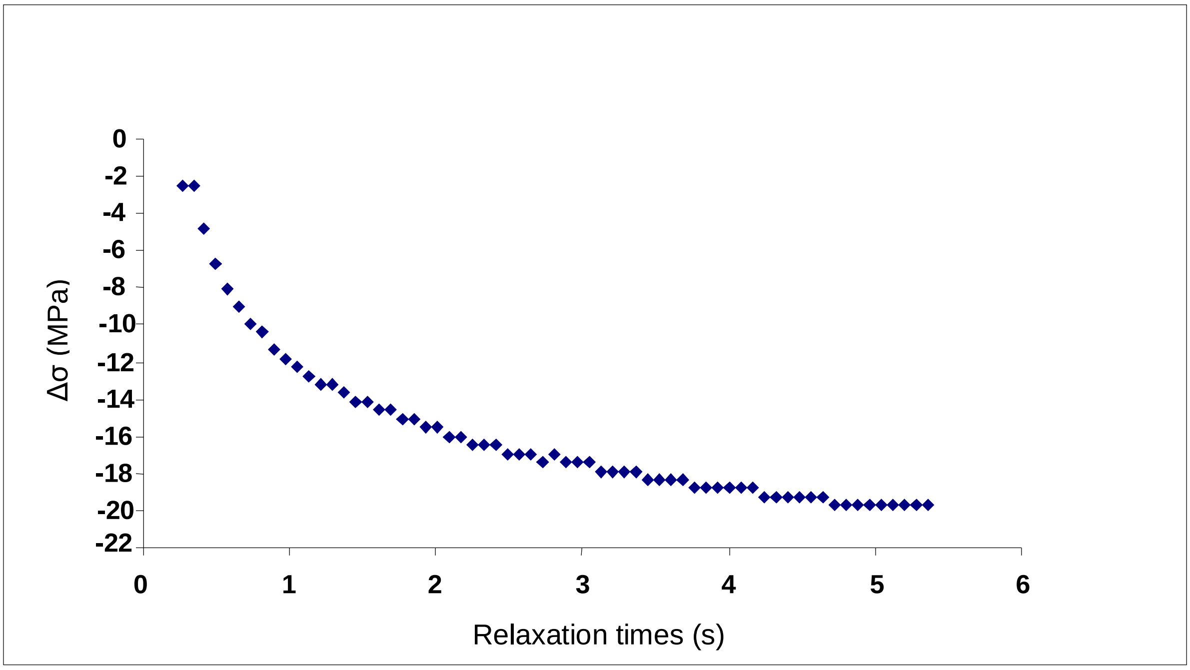

Fig. 11: Relaxation data from a test at 15 °C and an initial tensile strain rate of 2 x 10^{-3} s^{-1}.

These equal stress points were then time averaged to give a single time point to obtain relaxation curves such as shown in Fig. 12 below:

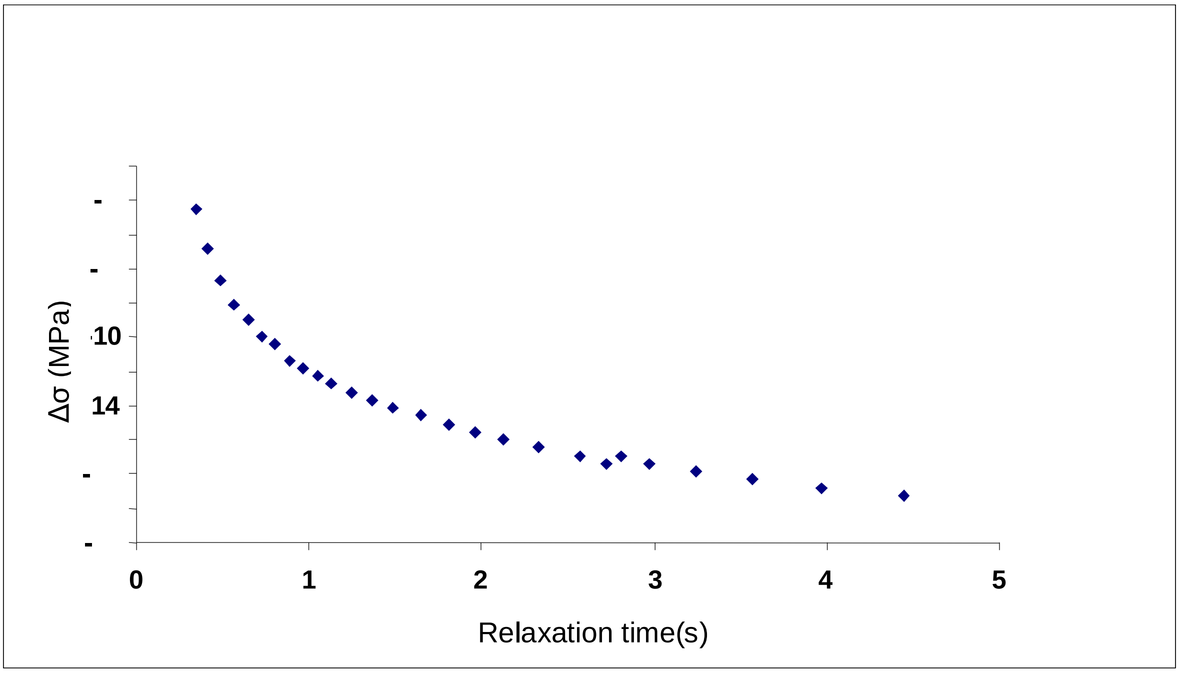

Fig. 12: Data from Fig.11, in which multiple points at the same stress have been time averaged

The slopes of these curves were then determined and data re-plotted as log (-$\dot{\sigma}$) versus $\Delta\sigma$ as shown in Fig. 13.

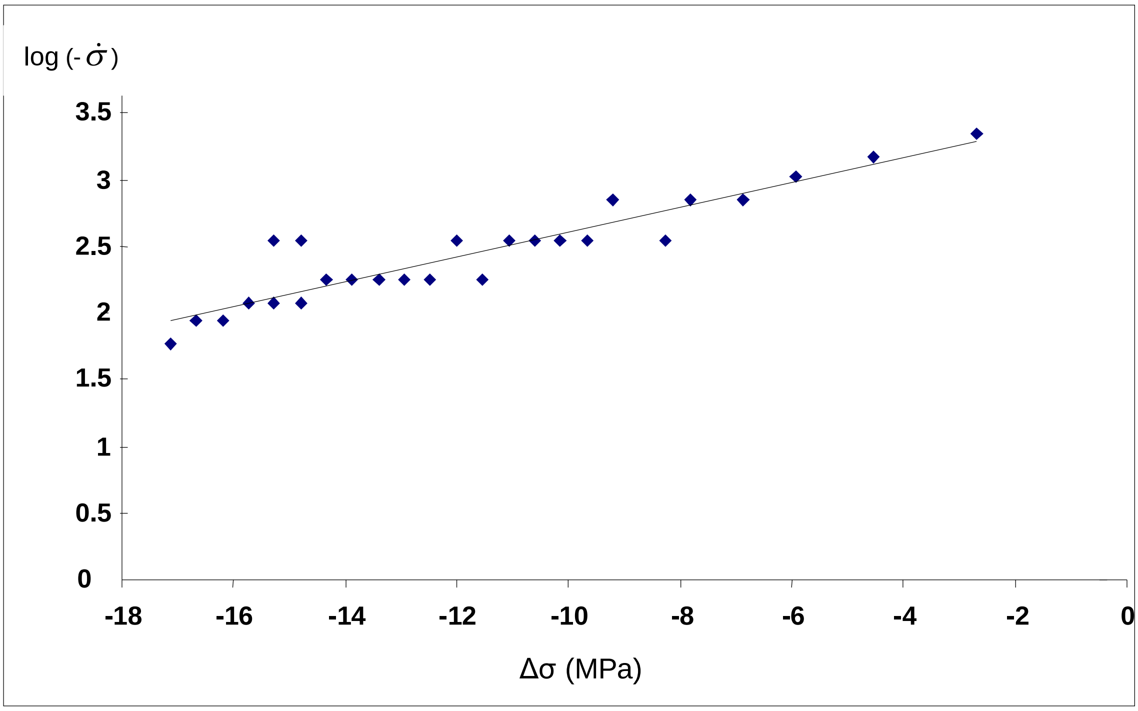

Fig. 13: Graph log ($-\dot{\sigma}$) vs. $\Delta\sigma$ calculated from Fig. 12 above.

The curves were found to be relatively linear within experimental scatter and were extrapolated to zero stress recovery to obtain values for stress rates at unloading stresses. The linearity that was observed in Fig.12; i.e. the Graph of log ($-\dot{\sigma}$) vs. $\Delta\sigma$, suggests that during relaxation, a constant mode of deformation is established rapidly after a short-lived transient which in most part is not detectable in the present tests [1].

Since stress levels were beyond the yield stress, inelastic true strains and true stresses were employed. This was done by first considering the total engineering strain, e_{tot} and elastic engineering strain, $e_e = \sigma/E$, where σ is the engineering stress and *E* the Young's modulus.

Then the inelastic engineering strain is given as:

$$e_P = e_{tot} - \frac{\sigma_e}{E} \tag{18}$$

During plastic deformation, the total volume was assumed to be conserved since the plastic strain due to stress relaxation is small, i.e. < 0.1%; stress relaxation takes place at a constant structure [63], so that true stress and inelastic true strain were, respectively, defined as following:

$$\sigma_t = \sigma_e(1 + e_P) \tag{19}$$

$$\varepsilon_P = \ln(1 + e_P) \tag{20}$$

Experimental data was then converted to true stress, strains, and strain rates immediately before and after the onset of relaxation (appendix B). These results are shown in Table 2. Strain rate immediately before and after the onset of relaxation were determined from the machine – specimen stiffness which was measured by partially unloading specimens following relaxation periods and then measuring the slope of force – displacement curves prior to the onset of yield during re-loading [1]. The relaxation periods were normalised with respect to the temperature compensated Young's modulus, (μ), of the material. A sample calculation for μ for different temperature measurements is given in appendix A. The calculated values are given in Table 3.

Table 3: Temperature compensated Young's modulus of low alloy steel

Temperature (K)	Temperature compensated Young's modulus (μ) (GPa)
288	217,561
373	206,504
673	167,473
773	154.456
863	142.741

In Table 2, it is noted that the Young's modulus is temperature dependent, i.e. it decreases with increasing temperature.

The linearity of the log $(-\dot{\sigma})$ vs. $\Delta\sigma$ curves suggests that, during relaxation, a constant mode of deformation is rapidly established after short-lived transients which for the most part were not detectable at the resolution of the present tests. Such transients have produced apparent strain rate ratios of unity as measured in some previous investigations on the "instantaneous" rate changes [34-36, 43, 44, 47, 53, 55]. Plastic strain rate immediately before halting the cross–head were determined from the total strain rate measured from specimen deformation rate curves from which contributions due to elastic strain rates were subtracted. Results obtained, are shown in Table 4 for specimen tested at the same displacement rate and different temperatures.

Table 4: Experimental results at different temperatures and a displacement rate corresponding to an initial strain rate of $2\times10^{-3}\text{s}^{-1}$.

Temperature (K)	Normalised interrupt stress $(x10^5)$	Plastic strain rate before $(\dot{\varepsilon}_p^- x10^5)$	Plastic strain rate after $(\dot{\varepsilon}_p^+ x10^5)$	Strain rate ratios (K)	Plastic strain rate difference $(\dot{\varepsilon}_p^- - \dot{\varepsilon}_p^+)x10^5)$
288	250	248	15	0.1	251
	384	778	67.7	0.1	717
	417	247	60.4	0.24	194
	437	225	74.5	0.33	157
	443	209	125	0.6	92
	374	267	88.4	0.33	179
	371	237	129	0.55	108
	438	216	118	0.55	98
373	694	574	16	0.1	552
	816	267	48	0.22	188
	860	231	62	0.3	207
	894	217	107	0.5	160
	934	207	64	0.3	138
	948	212	43	0.16	98.6
	948	215	57	0.25	145
473	364	205	78.5	0.33	85
	354	205	123	0.6	82
	422	216	53	0.25	163
	453	201	94	0.47	107
	477	330	109	0.33	221

Temperature (K)	Normalised interrupt stress $(x10^5)$	Plastic strain rate before $(\dot{\varepsilon}_p^- x10^5)$	Plastic strain rate after $(\dot{\varepsilon}_p^+ x10^5)$	Strain rate ratios (K)	Plastic strain rate difference $(\dot{\varepsilon}_p^- - \dot{\varepsilon}_p^+)x10^5)$
	752	216	79	0.35	171
	837	202	101	0.48	117
	884	866	95	0.41	814
673	166	206	111	0.54	95
	412	338	85	0.25	253
	436	228	124	0.54	104
	491	209	114	0.54	95
	500	207	108	0.52	99
773	378	116	77	0.33	109
	470	208	123	0.55	310
	471	214	135	0.66	335
	475	205	103	0.5	351
	497	204.5	146	0.71	336
873	265	116	73	0.1	43
	279	211	124	0.59	87
	364	229	111	0.48	118
	356	218	125	0.57	93
	339	208	132	0.63	76
	326	221	134	0.6	87
	329.3	214	124	0.58	90
	300.7	209	106	0.51	103

Plastic strain rates immediately prior to relaxation, $\dot{\varepsilon}_p^-$, and the onset rates minus the extrapolated relaxation rates $(\dot{\varepsilon}_p^- - \dot{\varepsilon}_p^+)$ are displayed in Table 4. The extrapolated strain rates associated with relaxation for all the tests was less than that associated with the rate prior to halting the cross-head. Comparison of plastic strain rates before and after stopping the cross-head, are also shown in Table 4. Strain rate ratios, $(\dot{\varepsilon}_p^+ / \dot{\varepsilon}_p^-)$ were found to lie in the range 0.1-0.71; values which are not dissimilar to the results obtained when “instantaneous” measurements of the relaxation strain rate were reported [27, 28, 30]. See details in Appendix C.

In prior studies where the calculated strain ratios were low, i.e. R < 1, it was concluded that probably the equations using the deformation variables stress and structure to describe the industrial cold working of brass could be correct [28]. This implies that the strain rate sensitivity of stress is negative and discontinuity in the plastic strain rate is observed. These studies were carried by Alden [27, 28, 31, 50, 64] and Oikawa et al [64], and corroborated by Yoshinaga and co-workers [46, 52]. They were, however, in disagreement with prior study by Holbrook et al [43] at room temperature. In a recent study, such low values were also observed [57]. It seems difficult to believe that the observed effect is purely because of athermal activation. Unless one is dealing with short transients, it may be of significance to compare deformation before stopping the cross-head with that established later during relaxation [1].

On re-loading after recovery, it was generally found that the yield stress was less than that at which the cross-head was stopped. This difference varied from less than 1MPa at low lower stresses to about 10 MPa at higher stresses, which indicates that a degree of softening, even during the short 5s recovery periods used for most tests had occurred. These relaxation strain rates were associated primarily with recovery processes [1]. This is assumed in the case in present study as well. Due to complex structures of carbides precipitates and dislocation tangles recovery is attributed both to carbide growth and to tangled dislocations re-arrangement and annihilation.

Higher deformation rates, during loading of the specimen, can probably be related primarily to simultaneous hardening and recovery; represented by the rate derived from extrapolating log $(-\dot{\sigma})$ vs. $\Delta\sigma$ curves [1]. The hardening component is thus identified as the difference between the strain rate before the cross-head is stopped and the recovery rate established during relaxation.

Furthermore, repeated stress relaxation experiments provide some insight into the phenomena of strain hardening. All experiments of this type presented so far are related to positive strain hardening coefficients. A closer analysis of the hardening component suggested that there is a poor correlation between strain rate and stress rate signifying that this deformation is probably not mechanically activated.

Rather, the hardening component of the strain rate was then analysed in terms of thermally activated glide using Eq. (7). This equation was re-arranged to calculate material hardness parameters in the form of a (0K) flow stress $\hat{\sigma}$ to:

$$\hat{\sigma} = \frac{\sigma}{\left[1-\left(kT/\Delta F\right)\ln\left(\dot{\varepsilon}_0/\dot{\varepsilon}\right)\right]} \qquad (21)$$

where values of ΔF and $\dot{\varepsilon}_0$ were taken from the literature [1] as $\Delta F = 2\mu_0 b^3$, μ_0 being the shear modulus of elasticity at 300K and 5.77 x 10^5 s^{-1} respectively.

Strain values, ε_h , due to the hardening component of the strain rates were estimated by multiplying the hardening strain rate by the time interval during which the specimen was being plastically strained in the loading phase. The strain increment was then added to the running total from previous straining cycles [1].

Flow stress-hardening curves could then be constructed as shown in Fig. 14.

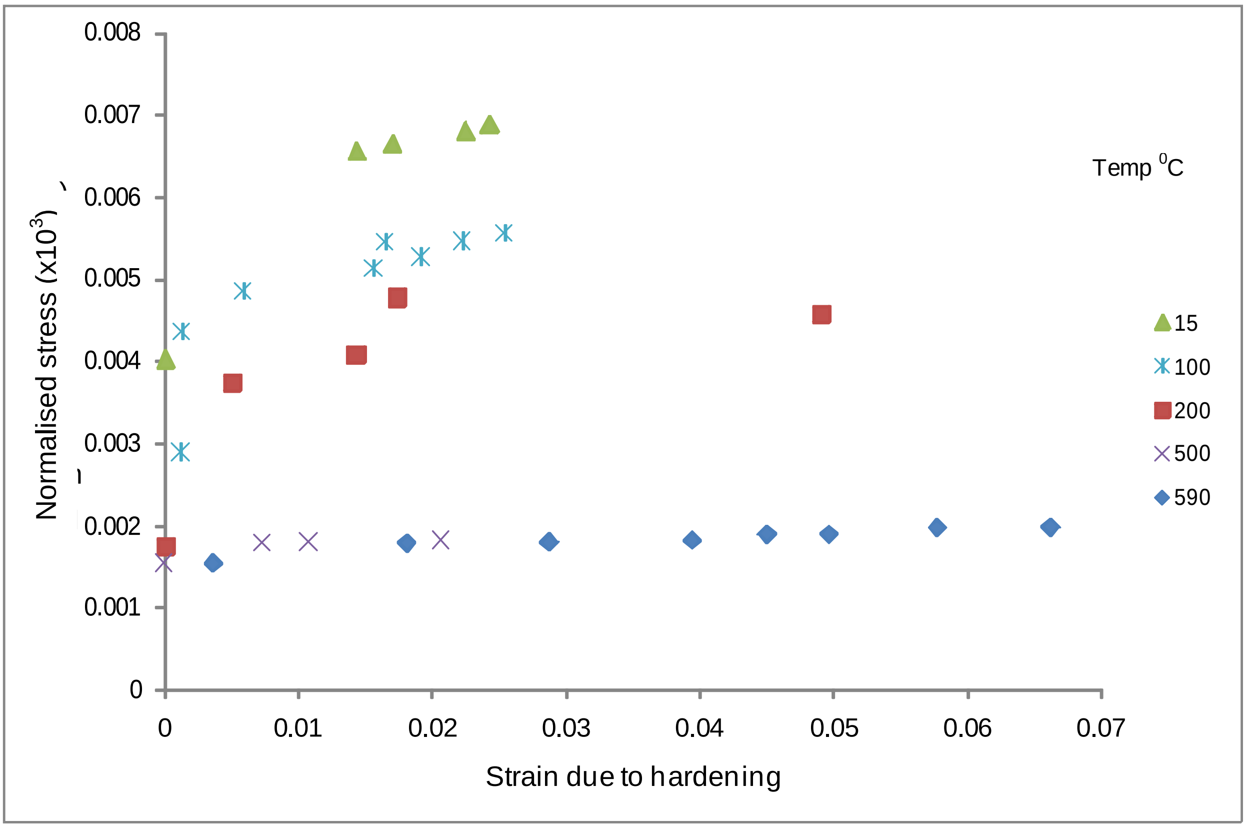

Fig. 14: Stress vs. the component of strain associated with hardening at different temperatures at initial strain rate of 2×10^{-3}s^{-1}.

Fig. 14 shows curves of the applied stress against hardening strain for tests at an initial rate of 2 x 10^{-3} s^{-1} and at different temperatures as derived from the results in Table 2. The applied stresses have been normalised with the temperature compensated Young's modulus of the material. The curves appear to follow parabolic curve profile as was previously noted in another study [1].

It is further observed that the slopes of the different flow stress decrease with increasing temperature. Temperature seems to have a significant effect on the flow stress of the material. This concurs with the results found in a previous study on the effects of temperature and strain rate in the dynamic flow behaviour of different steels [65]. It seems that as temperature of the material increase; dislocation movement occurs more readily; hence the resistance of the material to deformation decreases. The decreasing slope with an increase in stress could possibly be due to temperature and rate sensitivity. This is due to increasing dominance of recovery as the dislocation density increase. This decrease in slope was also observed in a prior study conducted on copper [1].

Fig. 15 shows curves of flow stress against hardening strain for tests at an initial rate of 2 x 10^{-3} s^{-1}

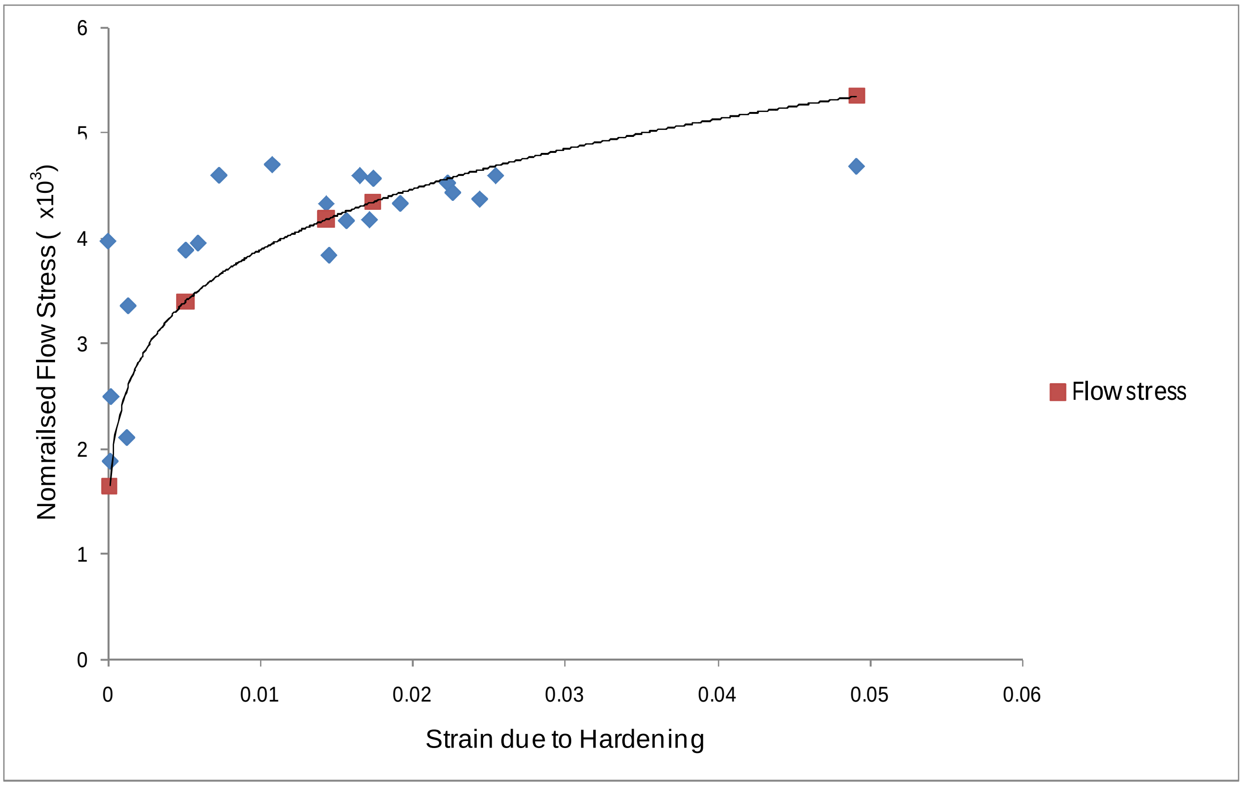

Fig. 15: Shown are values of flow stress determined from Eq. (21). The solid curve is plotted from Eq. (22).Flow stress vs. hardening strain. Results follow the same curve as in Fig 13.

The applied stresses have been normalised with the temperature compensated Young's modulus of the material. It is observed that the flow stress is larger than the applied stress because of the term (1 – kT) in Eq. (21). Results appear to lie close to a single parabolic curve represented by the solid line in Fig.14, which is described by:

$$\hat{\sigma} \Big/ E = A\varepsilon_h^{0.2} \tag{22}$$

where the constant A has a value of 9.78 x10^{-3}.

This is consistent with older theories where stress-strain curves found to be parabolic with little or no contribution from athermal activation [66, 67]. The value of A is close to that expected from such theories [1, 68].

In Fig. 15, the parabola does not begin at zero, but at approximately 1.7x10^3 normalised flow stress. The effects of the carbide precipitates could be the cause of this in the material. These precipitates cause obstacle fields resisting dislocation motion thus preventing the flow stress from being initiated from zero in the material.

Furthermore, the material seems to have regained its temperature dependence due to it being a sufficiently worked alloy. This phenomenon characterises forest hardening of the material. The density of the particles seems to be high, resulting in high flow strength (high τ).

In Fig. 16, flow stress vs. components of strain associated with hardening at different temperatures is plotted.

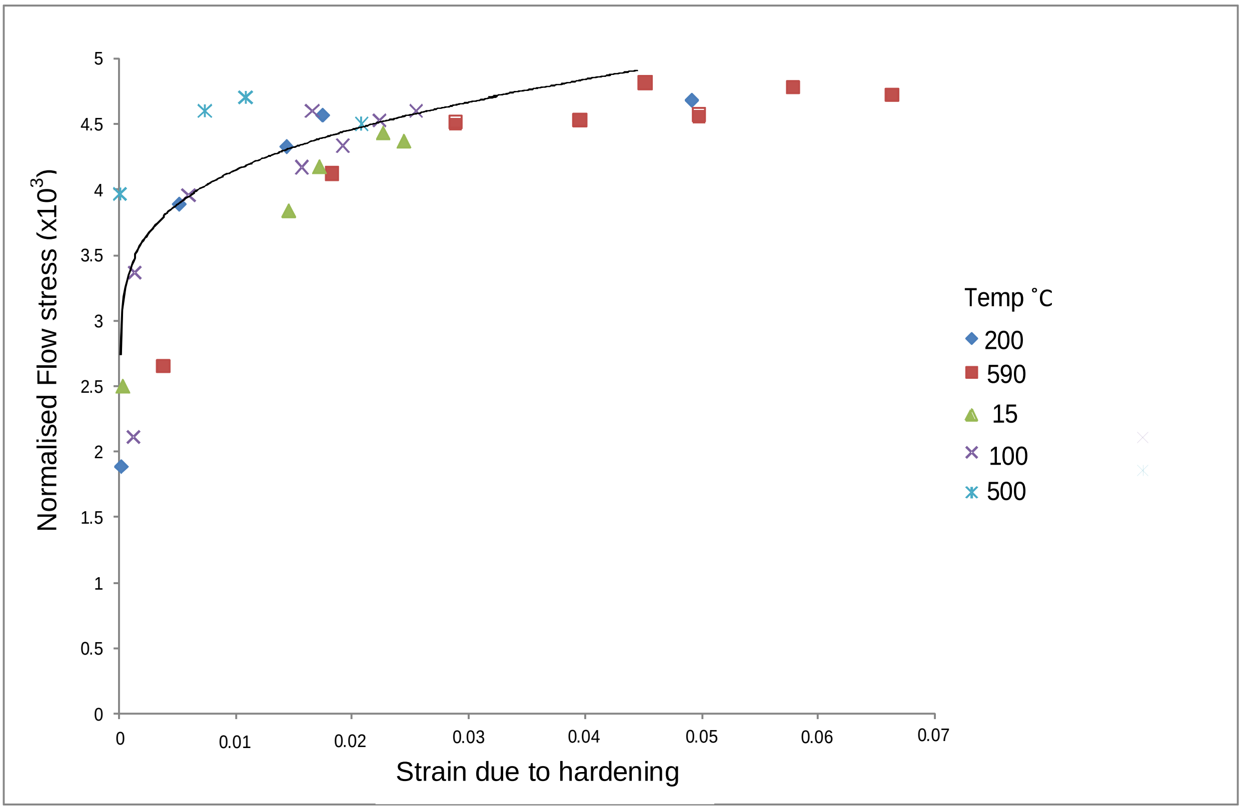

Fig. 16: Stress vs. the component of strain associated with hardening at different temperatures

In previous studies on creep behaviour of copper [37] and work hardening characteristics of copper from constant strain rate and stress relaxation testing [1] hardening curves similar to Fig. 16 were found [28].

The relationship of Eq. (7) suggests that curves of strain rate on log axis against applied stress should be linear. Curves for shear strain rate vs. normalised shear stress plotted in Fig. 17.

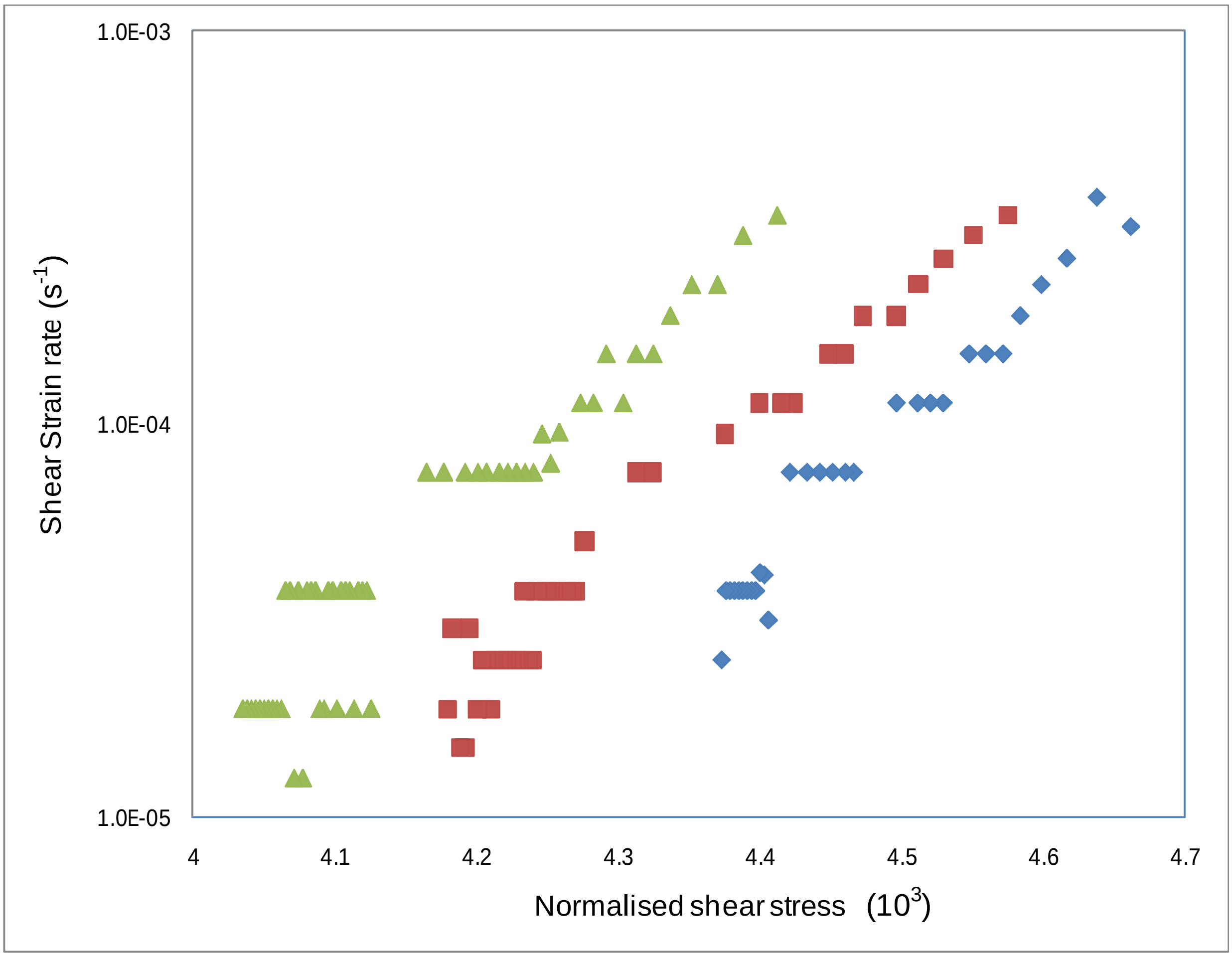

Fig. 17 Plastic strain rate – normalise stress rate curves determined from relaxation curves at a temperature of 500˚C. The relaxation after the loading increment was 5s.

Curve linearity is evidenced at least during the earlier stages of relaxation. Based on the established theory, the results should converge towards an intercept on the stress axis of $\log(\dot{\gamma}_0) - 0.435\Delta F / kT$, and have the slope of $\Delta F / \hat{\tau} kT$.

Relaxation curves were analysed in this way and although showing some scatter, intercept values were generally within +/-10% of the average value for a particular temperature. Fig. 18 shows average values of log ($\dot{\gamma}_0$) plotted against 1/*T*.

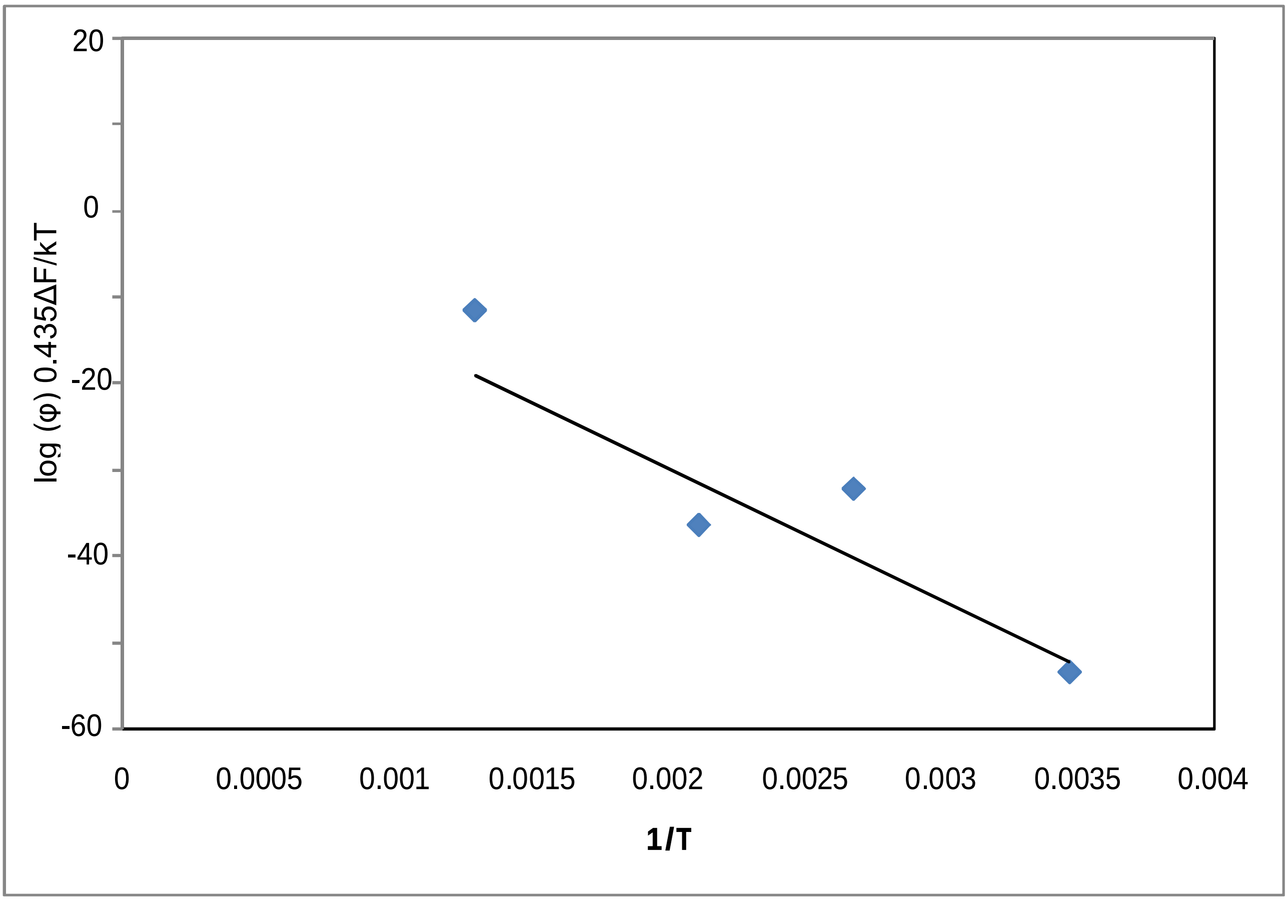

Fig. 18 Average values of $\log(\dot{\gamma}_0) - 0.435\Delta F / kT$ plotted against 1/T obtained with reference to Eq. (21), after the conversion stresses and strain rates to shear stresses and shear strain rate and using sets of relaxation curves from tests at temperatures ranging from 15- 590^0 C.

The solid line corresponds to a value for $\dot{\gamma}_0$ of 10^6 s^{-1} and for $\log(\dot{\gamma}_0) - 0.435\Delta F / kT$ of 124113 K^{-1} corresponding to a non-dimensionalised value of 2.3μb^3 as compared to a previously published value of 2μb^3 [5]. The low alloy steel is thus a precipitate hardened alloy as its activation energy corresponds to the activation energy of 2μb^3. This suggests existence of strong obstacles in the material, presumably carbides, and flow stress which when normalised is insensitive to temperature or strain rate.

In a recent study on a comparison between steady state creep and stress relaxation in copper, curves similar to the ones observed above could be determined [57]. In that study, it was observed that significant deviations from linearity corresponded to relaxation times of about 500 seconds (appendix D). In the current study, particular set of curves, for tests at lower temperatures, deviations from linearity occurred at longer times, at higher temperatures. It is deduced that the probable cause of such deviations is time dependent recovery of the work hardened structure. Evidence for this was obtained from recording the yield stresses on re-loading specimens following relaxation periods [57].

CONCLUSIONS AND RECOMMENDATIONS

Stress relaxation tests were carried out on low alloy steel specimen at different temperatures and strain rates. Strain rates ratios were found to be less than zero, i.e. discontinuity after commencement of relaxation periods was observed. The discontinuity was interpreted in terms of processes involving work hardening causing a component of strain rate, which could be isolated from a strain rate component caused by recovery. Comparable to previous studies, it was found that both components occurred during the constant rate testing with only recovery portion during stress relaxation.

Recovery is caused by complex structures of carbides precipitates while dislocation tangles recovery is attributed both to carbide growth and to tangled dislocations re-arrangement and annihilation. Therefore, creep of low alloy ferrite steel is recovery controlled. In a pure metal, two types of point defects are possible, namely a vacant atomic site or vacancy, and an interstitial atom [5]. The result obtained is inconsistent with glide control processes.

The material used in this study is thus a precipitate hardened alloy as its activation energy approximates $2\mu b^3$. This is attributed to strong obstacles in this material, presumably carbides, and flow stress which when normalised is insensitive to temperature or strain rate

The hardening component found was analysed in terms of thermally activated mechanism as opposed to using the mechanical activated analyses as has been done in previous studies. Contribution of mechanical activation of dislocation glide was thus not detected over the temperature range.

Results follow a single parabolic curve irrespective of temperature over the conditions investigated. When compared to results previously obtained by analysing creep deformation and work hardening, the current results were found to have hardening and recovery characteristics. Furthermore, they yielded similar stress-hardening strain curves obtained in a similar study where copper was used.

Additionally, the relaxation results obtained appear to be better described using expressions based on dislocation glide through obstacle field. A possible reason lies in the different internal states induced by the different deformation histories undergone in this type of test.

In conclusion, further experiments need to be carried out using pure Al and α-brass to validate results obtained by Alden, where deformation mechanism was found to be mechanically activated. This would be beneficial because effects previously attributed to machine effects can now be isolated by using better equipment.

REFERENCES

1. H.D. Chandler, Work Hardening characteristics of Copper from constant strain rate and stress relaxation testing. *Materials Science and Engineering*, 2009. **A 506**: p. 130–134.
2. U.F. Kocks, *J. Enging Mater, Tech (ASME H)*, 1976(98): p. 76.
3. U.F. Kocks and H. Mecking, in strengths of Metals and Alloys, P. Haasen, V. Gerold, and G. Kostorz, Editors. 1979, Perganom Press: Oxford. p. 345.
4. R.W. Evans and B. Wilshire, Creep of Metals and Alloys. 1985, Institute of Metals: London.
5. H.J. Frost and M.F. Ashby, Deformation – Mechanism Maps. 1982, UK: Pergamon Press, Oxford.
6. D. Hull and D. J. Bacon, Introduction to dislocations'; International series on material science and technology. 1984.
7. A.N. Latapie, Molecular Dynamics Investigation on the Fracture Behavior of Nanocrystalline Fe, in *Materials Science and Engineering*. 2002, Virginia Polytechnic Institute and State University: Blacksburg, Virginia. p. 120.
8. H. Kurishita, H. Yoshinaga, and H. Nakashima, *Acta Metall.* , 1989. **37**(2): p. 499-505.
9. A. G. Guy, Introduction to Materials Science. 1972, McGraw – Hill Inc.
10. U.F. Kocks, et al., *Progress in Materials Science*, 1975. **19** p. 1-288.
11. R.W. Bailey, note on the softening of strain-hardening metals and its relation to creep. *J. Inst. Metals*, 1926. **35**: p. 27.
12. E. Orowan, The creep of metals. *J. West Scotland Iron and Steel Inst* 1946-7.
13. A.H. Cottrell and R. J. Stokes, *Proc. R. Soc. London, Ser.*, 1955. **A, 233**: p. 17.
14. D. Mclean, *Reports Progr. Phys.*, 1966. **29**: p. 1.
15. R. Lagneborg, Creep of engineering materials and structures. *Applied Science Publishers*, 1978: p. 7-34.
16. K.R. Williams and B. Wilshire, Microstructural instability of 0.5Cr-0.5Mo-0.25V creep resistant steel during service at elevated temperatures. *Mat Sci. Eng*, 1981. **47**: p. 151-160.
17. A.S. Krausz and K. Krausz, The constitutive Law of Deformation Kinetics,'Unified Constitutive Laws of Plastic Deformation. 1996: Academic Press. 229-277.
18. F.R.N. Nabarro and H.L.d. Villiers, The Physics of Creep'. 1995, Taylor & Francis.
19. D.N. French, Creep and creep failures. Natural Board Classic Series.
20. H. D. Chandler, Creep of copper in the temperature range 423–623 K. *Materials Science and Engineering: A*, 1993. **169**(1-2): p. 27-32
21. H. Mecking and U.F. Kocks, *Acta Metall.*, 1981. **29**: p. 1865-121.
22. U.F Kocks, A.S Argon, and M.F Ashby, Thermodynamics and kinetics of slip" Progress in Materials Science. Vol. 19. 1975: Pergamon Press.

23. T. Matsuo, et al., Proc. 4th Int. Conf. On Creep and Fracture of Engineering Materials and Structures, R.W Evans and B. Wilshire, Editors. 1990, The Institute of Metals: London. p. 447-486.
24. T. Jamiru, Correlation between creep and tensile behaivour in low alloy steel, in *Mechanical, Aeronautical and Industrial Engineering* 2005, University of the Witwatersrand: Johannesburg.
25. Y. Estrin and H. Mecking, A unified phenomenological description of work hardening and creep based on one-parameter models. *Acta Metall.*, 1984. **32**(1): p. 57-70.
26. E. Orowan, *Proc. Phys. Soc.*, 1940. **52**: p. 8.
27. T.H. Alden, *Metall. Trans*, 1977. **8A**: p. 1675 - 1679.
28. T. H. Alden, *Metall. Trans.*, 1985. **16A**: p. 375-392.
29. T.H. Alden, *Acta Metall*, 1989. **37**: p. 1683.
30. T.H. Alden, *Mater. Sci. Eng.*, 1988. **A103**: p. 213-221
31. T.H. Alden, *Acta Metall.* , 1988. **36**: p. 1389-1396.
32. H.D. Chandler and J.N. Görtzen, *Materials Science and Engineering*, 1994. **A185**: p. 97-102.
33. U. F. Kocks, in Constitutive Equations in Plasticity (edited by Argon). 1975, Cambridge, Mass: MIT Press. 81.
34. C.-M. Kuo, et al., *Sripta Metall. Mater.*, 1990. **24**: p. 1623-1628.
35. C.-M Kuo and H.H. Chu, *Material Science and Engineering*, 2005. **A 409**: p. 59-66.
36. C.M. Kuo, C.H. Lin, and Y.C. Huang, *Mater. Sci. Eng.*, 2005. **A396**: p. 360-367.
37. A.H. Cottrell and V. Aytekin, *J. Inst. Metals*, 1950. **77**: p. 389.
38. J C. Gibeling and T.H. Alden, *Mater. Sci. Eng.*, 1986. **79**: p. 47-53.
39. X.F. Fang and W. Dahl, *Materials Science and Engineering*, 1981. **A203, 1995**(VNR International): p. 14-25.
40. H. D. Chandler and B. Wilshire, Proc. 4th Int. Conf. on creep and fracture of engineering materials and structures, R.W. Evans, Editor, Institute of metals.
41. D. P Dunham and J. C. Gibeling, *Acta Metall. Mater.*, 1989. **37**: p. 2651-2658.
42. W.D. Nix and J.C. Gibeling, Constitutive Equations in Plasticity, R. Raj, Editor. 1975, The MIT Press: Cambridge, MA. p. 81-115.
43. J. H. Holbrook, R.W. Rohde, and J.C. Swearengen., *Acta Metall*, 1981. **29**: p. 1099-1106.
44. J. C. Gibeling, J.H. Holbrook, and W. D. Nix, *Acta Metall*, 1984. **32**: p. 1287-1295.
45. F. Guiu and P.L. Pratt, *Phys. Status Solidi*, 1964. **6**: p. 1111.
46. K. Abe, H. Yoshinaga, and S. Morozumi, *Trans. Jpn. Inst. Met.*, 1976. **40**: p. 393.
47. D. P Dunham and J. C. Gibeling, *Acta Metall. Mater.*, 1993. **41**(4): p. 1173-1182.
48. J. C. Gibeling and T. H. Alden, *Mater. Sci. Engng*, 1986: p. 79, 47.
49. T.H. Alden, *Metall. Trans*, 1987. **18A**: p. 51.
50. T.H. Alden, *Metall. Trans*, 1987. **35**: p. 2621.

51. T. H. Alden, in Mechanical Testing for Deformation Model Development, R.W. Rohde and J.C. Swearengen, Editors. 1981, ASTM STP 765. p. 29.
52. H. Yoshinaga, Z. Horita, and H. Kurishita, *Acta Metall*, 1981. **29**: p. 1815.
53. J. C. Gibeling and T. H. Alden, *Acta Metall*, 1984. **32**: p. 2069-2075.
54. T.H. Alden and J.C. Gibeling, in *Proc. 6th Int. Conf. Strength of Metals and Alloys*, R.C. Gifkins, Editor. 1982, Pergamon Press, Oxford. p. 741.
55. D. P. Dunham and J. C. Gibeling, *Acta Metall.*, 1989. **37**: p. 2651.
56. T.H. Alden, *Metall. Trans*, 1987. **18A**: p. 811.
57. H.D. Chandler, A comparison between steady state creep and stress relaxation in copper. *Materials Science & Engineering A* 2010. **527**(23): p. 6219-6223.
58. J.L. Martin and T. Kruml, *Alloys and Compounds*, 2003.
59. C.M. Kuo, et al., *Sripta Metall. Mater.*, 1990. **24**: p. 1623-1628.
60. Kurushita, H., H. Yoshinaga, and H. Nakashima, The high temperature deformation mechanism in pure metals. *Acta Metall*, 1989. **37**(2): p. 499-505.
61. P. S. Follansbee, Metallurgical Applications of Shock Wave and High Strain Rate Phenomena, L.E. Murr and e. al., Editors. 1986, Marcel Dekker: New York. p. 451.
62. L. Hollang, et al., *Mater. Sci. Eng.*, 2006. **A 424**: p. 138.
63. I. Gupta and J.C.M. Li, Stress Relaxation, internal stress, and work hardening in some bcc metals and alloys. *Metallurgical Transaction*, 1970. **1**: p. 2330.
64. H. Oikawa, K. Sugawara, and S. Karashima, *Scr. Metall.*, 1976. **10**: p. 885.
65. J. Harding, *Met. Technol*, 1977. **4**: p. 6–16.
66. G.I. Taylor, *Proc. R. Soc. London, Ser.*, 1934. **A145** p. 362.
67. N.F. Mott, *Philos. Mag.*, 1952. **43**: p. 1151.

APPENDIX A Stress Data Manipulation

Force on the pan – Mg =9.81M

Cross section area of the specimen = πr^2 = $\pi(0.0025)^2$

Force on the pan = 9.81M x 11 =107.91M

Tensile Stress = $\frac{107.91M}{\pi(0.0025)^2}\frac{1}{\sqrt{3}}$ = $\frac{107.91M}{\pi(0.0025)^2}\frac{1}{\sqrt{3}}$

At temperature < 573K

$$*\mu = \mu_0(1+\frac{(T-300)}{T_M}\frac{T_M d\mu}{\mu_0 dT}$$

At temperature > 573K but < 923K

$$*\mu = \mu_0(1+\frac{(T-300)}{T_M}\frac{T_M d\mu}{\mu_0 dT}) - K(T-573)$$

where: $\mu_0 = 8.1x10^{-4}MPa, T_M = 1810K, \frac{T_M d\mu}{\mu_0 dT} = -1.09, K_i = 3.2x10^{-2}MPa/K$

APPENDIX B Tensile Test Data Manipulation

Table 5: Engineering stress, strain and true stress and strain at 500^{0}C

Engineering Strain (%)	True Strain (%)	Engineering Stress (MPa)	True Stress (MPa)
0	0	0	0
0.269893	0.521581	0.932548	0.65884
0.272054	0.55747	1.049117	0.717409
0.280893	0.608327	1.165686	0.772737
0.291107	0.630447	1.165686	0.772737
0.301321	0.652567	1.165686	0.772737
0.311536	0.711004	1.282254	0.825164
0.32175	0.77182	1.398823	0.874978
0.331572	0.795381	1.398823	0.874978
0.341785	0.859724	1.515391	0.922428
0.351804	0.884924	1.515391	0.922428
0.361821	0.910122	1.515391	0.922428
0.37184	0.978667	1.63196	0.967729
0.38225	1.006066	1.63196	0.967729
0.392465	0.987202	1.515391	0.922428
0.401893	1.010917	1.515391	0.922428
0.412304	1.037106	1.515391	0.922428
0.422125	1.012603	1.398823	0.874978
0.43234	1.037106	1.398823	0.874978
0.442357	1.112701	1.515391	0.922428
0.452767	1.191666	1.63196	0.967729
0.463375	1.435645	2.098234	1.130832
0.473982	1.689512	2.564508	1.271026
0.483804	2.006504	3.147351	1.42247
0.493625	2.33494	3.730194	1.553966
0.502857	2.613082	4.196468	1.647979
0.512089	2.899827	4.662743	1.733908
0.522304	3.262091	5.245585	1.831875
0.532321	3.572863	5.711859	1.903876
0.542929	3.960503	6.294702	1.987148
0.55275	4.35431	6.877545	2.064016
0.562768	4.761235	7.460388	2.135395

Engineering Strain (%)	True Strain (%)	Engineering Stress (MPa)	True Stress (MPa)
0.572785	5.17983	8.043231	2.202017
0.582804	5.610112	8.626074	2.264475
0.592821	6.052061	9.208917	2.323262
0.603232	6.509938	9.791759	2.378783
0.613053	6.973237	10.3746	2.431383
0.623267	7.452682	10.95744	2.481354
0.633286	7.867761	11.42372	2.519607
0.643106	8.364604	12.00656	2.565454
0.652928	8.872907	12.5894	2.60929
0.663142	9.320914	13.05568	2.643026
0.673357	9.856951	13.63852	2.683656
0.683374	10.40189	14.22136	2.7227
0.693393	10.87769	14.68764	2.752873
0.703607	11.53004	15.38705	2.796491
0.713428	12.1068	15.96989	2.831441
0.723446	12.78279	16.6693	2.871829
0.733661	13.4764	17.36872	2.910649
0.743285	14.08641	17.95156	2.941886
0.7535	14.89484	18.76754	2.984041
0.763321	15.62285	19.46695	3.018811
0.773339	16.36878	20.16636	3.052413
0.783553	17.22433	20.98234	3.090239
0.793571	17.99959	21.68175	3.121561
0.804178	18.89636	22.49773	3.156904
0.813999	19.79134	23.31371	3.19104
0.823821	20.70237	24.12969	3.22405
0.833838	21.5373	24.8291	3.251502
0.843857	22.48463	25.64508	3.282605
0.853874	23.54783	26.57763	3.317005
0.863893	24.42833	27.27704	3.34205
0.87391	25.52655	28.20959	3.374497
0.884125	26.54635	29.02557	3.402049
0.893749	27.56461	29.84155	3.428863
0.903964	28.72264	30.7741	3.458651

Engineering Strain (%)	True Strain (%)	Engineering Stress (MPa)	True Stress (MPa)
0.913981	29.78673	31.59008	3.484008
0.923803	30.96832	32.52263	3.512221
0.934017	32.07285	33.33861	3.53627
0.944036	33.29722	34.27116	3.563066
0.954249	34.54736	35.2037	3.589161
0.964464	35.81659	36.13625	3.614594
0.973892	37.07491	37.0688	3.639395
0.984107	38.3815	38.00135	3.663596
0.994124	39.58338	38.81733	3.684302
1.003553	40.89468	39.74988	3.707453
1.013571	42.24809	40.68243	3.73008
1.023786	43.74794	41.73154	3.754937
1.034589	45.17438	42.66409	3.776526
1.04441	46.57717	43.59664	3.797659
1.054428	48.00726	44.52919	3.818354
1.064445	49.58007	45.57831	3.841135
1.074071	51.03003	46.51086	3.860958
1.083892	52.50741	47.44341	3.880396
1.094303	54.15982	48.49252	3.901822
1.104124	55.54683	49.3085	3.918174
1.114339	57.35969	50.47419	3.94108
1.124553	59.06522	51.5233	3.961257
1.134178	60.62846	52.45585	3.978856
1.144196	62.23097	53.3884	3.996151
1.154017	63.97586	54.43752	4.015257
1.164428	65.7746	55.48663	4.034004
1.17425	67.56134	56.53575	4.052407
1.184464	69.39164	57.58487	4.070476
1.194875	71.25514	58.63398	4.088226
1.204696	73.10467	59.6831	4.105665
1.21491	74.99906	60.73222	4.122806
1.224731	76.89028	61.78134	4.139658
1.234357	78.78956	62.83045	4.15623
1.244571	80.74721	63.87957	4.172533

Engineering Strain (%)	True Strain (%)	Engineering Stress (MPa)	True Stress (MPa)
1.254195	82.68744	64.92869	4.188574
1.264214	84.67425	65.97781	4.204361
1.274624	86.85732	67.14349	4.221616
1.284839	89.05111	68.30917	4.238577
1.295053	91.26865	69.47486	4.255256
1.305071	93.34386	70.52398	4.270033
1.314892	95.57905	71.68967	4.286199
1.324714	97.83719	72.85535	4.302108
1.334535	99.9626	73.90446	4.316213
1.344553	102.2804	75.07015	4.331656
1.35457	104.6214	76.23584	4.346864
1.364589	106.9858	77.40153	4.361843
1.37441	109.3579	78.56721	4.376602
1.383642	111.5441	79.61633	4.389701
1.393463	113.9602	80.78201	4.404057
1.403285	116.3993	81.9477	4.41821
1.413499	118.8942	83.11338	4.432166
1.423517	121.3962	84.27907	4.445929
1.433928	124.1227	85.56133	4.460853
1.444731	126.9103	86.84357	4.475558
1.455535	129.7258	88.12583	4.490049
1.464767	132.0852	89.17495	4.501752
1.474588	134.8617	90.4572	4.515871
1.483624	137.2446	91.50632	4.527277
1.493838	140.105	92.78857	4.541043
1.503464	142.7603	93.95426	4.553395
1.513678	145.4946	95.11994	4.565597
1.524481	148.6655	96.51877	4.580045
1.53391	151.3731	97.68446	4.591927
1.544517	154.4002	98.96671	4.604837
1.554928	157.4348	100.249	4.617582
1.564552	160.2331	101.4146	4.62903
1.573981	163.0335	102.5803	4.640347
1.583802	165.897	103.746	4.651539

Engineering Strain (%)	True Strain (%)	Engineering Stress (MPa)	True Stress (MPa)
1.594017	169.0109	105.0283	4.663706
1.604034	172.1298	106.3105	4.675727
1.613856	175.2531	107.5928	4.687605
1.623481	178.1908	108.7585	4.698282
1.633499	181.3849	110.0407	4.709897
1.643517	184.6047	111.323	4.721378
1.653535	188.043	112.7218	4.733755
1.663552	191.3153	114.0041	4.744967
1.673767	194.6362	115.2863	4.756055
1.683588	197.937	116.5686	4.767022
1.693999	201.5307	117.9674	4.778849
1.70441	204.9546	119.2496	4.78957
1.714035	208.3099	120.5319	4.800177
1.723856	211.7139	121.8141	4.810672
1.733873	215.3696	123.213	4.821998
1.743695	218.8254	124.4952	4.832268
1.753516	222.3064	125.7775	4.842433
1.763731	226.2741	127.2929	4.854316
1.774534	230.1424	128.6917	4.86516
1.784553	233.9379	130.0905	4.875888
1.794963	237.8134	131.4893	4.886502
1.804785	241.6393	132.8882	4.897005
1.814213	245.2279	134.1704	4.906536
1.823838	248.8676	135.4527	4.915978
1.834052	252.8268	136.8515	4.926177
1.84407	256.7874	138.2503	4.936273
1.854088	260.7759	139.6491	4.946268
1.863517	264.7088	141.048	4.956165
1.873534	268.7524	142.4468	4.965964
1.883749	272.8527	143.8456	4.975668
1.893373	276.8953	145.2444	4.985279
1.903785	281.081	146.6432	4.994799
1.913606	285.2078	148.0421	5.004229
1.923428	289.5864	149.5575	5.014345

Engineering Strain (%)	True Strain (%)	Engineering Stress (MPa)	True Stress (MPa)
1.933641	293.829	150.9563	5.023593
1.944053	298.357	152.4717	5.033516
1.953874	302.5974	153.8705	5.042589
1.963891	307.1249	155.3859	5.052327
1.973516	311.1607	156.6681	5.060492
1.983142	315.4524	158.067	5.069325
1.99257	319.507	159.3492	5.077354
2.002588	323.9147	160.748	5.08604
2.012802	328.617	162.2634	5.095365
2.024588	334.0812	164.012	5.106018
2.034606	338.5804	165.4108	5.114459
2.04482	343.6171	167.0427	5.124218
2.054642	348.1417	168.4416	5.132508
2.064266	352.66	169.8404	5.14073
2.074481	357.5488	171.3558	5.149561
2.084302	362.1571	172.7546	5.157644
2.093731	366.7241	174.1534	5.165662
2.103159	371.3174	175.5522	5.173617
2.112588	375.9373	176.9511	5.181509
2.122605	380.9365	178.4665	5.189988
2.13282	386.2504	180.0984	5.199041
2.142641	391.0261	181.4973	5.206735
2.152856	396.1527	183.0126	5.215004
2.16248	401.2007	184.528	5.223206
2.172695	406.3883	186.0434	5.231341
2.182713	411.5697	187.5588	5.23941
2.192731	417.0372	189.1908	5.248028
2.202355	421.9484	190.5896	5.255356
2.21257	427.5163	192.2216	5.263837
2.222195	432.4844	193.6204	5.271051
2.232606	438.1541	195.2523	5.279401
2.242427	443.4797	196.7677	5.287093
2.252249	448.8352	198.2831	5.294727
2.263248	454.7208	199.9151	5.302882

Engineering Strain (%)	True Strain (%)	Engineering Stress (MPa)	True Stress (MPa)
2.272873	460.0987	201.4305	5.310396
2.283874	466.0528	203.0624	5.318426
2.293694	471.5327	204.5778	5.325825
2.30332	476.7334	205.9766	5.332606
2.313337	482.3124	207.492	5.339901
2.323159	487.8807	209.0074	5.347143
2.333373	493.8336	210.6394	5.354884
2.342999	499.4213	212.1548	5.362019
2.353016	505.1223	213.6702	5.369103
2.362838	510.8114	215.1856	5.376137
2.372462	516.4873	216.7009	5.383122
2.382481	522.2787	218.2163	5.390059
2.392498	528.3791	219.8483	5.397476
2.402713	534.5562	221.4803	5.404838
2.412534	540.3971	222.9957	5.411627
2.422749	546.639	224.6276	5.418886
2.433159	552.675	226.143	5.42558
2.442784	558.8479	227.775	5.432739
2.452605	564.5254	229.1738	5.438835
2.462427	570.8048	230.8058	5.4459
2.472248	576.8278	232.3212	5.452416
2.482266	583.2161	233.9531	5.459386
2.491302	588.8239	235.3519	5.465322
2.50132	593.5243	236.2845	5.46926
2.513105	601.594	238.3827	5.478064
2.523123	607.5214	239.7815	5.48389
2.533534	614.1628	241.4135	5.490645
2.543355	620.6942	243.0455	5.497355
2.552784	626.5662	244.4443	5.50307
2.561624	632.9163	246.0762	5.509697
2.571837	639.6371	247.7082	5.51628
2.581658	646.2927	249.3401	5.522821
2.59148	652.3765	250.739	5.528393
2.600909	658.9948	252.3709	5.534855

Engineering Strain (%)	True Strain (%)	Engineering Stress (MPa)	True Stress (MPa)
2.61132	666.5029	254.236	5.542189
2.621533	673.388	255.868	5.548562
2.631159	679.5409	257.2668	5.553993
2.641176	687.0542	259.1319	5.561189
2.651587	694.0898	260.7639	5.567443
2.661408	701.6244	262.629	5.574543
2.671427	708.6251	264.2609	5.580714
2.682034	715.8157	265.8929	5.586847
2.691266	722.6718	267.5248	5.592943
2.701087	729.7171	269.1568	5.599003
2.711695	737.0081	270.7888	5.605025
2.720926	743.9577	272.4207	5.611012
2.730748	751.0996	274.0527	5.616963
2.740766	758.3279	275.6847	5.622878
2.751176	766.3395	277.5497	5.629597
2.761784	773.8012	279.1817	5.635438
2.771801	781.7777	281.0468	5.642073
2.782605	790.0147	282.9119	5.648664
2.792034	797.2481	284.5439	5.654396
2.801462	803.8591	285.9427	5.659283
2.811284	811.2651	287.5746	5.664954
2.821694	819.5321	289.4397	5.671396
2.831516	827.6657	291.3048	5.677797
2.841534	835.2313	292.9368	5.683365
2.850962	842.6553	294.5687	5.688901
2.861176	851.0107	296.4338	5.695192
2.870998	858.6174	298.0658	5.700664
2.880819	866.2559	299.6978	5.706106
2.89123	874.7789	301.5629	5.712289
2.901052	882.4849	303.1948	5.717668
2.910873	890.9016	305.0599	5.723781
2.920891	898.7343	306.6919	5.729099
2.931302	907.4049	308.557	5.735142
2.94073	915.1228	310.189	5.7404

Engineering Strain (%)	True Strain (%)	Engineering Stress (MPa)	True Stress (MPa)
2.950552	923.6821	312.054	5.746376
2.958998	930.4654	313.4529	5.750834
2.969016	938.4607	315.0848	5.756011
2.978837	947.1209	316.9499	5.761894
2.988658	955.8178	318.815	5.767743
2.999855	965.6931	320.9133	5.774282
3.010658	974.786	322.7784	5.780059
3.021658	983.9833	324.6435	5.785803
3.031873	992.9642	326.5085	5.791514
3.041301	1001.015	328.1405	5.796485
3.050337	1008.967	329.7725	5.801431
3.059765	1017.079	331.4044	5.806352
3.069783	1026.135	333.2695	5.811948
3.079998	1035.294	335.1346	5.817512
3.089622	1044.291	336.9997	5.823045
3.099444	1052.669	338.6317	5.827862
3.110051	1062.072	340.4968	5.833338
3.119676	1071.178	342.3619	5.838785
3.130087	1080.59	344.227	5.844202
3.139908	1089.837	346.0921	5.84959
3.150516	1099.395	347.9572	5.854949
3.160337	1108.717	349.8223	5.86028
3.169569	1117.128	351.4542	5.864921
3.17998	1126.728	353.3193	5.870198
3.189408	1136.017	355.1844	5.875449
3.19923	1144.737	356.8164	5.88002
3.208855	1154.166	358.6815	5.885219
3.218676	1162.951	360.3134	5.889746
3.228498	1172.521	362.1785	5.894894
3.238319	1182.128	364.0436	5.900017
3.249319	1192.203	365.9087	5.905113
3.259926	1202.935	368.007	5.910816
3.27014	1212.804	369.872	5.915857
3.280354	1222.71	371.7372	5.920873

Engineering Strain (%)	True Strain (%)	Engineering Stress (MPa)	True Stress (MPa)
3.289587	1230.753	373.136	5.924619
3.299604	1241.424	375.2342	5.930212
3.30923	1250.446	376.8662	5.93454
3.318658	1260.198	378.7313	5.939464
3.329265	1270.435	380.5964	5.944363
3.338694	1280.261	382.4615	5.949239
3.347926	1289.264	384.0934	5.953486
3.357748	1299.309	385.9585	5.958317
3.368551	1309.772	387.8236	5.963126
3.378962	1320.91	389.9218	5.968508
3.387408	1328.95	391.3207	5.97208
3.398015	1340.241	393.4189	5.977414
3.407051	1349.366	395.0509	5.981543
3.417265	1359.784	396.916	5.986241
3.427087	1370.883	399.0142	5.9915
3.436515	1380.263	400.6461	5.995571
3.446533	1390.715	402.5113	6.000204
3.455962	1400.965	404.3763	6.004816
3.46539	1411.251	406.2415	6.009406
3.475801	1421.973	408.1065	6.013976
3.485622	1432.492	409.9716	6.018524
3.496819	1444.43	412.0699	6.023617
3.507819	1457.152	414.4012	6.029245
3.518426	1468.121	416.2663	6.033725
3.528051	1478.717	418.1314	6.038184
3.537283	1488.359	419.7634	6.042071
3.54789	1500.267	421.8616	6.047045
3.557319	1510.888	423.7267	6.051446
3.567337	1521.797	425.5918	6.055828
3.577158	1533.492	427.6901	6.060734
3.586194	1543.218	429.322	6.064534
3.596801	1555.33	431.4203	6.069398
3.607605	1567.571	433.5185	6.074238
3.618015	1578.842	435.3835	6.078522

Engineering Strain (%)	True Strain (%)	Engineering Stress (MPa)	True Stress (MPa)
3.626658	1589.378	437.2487	6.082786
3.636479	1600.465	439.1137	6.087033
3.646301	1611.588	440.9789	6.091262
3.655336	1622.399	442.8439	6.095473
3.665158	1633.594	444.709	6.099666
3.674979	1644.826	446.5741	6.103842
3.684801	1656.094	448.4392	6.108001
3.695211	1668.527	450.5375	6.112658
3.704836	1679.782	452.4026	6.11678
3.714658	1692.03	454.5008	6.121397
3.724872	1704.498	456.5991	6.125993
3.735676	1716.409	458.4642	6.130061
3.746479	1729.234	460.5624	6.134617
3.758069	1744.221	463.1269	6.140158
3.768283	1756.868	465.2251	6.144669
3.776926	1767.061	466.8571	6.148163
3.78714	1779.786	468.9553	6.152638
3.795979	1790.135	470.5873	6.156104
3.804819	1801.4	472.4524	6.160051
3.815622	1814.521	474.5506	6.164473
3.825051	1820.789	475.0169	6.165453
3.834676	1832.522	476.882	6.169364
3.845283	1844.763	478.7471	6.173259
3.855104	1858.462	481.0784	6.178107
3.865515	1870.691	482.9435	6.181968
3.874943	1882.481	484.8086	6.185815
3.885354	1898.408	487.6063	6.191557
3.895175	1910.472	489.4714	6.195367
3.904604	1922.379	491.3365	6.199162
3.915407	1936.826	493.6678	6.203887
3.92464	1948.713	495.5329	6.20765
3.934461	1960.928	497.398	6.211399
3.944283	1973.179	499.2631	6.215134
3.9543	1985.566	501.1282	6.218856

Engineering Strain (%)	True Strain (%)	Engineering Stress (MPa)	True Stress (MPa)
3.963729	1999.541	503.4596	6.223488
3.973747	2012.006	505.3247	6.227178
3.984943	2026.966	507.6561	6.231772
3.995747	2041.777	509.9874	6.236345
4.005765	2054.367	511.8525	6.239988
4.015979	2067.095	513.7177	6.243619
4.025604	2081.434	516.049	6.248138
4.035033	2093.835	517.9141	6.251738
4.044854	2106.476	519.7792	6.255326
4.054283	2120.838	522.1106	6.259793
4.063908	2133.453	523.9756	6.263352
4.072354	2145.482	525.8408	6.266898
4.083158	2158.789	527.7059	6.270432
4.093961	2175.955	530.5035	6.27571
4.104568	2189.248	532.3686	6.279213
4.114389	2204.078	534.7	6.283574
4.122836	2214.37	536.0988	6.286182
4.133836	2229.916	538.4302	6.290513
4.142872	2244.449	540.7615	6.294826
4.153872	2258.155	542.6266	6.298263
4.165068	2275.894	545.4243	6.303396
4.173122	2286.133	546.8231	6.305952
4.182943	2301.265	549.1545	6.310199
4.192961	2314.597	551.0196	6.313584
4.202783	2329.817	553.351	6.317798
4.212211	2342.899	555.2161	6.321157
4.222033	2356.237	557.0811	6.324504
4.233622	2374.549	559.8788	6.329505
4.244032	2388.303	561.7439	6.332825
4.253854	2403.748	564.0753	6.336959
4.264265	2417.584	565.9404	6.340254
4.27389	2434.997	568.738	6.345177
4.283514	2446.473	570.1368	6.347629
4.292747	2461.754	572.4682	6.351702

Engineering Strain (%)	True Strain (%)	Engineering Stress (MPa)	True Stress (MPa)
4.302175	2475.184	574.3333	6.354949
4.312193	2491.002	576.6647	6.358994
4.321425	2504.394	578.5297	6.362217
4.332622	2520.984	580.8611	6.366232
4.343425	2539.422	583.6588	6.371028
4.353443	2553.398	585.5239	6.374213
4.362872	2569.1	587.8552	6.37818
4.372104	2580.652	589.254	6.380553
4.383104	2599.407	592.0517	6.385282
4.391747	2612.724	593.9168	6.388422
4.402943	2629.65	596.2482	6.392333
4.412175	2645.45	598.5795	6.396229
4.421014	2658.995	600.4446	6.399334
4.430246	2672.811	602.3098	6.402431
4.440854	2689.564	604.6411	6.406288
4.450282	2703.574	606.5062	6.409362
4.460104	2722.018	609.3038	6.413957
4.470907	2736.951	611.1689	6.417008
4.481711	2756.103	613.9666	6.421568
4.493104	2771.489	615.8317	6.424596
4.503318	2790.388	618.6293	6.429121
4.513139	2806.995	620.9607	6.432877
4.522764	2821.417	622.8258	6.435871
4.5318	2835.506	624.6909	6.438857
4.540639	2851.623	627.0223	6.442576
4.550264	2864.032	628.4211	6.4448
4.560086	2880.845	630.7524	6.448498
4.569907	2897.704	633.0839	6.452181
4.580907	2915.359	635.4152	6.455851
4.590728	2932.312	637.7466	6.459508
4.601336	2947.669	639.6117	6.462423
4.609586	2961.552	641.4767	6.465331
4.619211	2978.505	643.8082	6.468953
4.629229	2995.757	646.1395	6.472562

Engineering Strain (%)	True Strain (%)	Engineering Stress (MPa)	True Stress (MPa)
4.638068	3010.127	648.0046	6.47544
4.646514	3024.275	649.8697	6.478309
4.657514	3042.293	652.201	6.481885
4.66655	3056.899	654.0662	6.484736
4.676568	3074.364	656.3975	6.488289
4.687371	3094.58	659.1952	6.492536
4.696603	3107.245	660.594	6.494652
4.707014	3127.301	663.3917	6.498872
4.717621	3145.347	665.723	6.502375
4.728229	3161.238	667.5881	6.505168
4.737461	3178.455	669.9195	6.508649
4.747478	3196.244	672.2509	6.512118
4.756907	3209.246	673.6497	6.514194
4.76555	3223.965	675.5148	6.516954
4.774782	3241.342	677.8462	6.520395
4.784407	3259.031	680.1776	6.523823
4.794621	3272.695	681.5764	6.525874
4.804442	3290.6	683.9077	6.529284
4.814068	3308.416	686.2391	6.532682
4.824282	3326.682	688.5705	6.536069
4.833907	3340.081	689.9693	6.538095
4.844121	3360.691	692.767	6.542136
4.854335	3376.831	694.632	6.544821
4.864943	3393.283	696.4971	6.547498
4.874764	3411.499	698.8285	6.550835
4.886746	3431.277	701.1599	6.554161
4.897157	3452.287	703.9575	6.558138
4.905603	3460.529	704.4238	6.558799
4.914639	3476.07	706.2889	6.561439
4.926032	3497.909	709.0865	6.565387
4.938014	3517.93	711.4179	6.568665
4.947639	3531.707	712.8167	6.570626
4.956675	3545.091	714.2156	6.572584
4.968068	3564.822	716.5469	6.575838

Engineering Strain (%)	True Strain (%)	Engineering Stress (MPa)	True Stress (MPa)
4.978674	3581.718	718.412	6.578434
4.989085	3596.187	719.8109	6.580377
4.999103	3612.732	721.676	6.582961
5.009907	3629.883	723.541	6.585538
5.019728	3644.021	724.9399	6.587467
5.029157	3660.245	726.8049	6.590033
5.037603	3668.741	727.2712	6.590674
5.045853	3681.808	728.67	6.592592
5.055282	3698.116	730.5352	6.595145
5.066478	3715.757	732.4003	6.597692
5.07846	3734.016	734.2653	6.600231
5.088675	3743.899	734.7316	6.600865
5.098496	3760.634	736.5967	6.603397
5.10871	3775.314	737.9955	6.605292
5.118728	3789.877	739.3943	6.607183
5.129139	3804.76	740.7932	6.609071
5.13896	3816.838	741.7257	6.610327
5.148389	3831.043	743.1246	6.612208
5.157621	3840.317	743.5908	6.612835
5.165674	3851.131	744.5234	6.614086
5.176281	3868.693	746.3885	6.616585
5.186103	3883.288	747.7873	6.618455
5.195728	3895.34	748.7198	6.6197
5.206335	3908.148	749.6524	6.620943
5.217532	3926.284	751.5175	6.623424
5.229907	3942.912	752.9163	6.625281
5.238942	3949.724	752.9163	6.625281
5.249156	3964.767	754.3151	6.627135
5.258585	3979.245	755.714	6.628985
5.267425	3990.846	756.6465	6.630217
5.277246	4003.208	757.579	6.631447
5.286478	4015.141	758.5116	6.632676
5.296299	4027.54	759.4442	6.633903
5.305728	4042.131	760.843	6.63574

Engineering Strain (%)	True Strain (%)	Engineering Stress (MPa)	True Stress (MPa)
5.316335	4055.17	761.7755	6.636964
5.327335	4066.045	762.2418	6.637575
5.337746	4081.457	763.6406	6.639406
5.346978	4093.503	764.5732	6.640625
5.356996	4106.168	765.5057	6.641842
5.366228	4118.249	766.4383	6.643058
5.376638	4133.759	767.8371	6.644879
5.38646	4143.822	768.3033	6.645485
5.396281	4156.41	769.2359	6.646697
5.406103	4169.016	770.1685	6.647907
5.416513	4184.621	771.5673	6.649719
5.425942	4194.435	772.0336	6.650322
5.436353	4202.483	772.0336	6.650322
5.445978	4217.541	773.4324	6.65213
5.457371	4233.998	774.8312	6.653935
5.46837	4247.632	775.7637	6.655136
5.479764	4264.147	777.1626	6.656935
5.489781	4274.502	777.6288	6.657534
5.498228	4283.642	778.0951	6.658133
5.507264	4295.818	779.0276	6.659329
5.517674	4306.511	779.494	6.659927
5.527299	4319.178	780.4265	6.661121
5.537317	4332.17	781.3591	6.662314
5.547335	4345.18	782.2916	6.663505
5.55696	4355.311	782.7579	6.6641
5.56737	4363.47	782.7579	6.6641
5.576995	4378.815	784.1567	6.665883
5.586227	4388.669	784.623	6.666477
5.596835	4402.221	785.5555	6.667663
5.606853	4415.329	786.488	6.668848
5.615888	4425.063	786.9543	6.66944
5.627085	4439.133	787.8869	6.670623
5.636906	4446.881	787.8869	6.670623
5.646728	4462.528	789.2857	6.672395

Engineering Strain (%)	True Strain (%)	Engineering Stress (MPa)	True Stress (MPa)
5.656549	4472.927	789.752	6.672984
5.666567	4486.133	790.6845	6.674163
5.674621	4492.509	790.6845	6.674163
5.685031	4506.053	791.6171	6.67534
5.695442	4519.616	792.5496	6.676516
5.707228	4534.291	793.4822	6.677691
5.719406	4543.966	793.4822	6.677691
5.728442	4553.816	793.9484	6.678277
5.738263	4564.299	794.4147	6.678864
5.748085	4577.472	795.3473	6.680035
5.757513	4587.664	795.8135	6.680621
5.767924	4601.339	796.7461	6.68179
5.777549	4611.711	797.2123	6.682375
5.787763	4622.563	797.6786	6.682959
5.797977	4636.128	798.6112	6.684126
5.807995	4646.846	799.0775	6.684709
5.818406	4657.889	799.5438	6.685291
5.828817	4668.941	800.01	6.685873
5.837852	4678.9	800.4763	6.686455
5.84846	4690.129	800.9426	6.687037
5.856906	4699.633	801.4088	6.687618
5.868299	4714.247	802.3414	6.68878
5.878317	4725.036	802.8077	6.68936
5.888335	4735.834	803.2739	6.68994
5.89796	4746.325	803.7402	6.69052
5.90837	4757.458	804.2065	6.691099
5.917406	4767.493	804.6727	6.691678
5.926442	4777.536	805.139	6.692256
5.937245	4783.477	804.6727	6.691678
5.949227	4801.452	806.0716	6.693412
5.959245	4812.316	806.5378	6.69399
5.970049	4826.608	807.4704	6.695144
5.97987	4837.336	807.9366	6.695721
5.989102	4847.597	808.403	6.696297

Engineering Strain (%)	True Strain (%)	Engineering Stress (MPa)	True Stress (MPa)
5.998727	4855.388	808.403	6.696297
6.009335	4869.577	809.3355	6.697448
6.019156	4880.342	809.8018	6.698024
6.028584	4890.798	810.2681	6.698599
6.037817	4898.288	810.2681	6.698599
6.047049	4908.597	810.7343	6.699173
6.057263	4919.713	811.2006	6.699747
6.066888	4930.359	811.6669	6.700321
6.076906	4941.333	812.1331	6.700895
6.088102	4956.115	813.0657	6.702041
6.09871	4967.594	813.532	6.702614
6.10912	4978.922	813.9982	6.703186
6.119334	4990.1	814.4645	6.703758
6.128959	5000.806	814.9308	6.70433
6.13937	5012.163	815.397	6.704901
6.149191	5023.049	815.8633	6.705472
6.157835	5030.109	815.8633	6.705472
6.16687	5037.49	815.8633	6.705472
6.177673	5052.076	816.7959	6.706613
6.188281	5066.521	817.7285	6.707752
6.200655	5076.653	817.7285	6.707752
6.211263	5088.233	818.1947	6.708322
6.221281	5099.341	818.661	6.708891
6.231298	5110.458	819.1273	6.70946
6.240334	5120.778	819.5935	6.710028
6.250352	5131.913	820.0598	6.710596
6.260959	5143.541	820.5261	6.711164
6.270191	5154.049	820.9924	6.711731
6.280406	5162.445	820.9924	6.711731
6.290423	5173.613	821.4586	6.712298
6.300048	5184.467	821.9249	6.712865
6.30987	5195.491	822.3912	6.713431
6.319298	5197.361	821.4586	6.712298
6.328138	5213.483	822.8574	6.713997

Engineering Strain (%)	True Strain (%)	Engineering Stress (MPa)	True Stress (MPa)
6.337763	5227.323	823.79	6.715129
6.347781	5235.586	823.79	6.715129
6.358191	5247.137	824.2563	6.715694
6.367227	5257.563	824.7225	6.716259
6.377048	5268.646	825.1888	6.716823
6.387656	5280.388	825.6551	6.717388
6.39787	5291.815	826.1214	6.717951
6.40828	5306.402	827.0539	6.719078
6.417316	5310.892	826.5876	6.718515
6.427727	5322.504	827.0539	6.719078
6.438923	5337.78	827.9865	6.720204
6.450512	5350.395	828.4528	6.720766
6.460923	5362.043	828.919	6.721328
6.469959	5369.542	828.919	6.721328
6.479191	5380.225	829.3853	6.72189
6.488816	5388.218	829.3853	6.72189
6.499619	5403.249	830.3178	6.723012
6.509441	5411.415	830.3178	6.723012
6.518281	5415.724	829.8516	6.722451
6.527905	5429.808	830.7841	6.723573
6.53812	5441.353	831.2504	6.724133
6.548138	5455.796	832.1829	6.725253
6.557959	5467.038	832.6492	6.725813
6.567388	5474.898	832.6492	6.725813
6.577405	5486.316	833.1155	6.726372
6.586834	5497.252	833.5818	6.726931
6.59528	5504.301	833.5818	6.726931
6.607066	5520.298	834.5143	6.728047
6.618066	5532.575	834.9807	6.728605
6.627691	5543.711	835.4468	6.729163
6.636923	5551.434	835.4468	6.729163
6.647138	5563.077	835.9132	6.72972
6.656763	5574.236	836.3794	6.730277
6.66678	5582.625	836.3794	6.730277

Engineering Strain (%)	True Strain (%)	Engineering Stress (MPa)	True Stress (MPa)
6.67778	5598.063	837.312	6.73139
6.690548	5615.006	838.2445	6.732502
6.700566	5623.413	838.2445	6.732502
6.709602	5630.997	838.2445	6.732502
6.720209	5643.032	838.7108	6.733058
6.729048	5650.455	838.7108	6.733058
6.739655	5662.504	839.1771	6.733613
6.749869	5674.233	839.6434	6.734168
6.760084	5685.971	840.1096	6.734722
6.770298	5697.72	840.5759	6.735276
6.779334	5705.324	840.5759	6.735276
6.789548	5717.086	841.0422	6.73583
6.799173	5728.361	841.5085	6.736384
6.808601	5739.479	841.9747	6.736937
6.818423	5747.758	841.9747	6.736937
6.827066	5758.228	842.441	6.73749
6.836691	5766.346	842.441	6.73749
6.847298	5781.677	843.3736	6.738595
6.858495	5797.527	844.3061	6.739699
6.869298	5800.254	843.3736	6.738595
6.879119	5811.754	843.8398	6.739147
6.889137	5826.642	844.7723	6.74025
6.899155	5838.332	845.2386	6.740801
6.909566	5850.363	845.7049	6.741352
6.919191	5861.739	846.1712	6.741903
6.930191	5877.521	847.1038	6.743003
6.941387	5890.253	847.57	6.743553
6.950619	5894.846	847.1038	6.743003
6.96103	5906.921	847.57	6.743553
6.970066	5917.839	848.0363	6.744102
6.978708	5925.177	848.0363	6.744102
6.988727	5936.941	848.5026	6.744651
7.000709	5953.648	849.4351	6.745748
7.010137	5961.666	849.4351	6.745748

Engineering Strain (%)	True Strain (%)	Engineering Stress (MPa)	True Stress (MPa)
7.020744	5973.961	849.9014	6.746296
7.029976	5981.817	849.9014	6.746296
7.039405	5989.84	849.9014	6.746296
7.047655	6000.145	850.3676	6.746844
7.05728	6011.631	850.834	6.747392
7.067298	6023.459	851.3002	6.747939
7.077119	6035.13	851.7665	6.748486
7.086744	6043.338	851.7665	6.748486
7.097744	6059.337	852.699	6.749579
7.107959	6071.372	853.1653	6.750125
7.118369	6080.264	853.1653	6.750125
7.128583	6092.313	853.6316	6.75067
7.138798	6104.371	854.0978	6.751216
7.148423	6115.934	854.5641	6.751761
7.159226	6128.515	855.0304	6.752306
7.16944	6137.259	855.0304	6.752306
7.181619	6154.381	855.9629	6.753395
7.191637	6166.32	856.4293	6.753939
7.201262	6171.214	855.9629	6.753395
7.21128	6183.162	856.4293	6.753939
7.219923	6190.573	856.4293	6.753939
7.228762	6198.152	856.4293	6.753939
7.239958	6214.504	857.3618	6.755026
7.250173	6226.651	857.828	6.755569
7.259994	6238.472	858.2943	6.756111
7.269815	6240.132	857.3618	6.755026
7.281208	6256.701	858.2943	6.756111
7.290833	6271.771	859.2269	6.757196
7.298691	6275.126	858.7606	6.756654
7.308905	6290.724	859.6931	6.757738
7.318923	6302.759	860.1594	6.75828
7.328155	6310.709	860.1594	6.75828
7.339155	6327.026	861.092	6.759362
7.349566	6339.428	861.5582	6.759903

Engineering Strain (%)	True Strain (%)	Engineering Stress (MPa)	True Stress (MPa)
7.359387	6347.9	861.5582	6.759903
7.369798	6360.316	862.0245	6.760443
7.379815	6372.402	862.4908	6.760983
7.389441	6380.714	862.4908	6.760983
7.399654	6396.434	863.4233	6.762063
7.410066	6405.433	863.4233	6.762063
7.420869	6418.233	863.8896	6.762602
7.432261	6431.551	864.3558	6.763141
7.443262	6444.542	864.8222	6.76368
7.452887	6452.875	864.8222	6.76368
7.461726	6460.528	864.8222	6.76368
7.469387	6467.161	864.8222	6.76368
7.480976	6484.171	865.7547	6.764756
7.490798	6496.177	866.2209	6.765294
7.501405	6505.375	866.2209	6.765294
7.511619	6517.736	866.6873	6.765831
7.521637	6529.935	867.1535	6.766369
7.532244	6542.656	867.6198	6.766906
7.540887	6550.164	867.6198	6.766906
7.550119	6558.183	867.6198	6.766906
7.560333	6574.106	868.5524	6.767979
7.570351	6582.816	868.5524	6.767979
7.579976	6591.186	868.5524	6.767979
7.590583	6607.488	869.4849	6.76905
7.60119	6620.265	869.9512	6.769586
7.610815	6628.648	869.9512	6.769586
7.621029	6641.098	870.4175	6.770121
7.63144	6653.728	870.8837	6.770656
7.640869	6661.949	870.8837	6.770656
7.651869	6675.108	871.35	6.771191
7.662279	6687.762	871.8162	6.771725
7.675243	6709.814	873.2151	6.773326
7.685458	6715.16	872.7488	6.772793
7.694886	6723.397	872.7488	6.772793

Engineering Strain (%)	True Strain (%)	Engineering Stress (MPa)	True Stress (MPa)
7.704119	6731.464	872.7488	6.772793
7.712173	6738.501	872.7488	6.772793
7.721404	6746.567	872.7488	6.772793
7.732601	6763.561	873.6813	6.77386
7.742815	6776.106	874.1476	6.774393
7.752636	6788.316	874.6139	6.774925
7.762654	6807.947	876.0128	6.776522
7.774243	6814.485	875.5464	6.77599
7.783869	6822.923	875.5464	6.77599
7.79153	6822.372	874.6139	6.774925
7.802333	6839.107	875.5464	6.77599
7.811761	6851.014	876.0128	6.776522
7.820993	6859.111	876.0128	6.776522
7.831993	6876.062	876.9453	6.777584
7.841815	6888.341	877.4116	6.778115
7.851833	6897.141	877.4116	6.778115
7.86185	6909.606	877.8779	6.778646
7.872065	6918.584	877.8779	6.778646
7.881691	6930.718	878.3441	6.779176
7.890922	6938.835	878.3441	6.779176
7.902316	6956.224	879.2766	6.780236
7.912922	6969.251	879.743	6.780766
7.923726	6982.46	880.2092	6.781295
7.934332	6991.806	880.2092	6.781295
7.945725	7005.551	880.6755	6.781824
7.954173	7012.999	880.6755	6.781824
7.961833	7016.04	880.2092	6.781295
7.973619	7033.862	881.1417	6.782353
7.983243	7042.352	881.1417	6.782353
7.993261	7054.916	881.608	6.782881
8.003082	7067.316	882.0743	6.783409
8.013886	7080.594	882.5406	6.783937
8.024886	7094.054	883.0068	6.784465
8.034315	7102.389	883.0068	6.784465

Engineering Strain (%)	True Strain (%)	Engineering Stress (MPa)	True Stress (MPa)
8.042368	7105.758	882.5406	6.783937
8.052976	7118.886	883.0068	6.784465
8.062993	7135.26	883.9394	6.785519
8.072029	7143.257	883.9394	6.785519
8.083422	7157.108	884.4057	6.786046
8.093047	7169.403	884.8719	6.786572
8.103065	7178.278	884.8719	6.786572
8.113672	7191.458	885.3383	6.787099
8.12369	7204.124	885.8044	6.787624
8.132922	7212.312	885.8044	6.787624
8.143332	7221.543	885.8044	6.787624
8.154333	7235.102	886.2708	6.78815
8.165726	7252.825	887.2034	6.789201
8.178101	7267.629	887.6696	6.789725
8.18635	7271.144	887.2034	6.789201
8.196958	7284.387	887.6696	6.789725
8.204422	7291.02	887.6696	6.789725
8.213457	7299.049	887.6696	6.789725
8.225047	7317.019	888.6021	6.790774
8.234475	7325.406	888.6021	6.790774
8.244297	7334.144	888.6021	6.790774
8.254707	7351.103	889.5347	6.791822
8.265118	7360.374	889.5347	6.791822
8.274547	7368.771	889.5347	6.791822
8.284958	7381.906	890.001	6.792346
8.294189	7393.998	890.4672	6.792869
8.303618	7402.404	890.4672	6.792869
8.313439	7411.159	890.4672	6.792869
8.323851	7424.321	890.9335	6.793392
8.334064	7437.317	891.3998	6.793914
8.343885	7449.972	891.8661	6.794437
8.353707	7458.742	891.8661	6.794437
8.364904	7472.64	892.3323	6.794959
8.37394	7480.711	892.3323	6.794959

Engineering Strain (%)	True Strain (%)	Engineering Stress (MPa)	True Stress (MPa)
8.38376	7493.394	892.7986	6.795481
8.394761	7507.14	893.2648	6.796002
8.405171	7520.369	893.7312	6.796523
8.418529	7536.245	894.1974	6.797044
8.42894	7549.496	894.6638	6.797565
8.438171	7553.829	894.1974	6.797044
8.447404	7562.094	894.1974	6.797044
8.455261	7569.128	894.1974	6.797044
8.46685	7583.451	894.6638	6.797565
8.477261	7596.727	895.1299	6.798085
8.486493	7608.958	895.5963	6.798606
8.495529	7613.098	895.1299	6.798085
8.506529	7630.888	896.0625	6.799126
8.517725	7644.904	896.5288	6.799645
8.526565	7652.837	896.5288	6.799645
8.535797	7661.124	896.5288	6.799645
8.545815	7674.099	896.9951	6.800165
8.55485	7682.213	896.9951	6.800165
8.565457	7695.732	897.4614	6.800684
8.575868	7709.084	897.9276	6.801203
8.585297	7717.56	897.9276	6.801203
8.595707	7730.927	898.3939	6.801721
8.605725	7739.937	898.3939	6.801721
8.615743	7752.964	898.8602	6.802239
8.624975	7761.272	898.8602	6.802239
8.635386	7774.666	899.3265	6.802757
8.646582	7788.778	899.7927	6.803275
8.657779	7802.901	900.259	6.803793
8.670939	7822.849	901.1916	6.804827
8.680368	7827.307	900.7252	6.80431
8.688618	7830.695	900.259	6.803793
8.697064	7838.308	900.259	6.803793
8.70669	7851.042	900.7252	6.80431
8.717886	7865.203	901.1916	6.804827

Engineering Strain (%)	True Strain (%)	Engineering Stress (MPa)	True Stress (MPa)
8.727118	7873.532	901.1916	6.804827
8.736154	7889.831	902.1241	6.80586
8.745975	7894.622	901.6578	6.805343
8.756779	7908.458	902.1241	6.80586
8.7666	7921.415	902.5903	6.806376
8.776814	7930.645	902.5903	6.806376
8.786832	7943.794	903.0566	6.806892
8.796064	7952.14	903.0566	6.806892
8.805492	7960.664	903.0566	6.806892
8.8161	7974.364	903.5229	6.807408
8.826118	7987.541	903.9892	6.807923
8.835546	7996.074	903.9892	6.807923
8.846153	8009.798	904.4554	6.808438
8.855975	8018.691	904.4554	6.808438
8.865796	8031.718	904.9218	6.808953
8.875225	8040.259	904.9218	6.808953
8.88485	8048.978	904.9218	6.808953
8.896242	8063.447	905.388	6.809467
8.909011	8083.329	906.3206	6.810496
8.920796	8098.182	906.7869	6.81101
8.929832	8102.22	906.3206	6.810496
8.938278	8109.884	906.3206	6.810496
8.949081	8123.859	906.7869	6.81101
8.9591	8132.953	906.7869	6.81101
8.968136	8141.156	906.7869	6.81101
8.97776	8154.079	907.2531	6.811523
8.987189	8162.643	907.2531	6.811523
8.9976	8176.294	907.7194	6.812036
9.008404	8190.311	908.1856	6.812549
9.018814	8203.982	908.652	6.813062
9.028635	8212.916	908.652	6.813062
9.03826	8221.672	908.652	6.813062
9.047493	8230.07	908.652	6.813062
9.0581	8243.941	909.1182	6.813574

Engineering Strain (%)	True Strain (%)	Engineering Stress (MPa)	True Stress (MPa)
9.067528	8252.522	909.1182	6.813574
9.07735	8265.694	909.5845	6.814087
9.087564	8274.995	909.5845	6.814087
9.097385	8288.18	910.0507	6.814599
9.107206	8297.127	910.0507	6.814599
9.117028	8310.326	910.517	6.81511
9.127635	8319.995	910.517	6.81511
9.137457	8333.208	910.9833	6.815622
9.148849	8347.864	911.4496	6.816133
9.160242	8362.53	911.9158	6.816644
9.17085	8372.214	911.9158	6.816644
9.181457	8381.897	911.9158	6.816644
9.191868	8395.688	912.3821	6.817154
9.201689	8404.658	912.3821	6.817154
9.211903	8413.987	912.3821	6.817154
9.219956	8421.344	912.3821	6.817154
9.229189	8429.776	912.3821	6.817154
9.239206	8443.234	912.8484	6.817665
9.249814	8457.241	913.3147	6.818175
9.260224	8466.759	913.3147	6.818175
9.270243	8480.241	913.7809	6.818685
9.279867	8489.046	913.7809	6.818685
9.289886	8498.21	913.7809	6.818685
9.299117	8506.655	913.7809	6.818685
9.309725	8520.7	914.2473	6.819194
9.319546	8534.034	914.7135	6.819704
9.329564	8543.208	914.7135	6.819704
9.339189	8552.021	914.7135	6.819704
9.3496	8565.915	915.1798	6.820213
9.359028	8574.552	915.1798	6.820213
9.369831	8588.818	915.646	6.820721
9.379457	8597.641	915.646	6.820721
9.390456	8612.104	916.1124	6.82123
9.402046	8627.116	916.5786	6.821738

Engineering Strain (%)	True Strain (%)	Engineering Stress (MPa)	True Stress (MPa)
9.413635	8642.14	917.0449	6.822246
9.423456	8651.156	917.0449	6.822246
9.433278	8660.173	917.0449	6.822246
9.443885	8669.911	917.0449	6.822246
9.452724	8678.026	917.0449	6.822246
9.460778	8676.597	916.1124	6.82123
9.470992	8694.796	917.0449	6.822246
9.480225	8703.272	917.0449	6.822246
9.490831	8717.434	917.5111	6.822754
9.501635	8731.788	917.9774	6.823262
9.511849	8745.61	918.4437	6.823769
9.520885	8753.918	918.4437	6.823769
9.531492	8763.67	918.4437	6.823769
9.541313	8777.149	918.91	6.824276
9.550546	8776.736	917.9774	6.823262
9.56076	8795.038	918.91	6.824276
9.570778	8808.716	919.3762	6.824783
9.580795	8817.936	919.3762	6.824783
9.590814	8831.629	919.8425	6.825289
9.599653	8835.293	919.3762	6.824783
9.609278	8848.632	919.8425	6.825289
9.619099	8862.16	920.3088	6.825795
9.630492	8877.148	920.7751	6.826301
9.641885	8887.649	920.7751	6.826301
9.652884	8902.289	921.2413	6.826807
9.662903	8911.528	921.2413	6.826807
9.672527	8920.404	921.2413	6.826807
9.682742	8929.825	921.2413	6.826807
9.692956	8943.765	921.7076	6.827312
9.701992	8952.102	921.7076	6.827312
9.711617	8960.983	921.7076	6.827312
9.721438	8970.046	921.7076	6.827312
9.731064	8983.464	922.1739	6.827818
9.742456	8998.524	922.6402	6.828323

Engineering Strain (%)	True Strain (%)	Engineering Stress (MPa)	True Stress (MPa)
9.752081	9007.414	922.6402	6.828323
9.76151	9016.123	922.6402	6.828323
9.771724	9025.557	922.6402	6.828323
9.781546	9039.189	923.1064	6.828827
9.790581	9042.974	922.6402	6.828323
9.800599	9052.227	922.6402	6.828323
9.811402	9071.355	923.5728	6.829332
9.82201	9081.163	923.5728	6.829332
9.831635	9094.645	924.0389	6.829836
9.84126	9103.549	924.0389	6.829836
9.850884	9112.452	924.0389	6.829836
9.860903	9121.719	924.0389	6.829836
9.87151	9136.135	924.5053	6.83034
9.882706	9151.104	924.9715	6.830843
9.894689	9171.427	925.9041	6.83185
9.905688	9177.004	925.4378	6.831347
9.914921	9185.557	925.4378	6.831347
9.924152	9189.482	924.9715	6.830843
9.934367	9203.573	925.4378	6.831347
9.944385	9212.854	925.4378	6.831347
9.953224	9221.043	925.4378	6.831347
9.963045	9230.142	925.4378	6.831347
9.972474	9243.527	925.9041	6.83185
9.984063	9263.579	926.8366	6.832856
9.993492	9267.668	926.3704	6.832353
10.00253	9276.047	926.3704	6.832353
10.01313	9285.885	926.3704	6.832353
10.02374	9300.395	926.8366	6.832856
10.03317	9309.143	926.8366	6.832856
10.04378	9323.668	927.3029	6.833358
10.05478	9338.567	927.7692	6.83386
10.0644	9347.507	927.7692	6.83386
10.07383	9351.566	927.3029	6.833358
10.08306	9360.137	927.3029	6.833358

Engineering Strain (%)	True Strain (%)	Engineering Stress (MPa)	True Stress (MPa)
10.09249	9368.889	927.3029	6.833358
10.10271	9383.082	927.7692	6.83386
10.11351	9397.831	928.2355	6.834362
10.12392	9407.506	928.2355	6.834362
10.13472	9422.27	928.7017	6.834864
10.14572	9432.496	928.7017	6.834864
10.15594	9446.729	929.168	6.835365
10.16713	9457.143	929.168	6.835365
10.17735	9466.645	929.168	6.835365
10.18697	9485.097	930.1006	6.836367
10.19444	9477.787	928.7017	6.834864
10.20406	9486.735	928.7017	6.834864
10.21369	9500.446	929.168	6.835365
10.22488	9515.628	929.6343	6.835866
10.2351	9525.134	929.6343	6.835866
10.24453	9533.908	929.6343	6.835866
10.25474	9548.196	930.1006	6.836367
10.26397	9552.005	929.6343	6.835866
10.2738	9565.937	930.1006	6.836367
10.28263	9574.167	930.1006	6.836367
10.29363	9584.409	930.1006	6.836367
10.30522	9604.81	931.0331	6.837368
10.31426	9608.421	930.5668	6.836868
10.32369	9617.204	930.5668	6.836868
10.33331	9630.99	931.0331	6.837368
10.34215	9634.405	930.5668	6.836868
10.35178	9648.199	931.0331	6.837368
10.36278	9663.282	931.4993	6.837868
10.37515	9679.661	931.9657	6.838368
10.38694	9695.499	932.4319	6.838868
10.39617	9699.27	931.9657	6.838368
10.40717	9714.385	932.4319	6.838868
10.41699	9723.552	932.4319	6.838868
10.42681	9727.859	931.9657	6.838368

Engineering Strain (%)	True Strain (%)	Engineering Stress (MPa)	True Stress (MPa)
10.43683	9737.205	931.9657	6.838368
10.44547	9750.138	932.4319	6.838868
10.45431	9753.515	931.9657	6.838368
10.46276	9761.395	931.9657	6.838368
10.47671	9789.061	933.3644	6.839867
10.48633	9798.055	933.3644	6.839867
10.49556	9801.787	932.8982	6.839367
10.50499	9810.593	932.8982	6.839367
10.51304	9818.113	932.8982	6.839367
10.52228	9826.735	932.8982	6.839367
10.53269	9841.369	933.3644	6.839867
10.54369	9856.564	933.8307	6.840365
10.55351	9865.745	933.8307	6.840365
10.56412	9875.661	933.8307	6.840365
10.57296	9883.924	933.8307	6.840365
10.58297	9893.289	933.8307	6.840365
10.59338	9907.96	934.297	6.840864
10.6038	9917.698	934.297	6.840864
10.6144	9932.568	934.7633	6.841363
10.62737	9949.654	935.2296	6.841861
10.63778	9959.402	935.2296	6.841861
10.64779	9968.78	935.2296	6.841861
10.6584	9978.71	935.2296	6.841861
10.66724	9982.013	934.7633	6.841363
10.67745	9996.549	935.2296	6.841861
10.68688	10005.38	935.2296	6.841861
10.69592	10013.84	935.2296	6.841861
10.70397	10016.38	934.7633	6.841363
10.71615	10032.78	935.2296	6.841861
10.72774	10053.63	936.1621	6.842856
10.73697	10057.28	935.6959	6.842359
10.74738	10067.03	935.6959	6.842359
10.75642	10075.49	935.6959	6.842359
10.76644	10084.88	935.6959	6.842359

Engineering Strain (%)	True Strain (%)	Engineering Stress (MPa)	True Stress (MPa)
10.77645	10094.26	935.6959	6.842359
10.78844	10115.55	936.6284	6.843354
10.79767	10114.13	935.6959	6.842359
10.80671	10127.63	936.1621	6.842856
10.81672	10142.07	936.6284	6.843354
10.82596	10150.72	936.6284	6.843354
10.8346	10153.78	936.1621	6.842856
10.84501	10168.59	936.6284	6.843354
10.85679	10184.7	937.0947	6.843851
10.86897	10206.26	938.0272	6.844844
10.87879	10210.41	937.561	6.844348
10.88881	10219.81	937.561	6.844348
10.89981	10230.14	937.561	6.844348
10.90904	10238.8	937.561	6.844348
10.91828	10247.47	937.561	6.844348
10.9277	10256.32	937.561	6.844348
10.93713	10265.17	937.561	6.844348
10.94578	10273.28	937.561	6.844348
10.9554	10277.2	937.0947	6.843851
10.96856	10304.89	938.4935	6.845341
10.97779	10313.57	938.4935	6.845341
10.98801	10323.16	938.4935	6.845341
10.99803	10327.45	938.0272	6.844844
11.00765	10341.62	938.4935	6.845341
11.01728	10350.66	938.4935	6.845341
11.02847	10361.18	938.4935	6.845341
11.03908	10376.29	938.9597	6.845837
11.04871	10385.34	938.9597	6.845837
11.05794	10388.86	938.4935	6.845341
11.06776	10403.25	938.9597	6.845837
11.07758	10412.48	938.9597	6.845837
11.08662	10410.63	938.0272	6.844844
11.09683	10430.57	938.9597	6.845837
11.10921	10447.39	939.4261	6.846333

Engineering Strain (%)	True Strain (%)	Engineering Stress (MPa)	True Stress (MPa)
11.1206	10463.28	939.8923	6.846829
11.13003	10466.97	939.4261	6.846333
11.14142	10482.88	939.8923	6.846829
11.15183	10492.67	939.8923	6.846829
11.15969	10494.86	939.4261	6.846333
11.1699	10504.47	939.4261	6.846333
11.17894	10512.96	939.4261	6.846333
11.18817	10521.65	939.4261	6.846333
11.19701	10529.96	939.4261	6.846333
11.20899	10546.45	939.8923	6.846829
11.21979	10567.08	940.8248	6.847819
11.22942	10570.91	940.3586	6.847324
11.23963	10580.53	940.3586	6.847324
11.24887	10589.22	940.3586	6.847324
11.25829	10598.09	940.3586	6.847324
11.26831	10602.27	939.8923	6.846829
11.28049	10624.25	940.8248	6.847819
11.28972	10638.21	941.2911	6.848314
11.29738	10634.89	940.3586	6.847324
11.30681	10643.76	940.3586	6.847324
11.31703	10658.66	940.8248	6.847819
11.32685	10667.91	940.8248	6.847819
11.33687	10677.34	940.8248	6.847819
11.34806	10693.18	941.2911	6.848314
11.36044	10710.14	941.7574	6.848809
11.37144	10720.51	941.7574	6.848809
11.38106	10729.58	941.7574	6.848809
11.39265	10745.82	942.2237	6.849303
11.40129	10743.34	941.2911	6.848314
11.41053	10752.04	941.2911	6.848314
11.42054	10761.48	941.2911	6.848314
11.42978	10770.18	941.2911	6.848314
11.43744	10772.06	940.8248	6.847819
11.44844	10787.76	941.2911	6.848314

Engineering Strain (%)	True Strain (%)	Engineering Stress (MPa)	True Stress (MPa)
11.46179	10816.38	942.6899	6.849798
11.47122	10819.93	942.2237	6.849303
11.48104	10829.19	942.2237	6.849303
11.48949	10831.8	941.7574	6.848809
11.49735	10833.85	941.2911	6.848314
11.50854	10849.76	941.7574	6.848809
11.51778	10863.84	942.2237	6.849303
11.5274	10867.54	941.7574	6.848809
11.53801	10882.92	942.2237	6.849303
11.54803	10897.76	942.6899	6.849798
11.55804	10907.21	942.6899	6.849798
11.56845	10917.03	942.6899	6.849798
11.57887	10926.86	942.6899	6.849798
11.58869	10936.13	942.6899	6.849798
11.60008	10952.29	943.1563	6.850292
11.61187	10968.83	943.6225	6.850785
11.6209	10971.95	943.1563	6.850292
11.63072	10975.8	942.6899	6.849798
11.63897	10983.58	942.6899	6.849798
11.64722	10985.94	942.2237	6.849303
11.65901	11007.93	943.1563	6.850292
11.66903	11017.38	943.1563	6.850292
11.67904	11026.84	943.1563	6.850292
11.68847	11035.74	943.1563	6.850292
11.69849	11039.75	942.6899	6.849798
11.70812	11054.29	943.1563	6.850292
11.71794	11063.56	943.1563	6.850292
11.72795	11078.49	943.6225	6.850785
11.73837	11088.32	943.6225	6.850785
11.74838	11097.79	943.6225	6.850785
11.75978	11114.03	944.0888	6.851279
11.7692	11122.94	944.0888	6.851279
11.77844	11126.18	943.6225	6.850785
11.78904	11136.2	943.6225	6.850785

Engineering Strain (%)	True Strain (%)	Engineering Stress (MPa)	True Stress (MPa)
11.79926	11151.35	944.0888	6.851279
11.80888	11160.44	944.0888	6.851279
11.82028	11171.21	944.0888	6.851279
11.83029	11186.19	944.5551	6.851772
11.84051	11190.33	944.0888	6.851279
11.85229	11207	944.5551	6.851772
11.86428	11223.86	945.0214	6.852265
11.8739	11227.43	944.5551	6.851772
11.8847	11215.48	942.6899	6.849798
11.89551	11253.4	945.0214	6.852265
11.90395	11244.74	943.6225	6.850785
11.9122	11258.09	944.0888	6.851279
11.92026	11260.14	943.6225	6.850785
11.92988	11269.24	943.6225	6.850785
11.94186	11291.69	944.5551	6.851772
11.95365	11308.41	945.0214	6.852265
11.96347	11312.12	944.5551	6.851772
11.97408	11333.32	945.4875	6.852758
11.9837	11331.25	944.5551	6.851772
11.99392	11340.91	944.5551	6.851772
12.00413	11356.17	945.0214	6.852265
12.01474	11366.2	945.0214	6.852265
12.02417	11369.51	944.5551	6.851772
12.03281	11377.69	944.5551	6.851772
12.04126	11380.06	944.0888	6.851279
12.05186	11395.7	944.5551	6.851772
12.06169	11404.99	944.5551	6.851772
12.07229	11420.65	945.0214	6.852265
12.08447	11437.8	945.4875	6.852758
12.09567	11448.4	945.4875	6.852758
12.10667	11464.46	945.9539	6.85325
12.1161	11467.73	945.4875	6.852758
12.1269	11477.96	945.4875	6.852758
12.13672	11487.26	945.4875	6.852758

Engineering Strain (%)	True Strain (%)	Engineering Stress (MPa)	True Stress (MPa)
12.14536	11489.77	945.0214	6.852265
12.15519	11499.07	945.0214	6.852265
12.16422	11507.61	945.0214	6.852265
12.17306	11515.98	945.0214	6.852265
12.1817	11518.47	944.5551	6.851772
12.1931	11534.93	945.0214	6.852265
12.20528	11557.83	945.9539	6.85325
12.21569	11567.69	945.9539	6.85325
12.22472	11570.55	945.4875	6.852758
12.23415	11579.47	945.4875	6.852758
12.24279	11581.94	945.0214	6.852265
12.25261	11591.24	945.0214	6.852265
12.26263	11612.15	945.9539	6.85325
12.27226	11615.54	945.4875	6.852758
12.28286	11625.58	945.4875	6.852758
12.29288	11635.06	945.4875	6.852758
12.30192	11643.61	945.4875	6.852758
12.31233	11653.47	945.4875	6.852758
12.32313	11669.44	945.9539	6.85325
12.33413	11679.85	945.9539	6.85325
12.34729	11698.07	946.4201	6.853743
12.3579	11713.89	946.8865	6.854235
12.36772	11717.43	946.4201	6.853743
12.37735	11720.78	945.9539	6.85325
12.38599	11723.19	945.4875	6.852758
12.39719	11739.56	945.9539	6.85325
12.40642	11748.31	945.9539	6.85325
12.41663	11757.98	945.9539	6.85325
12.42606	11766.91	945.9539	6.85325
12.43608	11776.39	945.9539	6.85325
12.4461	11785.88	945.9539	6.85325
12.45749	11802.48	946.4201	6.853743
12.46633	11805.04	945.9539	6.85325
12.47615	11814.34	945.9539	6.85325

Engineering Strain (%)	True Strain (%)	Engineering Stress (MPa)	True Stress (MPa)
12.48479	11822.52	945.9539	6.85325
12.49442	11825.81	945.4875	6.852758
12.50463	11841.31	945.9539	6.85325
12.51406	11850.24	945.9539	6.85325
12.52447	11860.1	945.9539	6.85325
12.53429	11869.4	945.9539	6.85325
12.54392	11878.51	945.9539	6.85325
12.55354	11887.63	945.9539	6.85325
12.56356	11897.11	945.9539	6.85325
12.57476	11913.58	946.4201	6.853743
12.58753	11931.55	946.8865	6.854235
12.59872	11942.16	946.8865	6.854235
12.60874	11951.65	946.8865	6.854235
12.61856	11955.08	946.4201	6.853743
12.62779	11963.83	946.4201	6.853743
12.63801	11967.61	945.9539	6.85325
12.64822	11983.18	946.4201	6.853743
12.65745	11986.03	945.9539	6.85325
12.66747	11995.51	945.9539	6.85325
12.67729	12004.81	945.9539	6.85325
12.68731	12014.3	945.9539	6.85325
12.69713	12023.6	945.9539	6.85325
12.70774	12039.57	946.4201	6.853743
12.71677	12054.06	946.8865	6.854235
12.72522	12050.2	945.9539	6.85325
12.73465	12053.19	945.4875	6.852758
12.74604	12075.86	946.4201	6.853743
12.75527	12078.66	945.9539	6.85325
12.76529	12088.14	945.9539	6.85325
12.7757	12103.96	946.4201	6.853743
12.78592	12113.64	946.4201	6.853743
12.79495	12116.23	945.9539	6.85325
12.80576	12126.46	945.9539	6.85325
12.81558	12141.74	946.4201	6.853743

Engineering Strain (%)	True Strain (%)	Engineering Stress (MPa)	True Stress (MPa)
12.82638	12151.97	946.4201	6.853743
12.83915	12170.06	946.8865	6.854235
12.84956	12179.92	946.8865	6.854235
12.85938	12183.24	946.4201	6.853743
12.86901	12186.36	945.9539	6.85325
12.87824	12189.09	945.4875	6.852758
12.88944	12205.7	945.9539	6.85325
12.89867	12214.44	945.9539	6.85325
12.9081	12223.37	945.9539	6.85325
12.91694	12225.72	945.4875	6.852758
12.92676	12235.01	945.4875	6.852758
12.93697	12250.72	945.9539	6.85325
12.94699	12254.16	945.4875	6.852758
12.9572	12263.83	945.4875	6.852758
12.96702	12279.17	945.9539	6.85325
12.97626	12281.87	945.4875	6.852758
12.98686	12291.91	945.4875	6.852758
12.99688	12301.39	945.4875	6.852758
13.00651	12310.5	945.4875	6.852758
13.01672	12320.17	945.4875	6.852758
13.02654	12329.46	945.4875	6.852758
13.03656	12338.94	945.4875	6.852758
13.04599	12347.87	945.4875	6.852758
13.05699	12364.37	945.9539	6.85325
13.0676	12368.32	945.4875	6.852758
13.0784	12378.54	945.4875	6.852758
13.09117	12396.73	945.9539	6.85325
13.1006	12399.55	945.4875	6.852758
13.11081	12409.22	945.4875	6.852758
13.11945	12411.28	945.0214	6.852265
13.12947	12420.76	945.0214	6.852265
13.14106	12431.72	945.0214	6.852265
13.14951	12445.84	945.4875	6.852758
13.15913	12442.68	944.5551	6.851772

Engineering Strain (%)	True Strain (%)	Engineering Stress (MPa)	True Stress (MPa)
13.17013	12453.08	944.5551	6.851772
13.17976	12462.19	944.5551	6.851772
13.1886	12464.39	944.0888	6.851279
13.19763	12466.78	943.6225	6.850785
13.20824	12482.96	944.0888	6.851279
13.21727	12491.5	944.0888	6.851279
13.2269	12494.43	943.6225	6.850785
13.2377	12510.81	944.0888	6.851279
13.24693	12513.35	943.6225	6.850785
13.25695	12522.82	943.6225	6.850785
13.26776	12533.02	943.6225	6.850785
13.27797	12542.67	943.6225	6.850785
13.2876	12545.57	943.1563	6.850292
13.29742	12554.84	943.1563	6.850292
13.30802	12564.85	943.1563	6.850292
13.31961	12575.8	943.1563	6.850292
13.3316	12593.33	943.6225	6.850785
13.34161	12596.57	943.1563	6.850292
13.35163	12599.8	942.6899	6.849798
13.36106	12602.47	942.2237	6.849303
13.37127	12605.87	941.7574	6.848809
13.38169	12615.68	941.7574	6.848809
13.39131	12618.51	941.2911	6.848314
13.40035	12620.78	940.8248	6.847819
13.40919	12629.1	940.8248	6.847819
13.4194	12638.72	940.8248	6.847819
13.4302	12648.9	940.8248	6.847819
13.43904	12650.96	940.3586	6.847324
13.44886	12660.2	940.3586	6.847324
13.45947	12670.19	940.3586	6.847324
13.46831	12665.95	939.4261	6.846333
13.47833	12675.37	939.4261	6.846333
13.48874	12685.16	939.4261	6.846333
13.49876	12688.29	938.9597	6.845837

Engineering Strain (%)	True Strain (%)	Engineering Stress (MPa)	True Stress (MPa)
13.50819	12697.15	938.9597	6.845837
13.51919	12707.49	938.9597	6.845837
13.52881	12710.23	938.4935	6.845341
13.53863	12713.14	938.0272	6.844844
13.54943	12723.29	938.0272	6.844844
13.56024	12727.11	937.561	6.844348
13.57222	12738.36	937.561	6.844348
13.58283	12748.31	937.561	6.844348
13.59265	12744.85	936.6284	6.843354
13.60208	12741.01	935.6959	6.842359
13.61092	12742.94	935.2296	6.841861
13.62074	12745.79	934.7633	6.841363
13.63311	12763.72	935.2296	6.841861
13.64352	12773.47	935.2296	6.841861
13.65236	12769.01	934.297	6.840864
13.66297	12772.56	933.8307	6.840365
13.6726	12775.19	933.3644	6.839867
13.68124	12770.5	932.4319	6.838868
13.69027	12772.56	931.9657	6.838368
13.70069	12782.27	931.9657	6.838368
13.70972	12784.31	931.4993	6.837868
13.72033	12794.2	931.4993	6.837868
13.73074	12803.9	931.4993	6.837868
13.74115	12807.21	931.0331	6.837368
13.75156	12810.5	930.5668	6.836868
13.76099	12812.86	930.1006	6.836367
13.77101	12809.35	929.168	6.835365
13.78142	12819.03	929.168	6.835365
13.79183	12822.29	928.7017	6.834864
13.80302	12826.26	928.2355	6.834362
13.81461	12837.03	928.2355	6.834362
13.82424	12833.08	927.3029	6.833358
13.83465	12836.29	926.8366	6.832856
13.84447	12838.95	926.3704	6.832353

Engineering Strain (%)	True Strain (%)	Engineering Stress (MPa)	True Stress (MPa)
13.85331	12834.23	925.4378	6.831347
13.86411	12837.77	924.9715	6.830843
13.87472	12847.6	924.9715	6.830843
13.88474	12843.92	924.0389	6.829836
13.89515	12847.08	923.5728	6.829332
13.90458	12849.31	923.1064	6.828827
13.91479	12852.26	922.6402	6.828323
13.92383	12854.11	922.1739	6.827818
13.93345	12850.01	921.2413	6.826807
13.94249	12851.84	920.7751	6.826301
13.95192	12854.02	920.3088	6.825795
13.96135	12856.2	919.8425	6.825289
13.97215	12866.15	919.8425	6.825289
13.98315	12869.76	919.3762	6.824783
13.99297	12872.27	918.91	6.824276
14.00318	12875.14	918.4437	6.823769
14.01477	12879.26	917.9774	6.823262
14.0246	12881.75	917.5111	6.822754
14.03501	12878.22	916.5786	6.821738
14.04522	12881.05	916.1124	6.82123
14.05661	12891.49	916.1124	6.82123
14.06643	12887.38	915.1798	6.820213
14.07606	12876.51	913.7809	6.818685
14.08667	12886.21	913.7809	6.818685
14.09531	12880.98	912.8484	6.817665
14.10454	12876.26	911.9158	6.816644
14.11633	12893.6	912.3821	6.817154
14.12654	12889.76	911.4496	6.816133
14.13656	12892.31	910.9833	6.815622
14.14658	12894.85	910.517	6.81511
14.15679	12897.56	910.0507	6.814599
14.16622	12892.93	909.1182	6.813574
14.17585	12888.47	908.1856	6.812549
14.18606	12891.15	907.7194	6.812036

Engineering Strain (%)	True Strain (%)	Engineering Stress (MPa)	True Stress (MPa)
14.1949	12892.56	907.2531	6.811523
14.20374	12887.34	906.3206	6.810496
14.21415	12890.16	905.8543	6.809982
14.22593	12907.48	906.3206	6.810496
14.23615	12903.47	905.388	6.809467
14.24617	12905.91	904.9218	6.808953
14.25638	12901.87	903.9892	6.807923
14.26679	12904.64	903.5229	6.807408
14.2772	12907.4	903.0566	6.806892
14.28742	12903.31	902.1241	6.80586
14.29802	12906.22	901.6578	6.805343
14.30883	12915.97	901.6578	6.805343
14.31884	12904.99	900.259	6.803793
14.32827	12900.12	899.3265	6.802757
14.33809	12902.28	898.8602	6.802239
14.34733	12897.21	897.9276	6.801203
14.35754	12899.7	897.4614	6.800684
14.36835	12902.7	896.9951	6.800165
14.37836	12904.99	896.5288	6.799645
14.38838	12900.57	895.5963	6.798606
14.39859	12896.3	894.6638	6.797565
14.40861	12905.27	894.6638	6.797565
14.41765	12893.2	893.2648	6.796002
14.42767	12902.15	893.2648	6.796002
14.4367	12890.04	891.8661	6.794437
14.44731	12899.51	891.8661	6.794437
14.45674	12894.45	890.9335	6.793392
14.46735	12897.16	890.4672	6.792869
14.47756	12899.52	890.001	6.792346
14.48758	12901.69	889.5347	6.791822
14.49799	12897.44	888.6021	6.790774
14.5082	12899.76	888.1359	6.79025
14.51861	12895.48	887.2034	6.789201
14.52942	12898.3	886.737	6.788676

Engineering Strain (%)	True Strain (%)	Engineering Stress (MPa)	True Stress (MPa)
14.53983	12893.98	885.8044	6.787624
14.55142	12897.48	885.3383	6.787099
14.56261	12900.61	884.8719	6.786572
14.57224	12888.75	883.4731	6.784992
14.58186	12883.67	882.5406	6.783937
14.59051	12877.7	881.608	6.782881
14.59954	12872.06	880.6755	6.781824
14.61054	12881.76	880.6755	6.781824
14.62115	12884.29	880.2092	6.781295
14.63195	12886.99	879.743	6.780766
14.64177	12881.98	878.8104	6.779706
14.65258	12884.66	878.3441	6.779176
14.66083	12871.4	876.9453	6.777584
14.67026	12872.84	876.479	6.777053
14.68008	12867.77	875.5464	6.77599
14.68951	12869.18	875.0802	6.775458
14.70011	12871.62	874.6139	6.774925
14.71013	12866.68	873.6813	6.77386
14.71995	12868.4	873.2151	6.773326
14.73036	12863.77	872.2826	6.772259
14.74077	12865.99	871.8162	6.771725
14.75079	12860.97	870.8837	6.770656
14.76022	12855.43	869.9512	6.769586
14.77142	12858.29	869.4849	6.76905
14.78202	12860.64	869.0186	6.768515
14.7944	12864.5	868.5524	6.767979
14.80461	12852.68	867.1535	6.766369
14.81463	12847.56	866.2209	6.765294
14.82465	12842.42	865.2884	6.764218
14.83368	12836.41	864.3558	6.763141
14.84351	12831.07	863.4233	6.762063
14.85411	12833.32	862.9571	6.761523
14.86433	12835.21	862.4908	6.760983
14.87474	12830.33	861.5582	6.759903

Engineering Strain (%)	True Strain (%)	Engineering Stress (MPa)	True Stress (MPa)
14.88436	12824.75	860.6257	6.758821
14.89497	12820	859.6931	6.757738
14.90499	12821.67	859.2269	6.757196
14.91422	12815.7	858.2943	6.756111
14.92326	12802.59	856.8954	6.754482
14.93386	12811.69	856.8954	6.754482
14.94349	12806.01	855.9629	6.753395
14.95351	12800.66	855.0304	6.752306
14.96392	12802.59	854.5641	6.751761
14.97354	12796.86	853.6316	6.75067
14.98356	12791.45	852.699	6.749579
14.99417	12793.51	852.2327	6.749032
15.00438	12788.24	851.3002	6.747939
15.0146	12782.94	850.3676	6.746844
15.02501	12784.8	849.9014	6.746296
15.0362	12780.3	848.9689	6.7452
15.04779	12783.14	848.5026	6.744651
15.0584	12771.08	847.1038	6.743003
15.06881	12765.86	846.1712	6.741903
15.07745	12752.09	844.7723	6.74025
15.08531	12737.64	843.3736	6.738595
15.09709	12747.59	843.3736	6.738595
15.10652	12741.46	842.441	6.73749
15.11615	12735.48	841.5085	6.736384
15.12636	12737.03	841.0422	6.73583
15.13717	12732.02	840.1096	6.734722
15.1466	12725.82	839.1771	6.733613
15.1574	12727.83	838.7108	6.733058
15.16643	12714.2	837.312	6.73139
15.17626	12708.28	836.3794	6.730277
15.18647	12709.76	835.9132	6.72972
15.19629	12703.81	834.9807	6.728605
15.2065	12698.16	834.048	6.727489
15.21633	12692.17	833.1155	6.726372

Engineering Strain (%)	True Strain (%)	Engineering Stress (MPa)	True Stress (MPa)
15.22654	12693.59	832.6492	6.725813
15.23715	12688.23	831.7167	6.724693
15.24638	12674.59	830.3178	6.723012
15.2564	12668.69	829.3853	6.72189
15.2674	12663.59	828.4528	6.720766
15.27781	12665.1	827.9865	6.720204
15.28979	12667.9	827.5202	6.719641
15.30138	12663.23	826.5876	6.718515
15.31061	12649.46	825.1888	6.716823
15.32102	12636.63	823.79	6.715129
15.32849	12614.19	821.9249	6.712865
15.33929	12615.93	821.4586	6.712298
15.35108	12625.62	821.4586	6.712298
15.36011	12611.57	820.0598	6.710596
15.36974	12605.14	819.1273	6.70946
15.37995	12599.17	818.1947	6.708322
15.39095	12593.83	817.2621	6.707183
15.40058	12587.35	816.3296	6.706042
15.41059	12581.16	815.397	6.704901
15.41943	12566.81	813.9982	6.703186
15.42808	12559.47	813.0657	6.702041
15.43868	12553.7	812.1331	6.700895
15.4487	12554.65	811.6669	6.700321
15.45872	12548.37	810.7343	6.699173
15.46913	12542.4	809.8018	6.698024
15.47915	12536.09	808.8692	6.696873
15.48917	12522.53	807.4704	6.695144
15.49899	12516.02	806.5378	6.69399
15.50959	12510.12	805.6053	6.692834
15.52059	12504.52	804.6727	6.691678
15.53297	12507.25	804.2065	6.691099
15.54377	12494.2	802.8077	6.68936
15.55359	12480.34	801.4088	6.687618
15.56342	12466.45	800.01	6.685873

Engineering Strain (%)	True Strain (%)	Engineering Stress (MPa)	True Stress (MPa)
15.57265	12452.06	798.6112	6.684126
15.58286	12445.7	797.6786	6.682959
15.59347	12446.9	797.2123	6.682375
15.60329	12447.46	796.7461	6.68179
15.61213	12418.12	794.4147	6.678864
15.62254	12419.11	793.9484	6.678277
15.63315	12412.97	793.0159	6.677103
15.64297	12398.89	791.6171	6.67534
15.65338	12392.54	790.6845	6.674163
15.6632	12385.71	789.752	6.672984
15.67263	12371.24	788.3531	6.671214
15.68245	12364.37	787.4206	6.670032
15.69227	12350.16	786.0218	6.668256
15.70249	12343.56	785.0892	6.66707
15.71211	12336.47	784.1567	6.665883
15.72272	12330.14	783.2241	6.664695
15.73254	12315.83	781.8253	6.66291
15.74236	12301.5	780.4265	6.661121
15.75277	12294.94	779.494	6.659927
15.76279	12288.06	778.5614	6.658731
15.77438	12275.03	777.1626	6.656935
15.78577	12269.18	776.23	6.655736
15.79756	12263.61	775.2975	6.654536
15.80699	12241.44	773.4324	6.65213
15.817	12219.7	771.5673	6.649719
15.82663	12212.38	770.6348	6.648511
15.83743	12205.94	769.7022	6.647302
15.84647	12190.74	768.3033	6.645485
15.85491	12175.06	766.9045	6.643665
15.86474	12160.41	765.5057	6.641842
15.87515	12160.99	765.0394	6.641234
15.88595	12154.45	764.1069	6.640016
15.89715	12140.78	762.7081	6.638186
15.90795	12126.78	761.3093	6.636352

Engineering Strain (%)	True Strain (%)	Engineering Stress (MPa)	True Stress (MPa)
15.91659	12103.68	759.4442	6.633903
15.92543	12088.13	758.0453	6.632062
15.93565	12081.02	757.1128	6.630832
15.94508	12065.86	755.714	6.628985
15.95549	12058.86	754.7814	6.627752
15.9655	12044.1	753.3826	6.6259
15.97572	12029.46	751.9838	6.624044
15.98534	12014.34	750.585	6.622184
15.99576	12007.25	749.6524	6.620943
16.00597	11992.53	748.2536	6.619078
16.01638	11977.93	746.8547	6.617209
16.02954	11972.82	745.9222	6.615961
16.03975	11950.53	744.0571	6.613461
16.05017	11928.35	742.192	6.610954
16.06018	11905.85	740.3269	6.608442
16.06981	11883.01	738.4618	6.605923
16.08061	11868.5	737.063	6.604029
16.09024	11845.6	735.1979	6.601499
16.09966	11815	732.8665	6.598327
16.1087	11776.57	730.0688	6.594508

APPENDIX C

Fig. 19 is a plot of strain rate ratio obtained from the experiments.

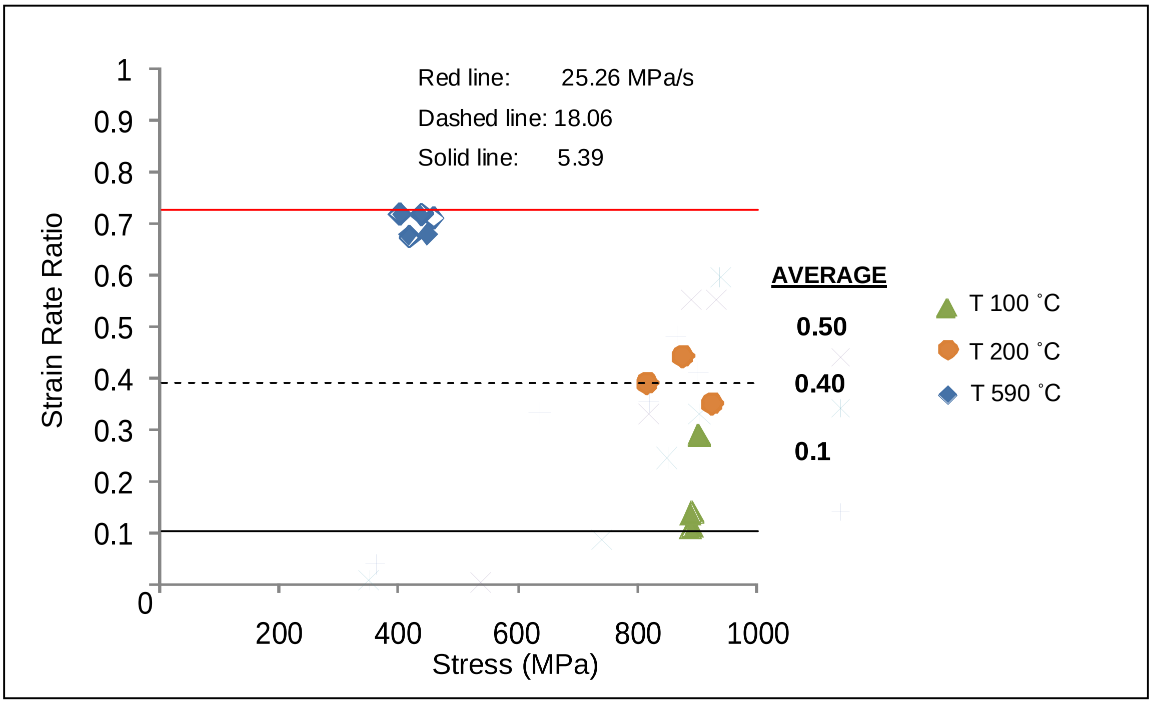

Fig. 19: Strain rate ratios for low Alloy Steel tested at various temperatures plotted as a function of Stress. The strain rate ratio is weakly dependant on the stress, if at all.

Data points as shown in Fig. 19 are scattered, with no clear trend of decrease or increase of the ratio with increase of stress. The minimum value for R found in the present study is 0.1 at 39.2 MPa/s, as shown in Fig. 19. This implies that almost 98% might initially have been thought to be mechanically activated at this stress rate. These values are not different to results that have been obtained "when instantaneous measurements of relaxation strain rate were reported [1]. The strain rate ratios tended to increase with higher stresses since at higher stresses, stress versus strain graphs became "flatter" due to recovery processes becoming more dominant. Even at high temperatures of low alloy steel at 200^{0}C and 590^{0}C we found that the result obtained is consistent with the recovery control, but inconsistent with the glide control. This observation was evidenced by Kurishita et al as well [8].

Fig. 20 shows a plot strain ratio at different temperatures.

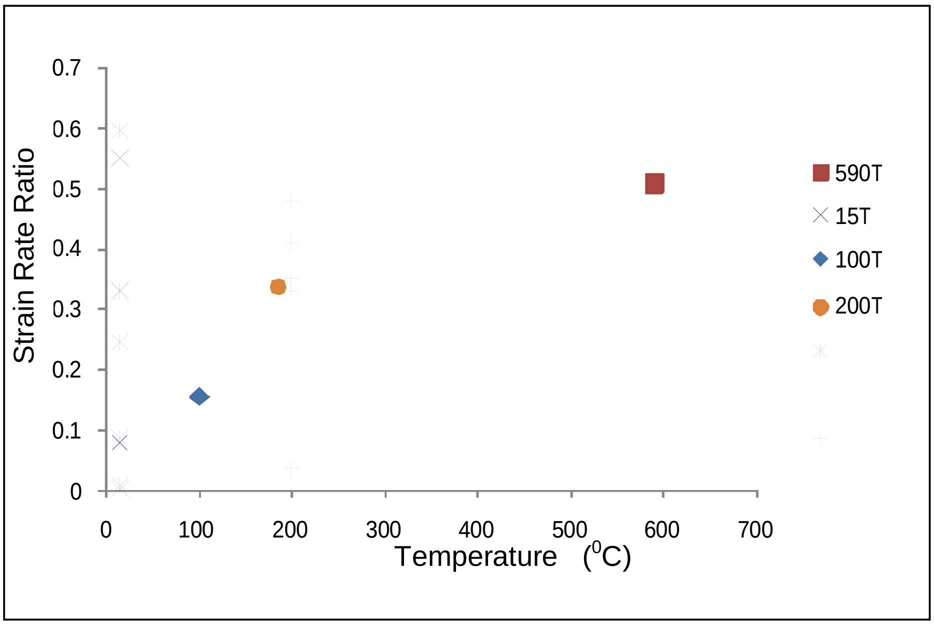

Fig. 20: Strain rate ratio for low Alloy Steel measured at 1% strain as a function of Temperature (^{0}C).

It was observed that higher temperatures tended to produce higher strain rate ratios. This indicates strain rate sensitivity and activation volume of low alloy steel, which is a signature of the deformation (dislocation) mechanism.

Furthermore, at these temperatures an important phenomenon sets in and there is a presence of diffusing effects which slow down or pin dislocations as was observed by Kruml et al [58]. As shown in Fig. 20, this effect can be observed during a repeated stress relaxation test. Apparently the previous load relaxation results of Alden [27, 28, 31, 50] and Abe et al [46] as well as the strain rate change data of Yoshinaga et al [52] are correct as opposed to what Gibeling et al [48] called results because of the limitations of experimental resolution[43, 44].

APPENDIX D

Plastic shear strain rate- normalised shear stress curves determined from relaxation curves at different temperatures.

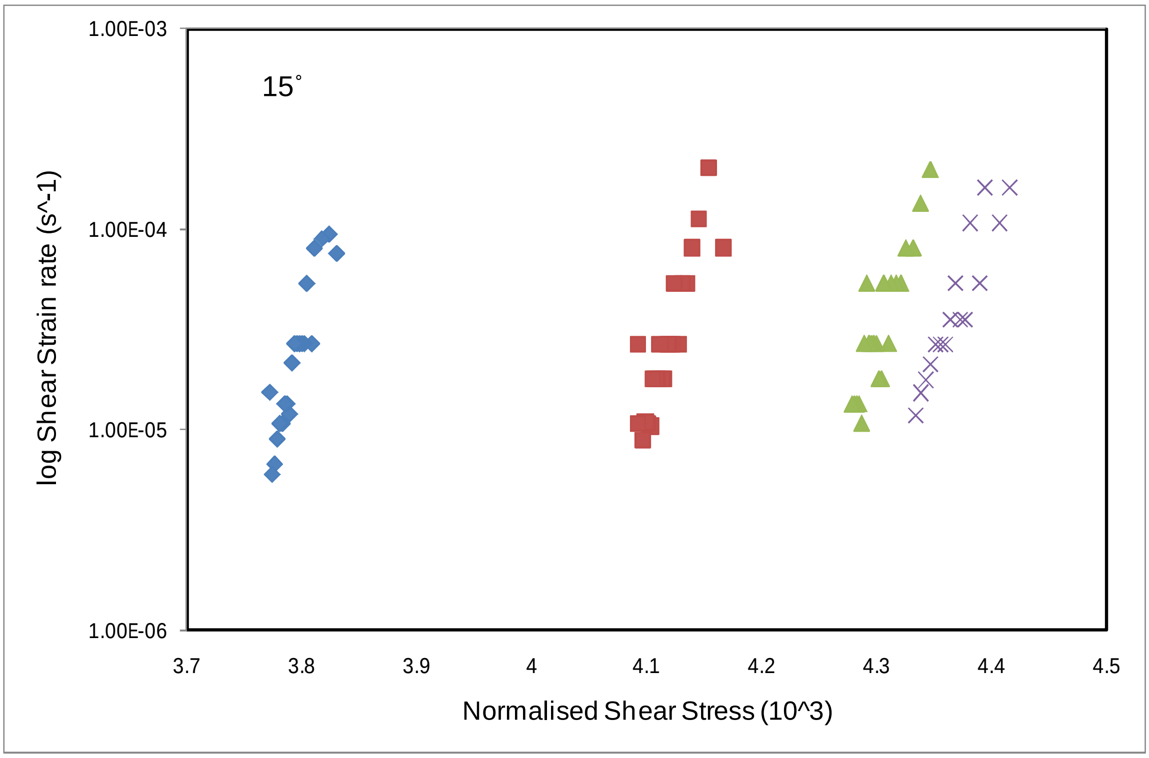

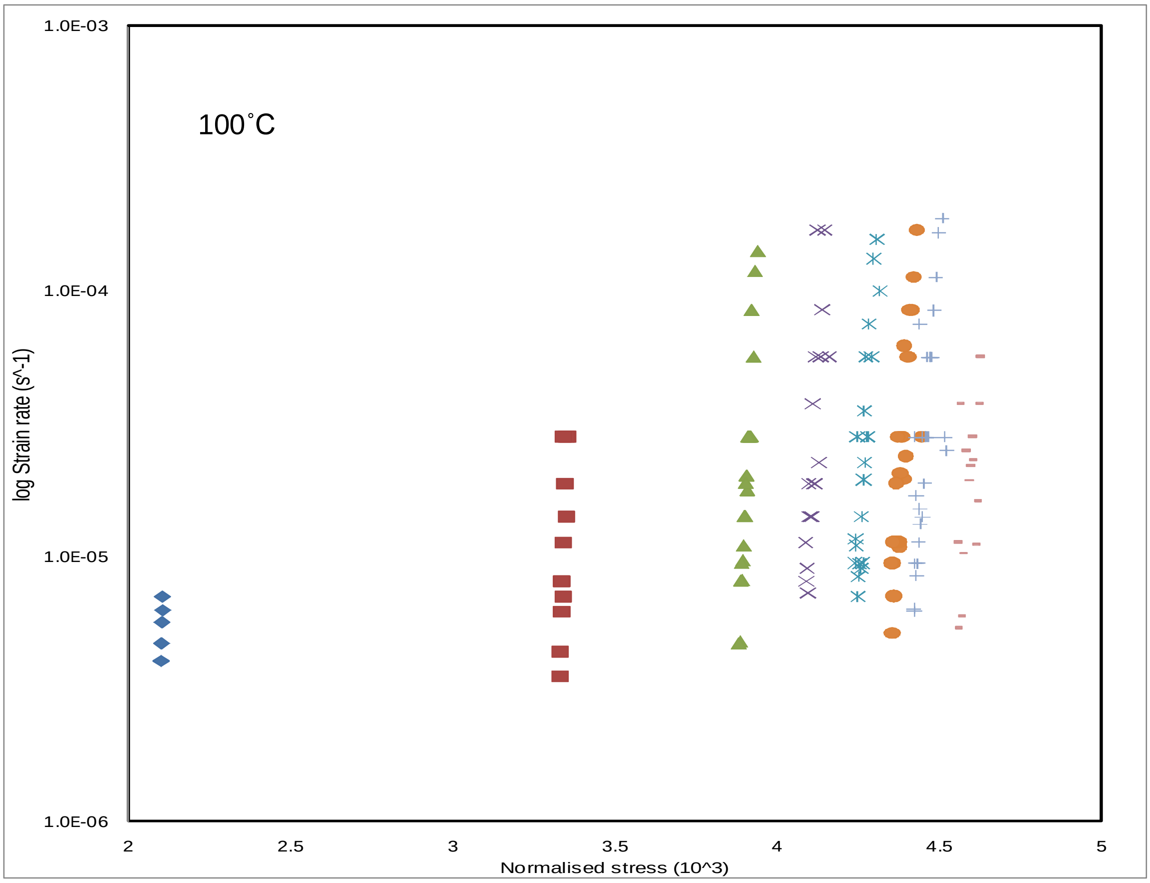
100˚C
1.0E-03
1.0E-04
1.0E-05
1.0E-06
log Strain rate (s^-1)
2
2.5
3
3.5
4
4.5
5
Normalised stress (10^3)

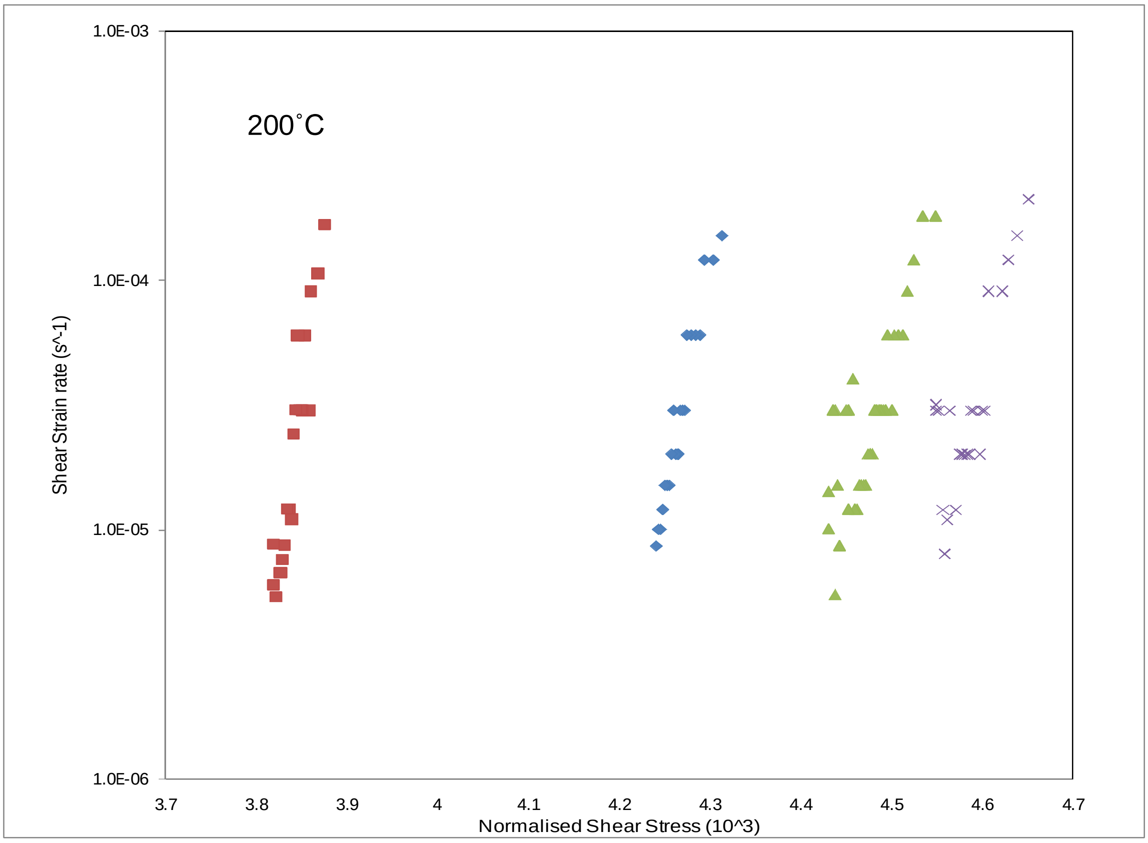

200˚C
Shear Strain rate (s^-1)
1.0E-03
1.0E-04
1.0E-05
1.0E-06
3.7
3.8
3.9
4
4.1
4.2
4.3
4.4
4.5
4.6
4.7
Normalised Shear Stress (10^3)

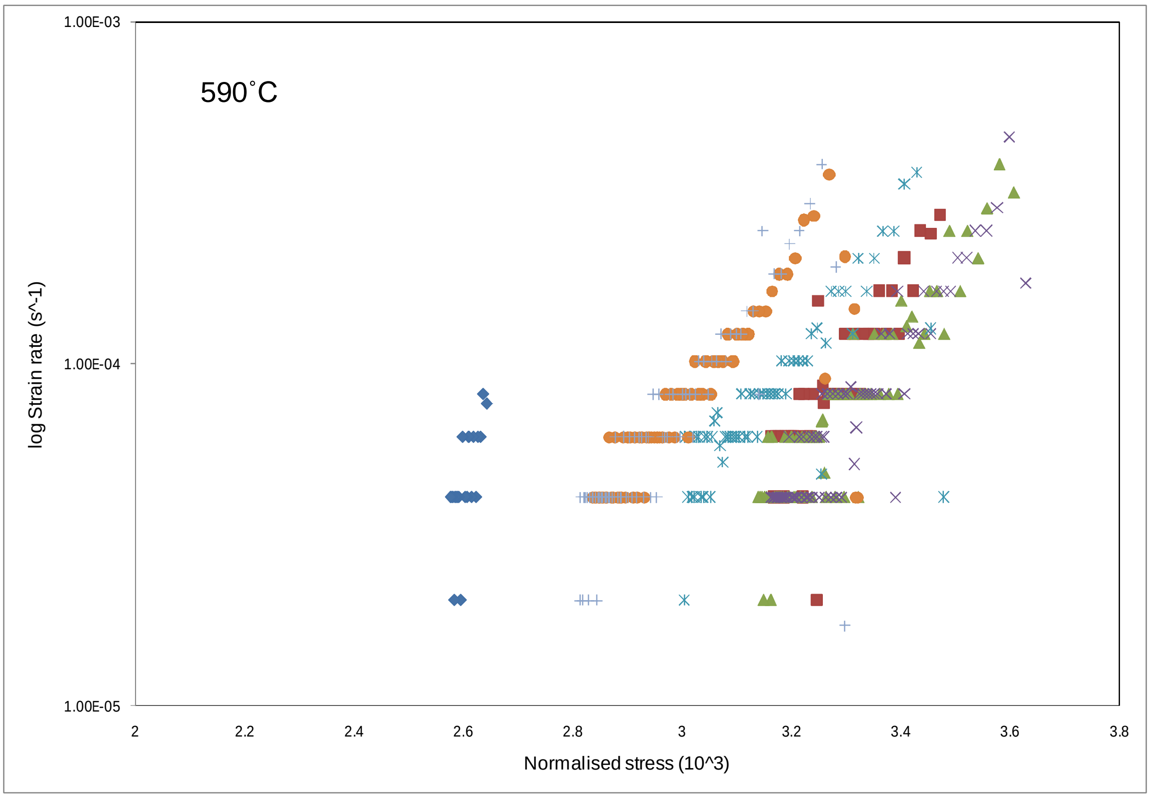

590˚C
log Strain rate (s^-1)
1.00E-03
1.00E-04
1.00E-05
2
2.2
2.4
2.6
2.8
3
3.2
3.4
3.6
3.8
Normalised stress (10^3)